Development of systems to produce antibodies to target tumor-stroma crosstalk

by

Ömrüm Naz Nalkıran

A Dissertation Submitted to the
Graduate School of Health Sciences
in Partial Fulfillment of the Requirements for
the Degree of

Master of Science

in

Cellular and Molecular Medicine

August 29, 2025

Development of systems to produce antibodies to target tumor-stroma crosstalk

Koç University

Graduate School of Health Sciences

This is to certify that I have examined this copy of a master's thesis by

Ömrüm Naz Nalkıran

and have found that it is complete and satisfactory in all respects,
and that any and all revisions required by the final
examining committee have been made.

Committee Members:

Prof. Dr. Devrim Gözüaçık (Advisor)

Dr. Yunus Akkoç (Co-Advisor)

Assist. Prof. Sibel Çetinel Memiş

Assoc. Prof. Safacan Kölemen

Prof. Dr. Elif Damla Arısan

Date: 29.08.2025

To the strongest person I know, C. Ezgi Güneş

ABSTRACT

Development of systems to produce antibodies to target tumor-stroma crosstalk

Ömrüm Naz Nalkıran

Master of Science in Cellular and Molecular Medicine

August 29, 2025

Cancer cells can program their tumor microenvironment (TME) in a manner that facilitates their adaptation, thereby influencing cancer survival, progression, and metastasis. In this context, it is crucial to elucidate the stroma components and their roles in various cancer types, as well as to investigate their potential applications in diagnosis, treatment, and follow-up. Previously, we demonstrated that cancer-derived secreted factors, cytokines, alter tumor fate through regulating stromal autophagy, cancer-stroma signaling. This thesis aims to develop systems for producing antibody-based drugs that target cytokines in the tumor microenvironment. To achieve this, we developed systems to produce recombinant cytokines and established a mouse single-chain variable fragment (scFv) library. To obtain these, we first cloned cDNA of cytokines into different IPTG-inducible, lac-promoter-containing vectors, including pGEX4T2 and pGEX4T1-3xFLAG. We validated our positive clones and further optimized the protocols to produce recombinant GST- and GST-FLAG-tagged cytokines using *BL21* E. coli cells. In the second part, we focus on optimizing protocols and establishing recombinant scFv antibodies through phage display technology. Hence, we first determined the sequences of the antibody variable light (VL) and variable heavy (VH) chains. To establish a diverse scFv antibody library, we designed at least 36 oligos to produce VL and VH fragments. Fragments were further combined by SOE-PCR (splicing by overlap extension) and cloned into the pCANTAB-5E phage display plasmid for further phage display studies against recombinant cytokines. Overall, we established systems for producing recombinant cytokines and recombinant scFv antibodies. This study could lead to the discovery of new, specific, and drug-

potential antibodies that target specific cytokines in the tumor stroma context, potentially serving as a new cancer therapeutic.

Keywords: Cytokines, scFv, antibody drugs, tumor stroma

ÖZETÇE

Tümör-stroma etkileşimini hedef alan antikorlar üretmek için sistemlerin geliştirilmesi

Ömrüm Naz Nalkıran

Hücresel ve Moleküler Tıp, Yüksek Lisans

29 Ağustos, 2015

Kanser hücreleri, tümör mikroçevrelerini (TME) adaptasyonlarını kolaylaştıracak şekilde programlayabilir ve böylece kanser sağ kalımını, ilerlemesini ve metastazını etkileyebilir. Bu bağlamda, stroma bileşenlerini ve çeşitli kanser türlerindeki rollerini açıklamak ve tanı, tedavi ve takipteki potansiyel uygulamalarını araştırmak çok önemlidir. Daha önce, kanser kaynaklı salgılanan faktörlerin, sitokinlerin, stromal otofajiyi ve kanser-stroma sinyalleşmesini düzenleyerek tümör kaderini değiştirdiğini gösterilmiştir. Bu tez, tümör mikroçevresindeki sitokinleri hedef alan antikor bazlı ilaçlar üretmek için sistemler geliştirmeyi amaçlamaktadır. Bunu başarmak için, rekombinant sitokinler üretmek için sistemler geliştirdik ve bir fare tek zincirli değişken fragman (scFv) kütüphanesi oluşturduk. Bunları elde etmek için öncelikle sitokinlerin cDNA'sını pGEX4T2 ve pGEX4T1-3xFLAG dahil olmak üzere farklı IPTG ile indüklenebilir, lac-promotör içeren vektörlere klonladık. Pozitif klonlarımızı doğruladık ve BL21 E. coli hücreleri kullanarak rekombinant GST ve GST-FLAG etiketli sitokinler üretmek için protokolleri daha da optimize ettik. İkinci bölümde, protokolleri optimize etmeye ve faj görüntüleme teknolojisiyle rekombinant scFv antikorları oluşturmaya odaklanıyoruz. Bu nedenle, öncelikle antikor değişken hafif (VL) ve değişken ağır (VH) zincirlerinin dizilerini belirledik. Çeşitli bir scFv antikor kütüphanesi oluşturmak için, VL ve VH fragmanları üretmek üzere en az 36 oligo tasarladık. Fragmanlar, SOE-PCR (örtüşme uzatma yoluyla ekleme) ile daha da birleştirildi ve rekombinant sitokinlere karşı daha ileri faj görüntüleme çalışmaları için pCANTAB-5E faj görüntüleme plazmidine klonlandı. Genel olarak, rekombinant sitokinler ve rekombinant scFv antikorları üretmek için sistemler oluşturduk. Bu çalışma, tümör stromasında spesifik

sitokinleri hedef alan yeni, spesifik ve ilaç potansiyeline sahip antikorların keşfine yol açabilir ve potansiyel olarak yeni bir kanser tedavisi olarak kullanılabilir.

Anahtar kelimeler: Sitokinler, scFv, antikor ilaçlar, tümör stroma

AKNOWLEDGEMENTS

I sincerely thank everyone who helped me complete my master's degree in Cellular and Molecular Medicine.

First and foremost, I would like to thank my supervisor, Prof. Dr Devrim Gözüaçık, for their guidance, expertise, and support throughout this journey. His invaluable insights have been instrumental in guiding my research and academic growth. Furthermore, I would express my gratitude to my co-advisor, Dr. Yunus Akkoç. This thesis wouldn't be complete without his guidance, support and patience. I learned a lot about doing science with him during this process. I thank him for always looking at the bright side of every experiment I conducted, even when I thought it wasn't very good, and for his endless patience; I never felt judged. His perspective on science has helped me become a better scientist throughout my studies. I learned something new from him every day. Doing science is challenging, especially when you're just starting. But I'm deeply grateful for the scientific and emotional support he provided me throughout my master's thesis journey, facing these challenges. Moreover, I would like to thank my jury members, Assist. Prof. Sibel Çetinel Memiş and Assoc. Prof. Safacan Kölemen and Prof. Dr. Elif Damla Arısan for their guidance and contributions to my thesis.

I extend my heartfelt thanks to all the members of the Gözüaçık Laboratory. The nature of our work means we work very long hours in the lab. It can quickly become unbearable if you don't work with the right people. But I believe I've found the right people. I've never felt lonely working in this lab, even when I was at my lowest and most anxious to quit. Even when I was working late into the night, someone was always there, either working alongside me or waiting for me to finish. I want to thank everyone at the Gözüaçık Lab, who made me feel like family with countless lunch orders, dance breaks, birthday cakes, gossip between experiments, and scientific chats about our projects.

I want to express my love for my mother and father. Their support is the reason I confidently chose this career path. They have supported me throughout my life, always by my side and showing their endless love and trust. Also, I want to thank my friends, who have been with me since high school and who showed up to every presentation and graduation of mine. They always supported me, gave me joy when I was sad, and challenged me with interesting scientific questions.

Finally, I want to thank to KUTTAM and TÜBİTAK for their financial and technical support for my research.

Table of Contents

LIST OF TABLES

TABLE OF FIGURES

ABBREVIATIONS

CTF1 Cardiotrophin-1

JAK Janus tyrosine kinase

STAT Signal transducers and activators of transcription

ERK Extracellular signal-regulated kinase

ECM Extracellular matrix

MMP Matrix metalloproteinase

TNF Tumor Necrosis Factor

TGF-ß Transforming growth factor beta

SOE Splicing by Overlap Extension

scFv Single Chain Variable Fragment

AMPK AMP-activated protein kinase

PI3K Phosphoinositide 3-kinases

IL-6 Interleukin 6

LIFR Leukemia Inhibitory Receptor

OSM Oncostatin M

Chapter I:

INTRODUCTION

1.1 CTF1 protein

Cardiotrophin-1 is an IL-6 family cytokine with 21.5 kilodaltons in size and located at position 16p11.1-16p11.2 on the human chromosome. The CTF1 protein is called "Cardiotrophin-1" because it increases hypertrophy in heart muscle cells under *in vitro* conditions. Because CTF1 is an IL-6 family cytokine, like most IL-6 family cytokines, it binds gp130 and LIFR receptor. Even though some studies indicate that CTF1 has a third receptor component. CTF1 cytokine activates the JAK/STAT signaling pathway by interacting with GP130 and LIFR receptors.(J. Liu et al., 2008) However, in addition to these two receptors, there are publications in the literature that mention the existence of a third receptor, and that this receptor is likely to be a glycosylphosphatidylinositol (GPI)-anchored protein, in experiments using PI-PLC (phosphatidylinositol-specific phospholipase C). (Pennica, Arce, et al., 1996)

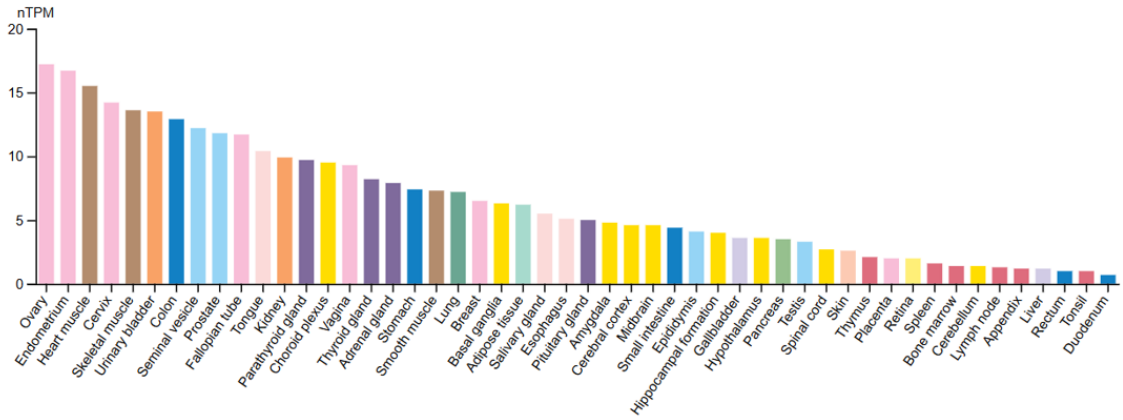

Figure 1.1 CTF1 RNA expression data according to tissues. Each color code represents certain tissue groups. Most CTF1 RNA expression is in ovary, endometrium and heart muscle. (Human Protein Atlas)

Human and mouse CTF1 bind both human LIFR and mouse LIFR receptor. This cross-reactivity can occur due to some conserved regions (FXXK motif) also contained in

CTF1 orthologs and needed for LIFR binding. The FXXK motif is highly conserved in all CTF1 sequences (across seven vertebrate classes) and crucial in LIFR binding. CTF1 sequences are present in Amphibia, Mammals, Reptiles, and Sarcopterygii (infraclass Coelacanthimorpha, now categorised as a clade). CTF1 is the only IL6 family protein with a sequence in the Sarcopterygii (salamanders) class. Since the CTF1 gene is located on chromosome 16, unlike LIF and OSM on chromosome 11, it may have a

Neighbour	Description	Correlation	Cluster
EFEMP2	EGF containing fibulin extracellular matrix protein 2	0.9140	62
ARMCX1	Armadillo repeat containing X-linked 1	0.8860	64
MAGED2	MAGE family member D2	0.8667	62
ME3	Malic enzyme 3	0.8351	62
CBY1	Chibby family member 1, beta catenin antagonist	0.8298	62
RAMP1	Receptor activity modifying protein 1	0.8105	64
KLHDC8B	Kelch domain containing 8B	0.8070	41
GLT8D2	Glycosyltransferase 8 domain containing 2	0.8070	62
GSTM2	Glutathione S-transferase mu 2	0.7965	66
EDA2R	Ectodysplasin A2 receptor	0.7947	62
OMD	Osteomodulin	0.7877	62
TCEAL4	Transcription elongation factor A like 4	0.7860	64
WTIP	WT1 interacting protein	0.7807	62
PDZRN3	PDZ domain containing ring finger 3	0.7807	41
SMOC2	SPARC related modular calcium binding 2	0.7807	62

Figure 1.1.1 CTF1 and associated genes. According to expression clustering and correlation data from the Human Protein Atlas, CTF1 is part of cluster 62, which is associated with connective tissue—ECM organization and has a confidence score of 0.74 (389 genes in the cluster). Data is provided from the Human Protein Atlas.
different evolutionary origin. (Costa et al., 2022)

Some transcription factors possibly bind to the binding sites of the CTF1 gene. There are two CAAT boxes in the positions of -1043 and -1076. Notably, the broadly transcriptional activator C/EBP beta binds to position -1076. C/EBP beta is a well-known transcriptional activator and stimulates IL-6 expression *in vivo* and *in vitro* conditions. In position -934, a putative STAT site explains that CTF1 is a STAT3 activator. In position -582, the Sp1 site appears. Sp1 is a DNA-binding protein that binds promoter regions, especially GC-box elements. Additionally, nine AP-2 binding sites at positions -716, -438, -266, -251, -248, -207, -181, -73, and -72 are present in the CTF1 gene. AP-2 is a transcription factor family associated with gene expression regulation in early embryonic development. (Hilger-Eversheim et al., 2000) There is also cAMP response element (CRE) in position -639. CREs control diverse transcriptional processes and some growth control genes, such as FOS have CRE

regions in the gene. Moreover, the CTF1 gene contains a GATA-binding factor region in position -484. GATA-binding proteins are essential transcription factors that control gene expression and differentiation in different cell types. These family member proteins target and bind the GATA motif, which is usually located in the promoter site of the gene. Many studies suggested that this factor may regulate genes for myocardial differentiation, including troponin C, cardiac alpha-myosin heavy chain, and brain type natriuretic factor (BNP). (Erdmann et al., 1998) Human CTF1, like the mouse protein, lacks a typical, hydrophobic, N-terminal amino acid sequence that would indicate a secretion signal. Human CTF1 contains two cysteine residues and no potential N-linked glycosylation sites, but the mouse protein contains one cysteine and one potential glycosylation site. The 3'untranslated regions of both the human and mouse clones have an Alu or B1-like repeat sequence. (Pennica, Swanson, et al., 1996)

1.2 Signaling pathway of the CTF1 protein

The signaling of the CTF1 protein begins with gp130/LIFR. Gp130 and LIFR phosphorylate, thus enabling the phosphorylation of Jak1 and Jak2. Then, it migrates to the nucleus by forming STAT1 or STAT3 homodimers and stimulates the activity of the related genes. It is known that CTF1 protein also affects Akt/BAD, MAPK signalling pathways, thus stimulating cardiac fibroblasts and causing hypertrophy. There are also studies showing that CTF1 increases IL-6 mRNA and protein expression in monocytes, depending on time and dose (100 ng/ul), thus STAT3 phosphorylation occurs. (Fritzenwanger et al., 2007)

As mentioned before, CTF1's primary role is contributing to cardiac hypertrophy. CTF1 phosphorylates STAT3 via the JAK/STAT signaling pathway and increases the expression of genes associated with hypertrophy. These genes include biomarkers to detect hypertrophy, such as atrial natriuretic peptide (ANP). The expression of hypertrophy-associated proteins decreased by 88% in the application of parthenolide (STAT inhibitor), proving that the STAT3 signaling pathway stimulated by CTF1 is one of the main pathways for hypertrophic effects.(Z. Tian et al., 2004)

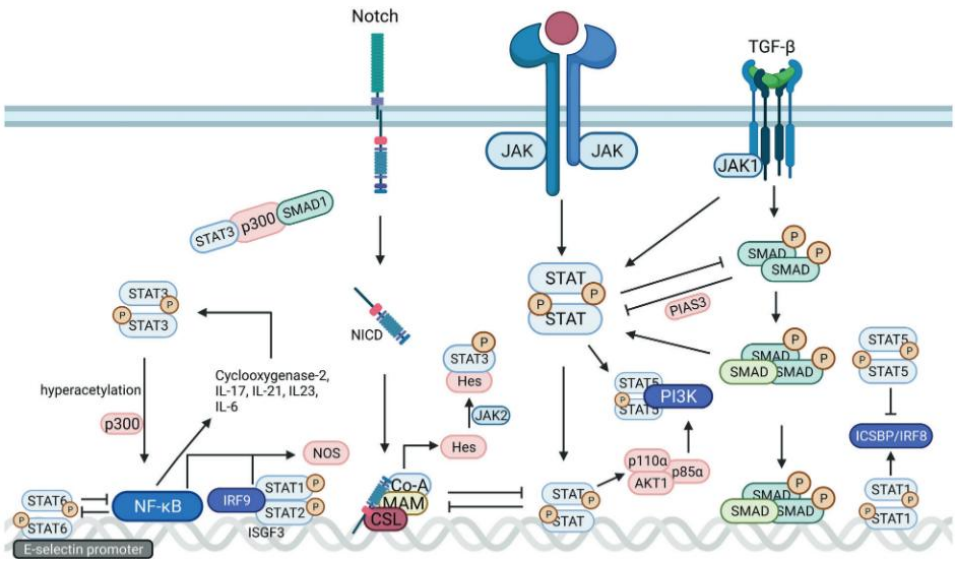

Figure 1.2 The signalling crosstalk between JAK-STAT and other pathways. (Hu et al. 2021) (Copyright © 2021 Xiaoyi Hu et al. This is an open-access article distributed under the Creative Commons Attribution License, which permits unrestricted use, distribution, and reproduction in any medium, provided the original work is properly cited.

Additionally, it has been discovered that CTF1 may have a role in the ADMA/DDAH signalling pathway. The ADMA/DDAH signaling pathway is a crucial pathway that regulates NO synthesis. This pathway is vital for endothelial function, atherosclerosis, inflammation, oxidative stress and cardiovascular disease. In this pathway, ADMA inhibits NO synthesis, and DDAH suppresses ADMA function, thus NO can be synthesized. (Vallance et al., 1992) It has been discovered that CTF1 increases cell proliferation, but when cells are treated with ADMA in addition to CTF1, cell proliferation, migration and tube formation decrease. CTF1 also increases eNOS levels, a type of NOS usually found in endothelial cells, but when ADMA is applied, this effect is diminished. Moreover, levels of DDAH1 and DDAH2 (two isoforms of DDAH enzyme) are increased only in the CTF1 group, but when ADMA is treated, DDAH' levels decrease. Finally, NOS activity is reduced in ADMA + CTF1 group at 48 hours. These results indicate that CTF1 could be associated with ADMA/DDAH signaling pathway activation. (Zheng et al., 2015) Another study conducted with CTF1 induction and CIS (cytokine inducible SH2 protein) family proteins JAB/SOCS-1/SSI-1 and CIS3/SOCS-3/SSI-3. JAB and CIS3 proteins act as inhibitors of CTF1 via the JAK-STAT signalling pathway. Therefore, with suppressing CTF1, they can have a stabiliser role in the cardiovascular system. (Hamanaka et al., 2001) Finally, Akkoç et al. showed

that CTF1 phosphorylated and caused the nuclear transportation of p-STAT3. This activated several essential autophagy proteins, like the LC3-1 to LC3-2 shift, SQSTM1 and NBR1 accumulation, and ULK1 and AMPK activation in fibroblast cells. (Akkoc et al., 2023)

1.3 CTF1s role in diseases

1.3.1 Cardiovascular disease

1.3.1.1 Cardiac hypertrophy

Cardiac muscle cell hypertrophy is one of the heart's most essential adaptive reactions and is a common hallmark of many human cardiac disorders. Following long-term hypertension, myocardial injury, or other demands for increased cardiac output, the heart adapts by activating a hypertrophic response, defined by myocardial cell enlargement and the accumulation of sarcomeric proteins in the absence of cell division. Although this process is initially compensatory, there may be a pathological shift in which the myocardium becomes irreversibly enlarged and dilated, resulting in the development of overt cardiac muscle failure. The discovery of the mechanisms that mediate the start of these multiple stages of ventricular hypertrophy and failure remains an essential goal in cardiac biology and medicine. (Schirone et al., 2017) 1995 D.Pennica discovered that Cardiotrophin-1 induces cardiac muscle cell hypertrophy, judged by cell enlargement, atrial natriuretic peptide (ANP) induction, and myosin light chain (MLC) organisation using hypertrophy assay in vitro studies. (Pennica et al., 1995)

Cardiotrophin-1, unlike other cardiac cell hypertrophy stimulators (exp., alpha-adrenergic stimulation), causes hypertrophy by increasing cell length and serial arrangement of sarcomeres without significant change in cell width. CTF1 also upregulates the atrial natriuretic factor (ANF) gene but does not alter skeletal alpha-actin and myosin light chain-2v expression. Alpha-adrenergic stimulation exhibits a different gene expression pattern. In addition, alpha-adrenergic stimulation works through regulatory elements within the proximal 5’-flanking region of the ANF gene, whereas CTF1 acts through regulatory elements outside this region. (Wollert et al., 1996) The hypertrophic impact of CTF1 was mediated mainly by STAT3, independent of PI3-K, and was negatively controlled by ERK1/2 via reducing STAT3 phosphorylation. The interplay of STAT3 and ERK1/2 in CTF1-induced signaling

promotes cardiac hypertrophy. (Z. Tian et al., 2004) Research was conducted on cardiomyocyte hypertrophy controlled by gp130 using neonatal ventricular myocytes. CTF1 increased cell viability and ANP expression with MEK1 inhibitor PD098059 and PKC inhibitor calphostin C. These results showed that CTF1 can regulate ANP transcription in hypertrophic ventricular myocytes in a time and dose-dependent manner, and the p42/p44 MAPK signalling pathway may play a role in this regulation. (Dong et al., 2014) In another study, CTF1 levels and STAT3 activation were measured in babies with congenital heart defects and their relationship with left ventricular wall thickening due to hypertrophy was examined. They discovered that patients with congenital heart disease have greater CTF1 expression, linked to JAK/STAT pathway activation and increased cardiac troponin I degradation, a biomarker for cardiac defects. (Heying et al., 2014) Moreover, 124 patients with hypertrophic cardiomyopathy (HCM) had plasma CTF1 levels examined. The relationship between these results and the development of left ventricular wall thickness (LVH) due to hypertrophy was investigated. The results showed that HCM patients had higher CTF1 levels than controls. A correlation was observed between CTF1 and maximal left ventricular wall thickness. In addition, higher CTF1 was seen in advanced LVH patients compared to moderate and mild LVH patients.(Monserrat et al., 2011) All these results reveal the role of CTF1 protein in hypertrophy and its importance as a biomarker in cardiomyopathic hypertrophy.

1.3.1.2 Hypertension

Hypertension is a common cardiovascular disorder characterised by consistently high blood pressure. It is a significant risk factor for a variety of cardiovascular disorders, including heart failure, stroke, and renal disease. (Harrison et al., 2021) The most common cardiac disorder In hypertensive heart disease, the key feature is left ventricular hypertrophy (LVH), which is an important biomarker of preclinical cardiovascular diseases. One of the most critical proteins to induce LVH is the CTF1 protein. (González et al., 2005) In 1996, Iskikawa revealed increased CTF1 mRNA in 12-week spontaneous hypertensive rats (SHR) ventricles compared to the control (Wistar) rats. (Ishikawa et al., 1996) In cardiomyocytes isolated from normotensive (Wistar) and spontaneously hypertensive rats (SHR), CTF1 increased *c-fos* and ANP levels in both cardiomyocyte types. Also, CTF1 increased cell length in Wistar cells, but did not change transverse diameter or cell depth. Conversely, in SHR cells, the cell

length, width, and depth all increased. Additionally, levels of total and phosphorylated myosin light chain 2v (MLC-2v) and skeletal α-actin were elevated. CTF1 treatment triggered activation of PI3K, Akt, p42/44, STAT3, and ERK5 signalling pathways in both SHR and Wistar cells. Basal angiotensinogen mRNA expression was higher in SHR cells than in Wistar cells, but CTF1 increased this expression in Wistar cells. Applying the angiotensin II receptor AT1 inhibitor losartan significantly reduced the CTF1 effects observed in SHR cells. In conclusion, based on the effect observed in cells from hypertensive mice, the hypertensive phenotype of these cells may enhance the hypertrophic effect of CTF1, most likely by increasing angiotensinogen expression. (N. López et al., 2006) Another study on Angiotensin II investigated the contribution of Angiotensin II (Ang II) and aldosterone to hypertension, oxidative stress and cardiovascular damage. Ang II infusion increased cardiac CTF1 protein expression by 42%, while ARB and combination therapy completely prevented the increase in cardiac CTF1. This suggests that blocking the AT1 receptor suppresses the effects on CTF1. Eplerenone treatment reduced cardiac CTF1 levels by 25% compared to Ang II, but did not completely restore them to normal levels. Ang II infusion increased plasma CTF1 levels by 27%. ARB treatment reduced CTF1 levels to 81%, eplerenone treatment reduced CTF1 levels to 88%. Notably, the combination treatment of two drugs reduced CTF1 levels to 84%. These findings suggest that CTF1 levels are regulated by AT1 and MR pathways. These pathways are crucial in the development of hypertension and cardiovascular damage. Suppression of CTF1 may be an important target in treatment strategies to reduce Ang II-induced oxidative stress and cardiovascular damage. (Minas et al., 2015) Furthermore, recent research has demonstrated that some cytokines, such as cardiotrophin-1 (CTF1) and interleukin-2, stimulate NO production, decreasing NO-dependent arterial blood pressure. (Nomura et al., 2003) Researchers examined the hemodynamic effects of CTF1 and heart function and the role of nitric oxide (NO) in this mechanism. The researchers targeted mean arterial pressure (MAP), heart rate (HR), cardiac output, systemic vascular resistance, and ventricular contractility (dP/dt). At the same time, an NO synthase inhibitor, N^{ω}-nitro-L-arginine methyl ester (L-NAME) was used to assess the role of the nitric oxide (NO) system in these effects in rats. As a result, the CTF1 application decreased MAP, systemic vascular resistance, and increased HR and cardiac output. In L-NAME application with CTF1 treatment, the decrease in blood pressure (depressor response) and the increase in heart rate (tachycardic response) caused by CTF1 were significantly reduced, indicating that the

hemodynamic effects of CTF1 are mediated to a significant extent by nitric oxide. (Jin et al., 1998) In a study investigating the genetic background of left ventricular hypertrophy and essential hypertension, 900 individuals were genotyped for the 1742(C/G) polymorphism. Serum CTF1 levels were screened in 681 individuals, and left ventricular parameters were screened in 297 individuals. The GG genotype for the 1742(C/G) polymorphism in essential hypertension, the prevalence of the GG genotype was shown to be lower (8.4% in normotensive individuals, 4.9% in hypertensive patients, when compared to CC/CG individuals). The GG genotype was lower in patients with left ventricular hypertrophy (LVH). GG people showed lower serum CTF1 levels and a lower left ventricular mass index. Multivariate analysis revealed that the 1742(C/G) polymorphism could predict left ventricular mass index and serum CTF1 levels, indicating that this genetic variation is strongly connected with these parameters. The 1742(C/G) polymorphism is linked to LVH in essential hypertension, and the GG genotype found in this study may have a protective impact. (Robador et al., 2010) Lastly, studies revealed that patients who have hypertension with LVH and suspiciously high LVH levels have higher CTF1 levels, especially with patients with systolic function disruption. (Ravassa et al., 2013) Another study revealed that CTF1 can be a biomarker in hypertensive patients. A study was conducted with 31 normotensive, 111 essential hypertension patients (with or without LVH). The hypertensive group's CTF1 level is much higher than the normotensive group's. Also, it has been found to directly correlate with LVH index and CTF1 level. All of these results prove that CTF1 can be a biomarker in hypertension and hypertensive heart diseases. (B. López et al., 2005)

1.3.1.3 Heart Failure

Myocardial infarction (MI) is known as an infarction in the coronary arteries due to the interruption of blood flow to the heart for certain reasons, and this is a common problem in all countries of the world. Suppose the rupture in the MI infarction is relatively large. In that case, these patients develop congestive heart failure rapidly, and at the same time, this condition evolves into chronic heart failure, and patients have a poor prognosis. Cardiac recovery after MI depends on the ventricular architecture of the non-MI portions of the heart, time, and various factors. Cardiac recovery after MI depends on the ventricular architecture of the non-MI portions of the heart, time, and several factors. This process is controlled by trophic factors and chemokines, led by myofibroblast cells. Therefore, it is important to discover new molecules that will

support heart regeneration in MI-based heart diseases and identify biomarkers to diagnose the disease early. CTF1 protein was discovered to be related to MI in various studies. A blood proteome study of 618,717 European participants found that high levels of CTF1 in the blood were associated with MI. (Wang et al., 2024) A chronic heart failure (CHF) study showed that CTF1 gene expression increased in CHF. Left ventricular hypertrophy, which is known to be associated with diseases such as heart failure and hypertension, increased in the experimental groups in CHF, and this increase was observed to be correlated with the increase in CTF1 levels. (Jougasaki et al., 2000) At the same time, S. Sasayama et al. collected infarcted rat tissues after coronary artery ligation on days 1, 3, 7, 14, 28 and 65 to understand the role of CTF1 and gp130 signalling during ventricular remodelling after myocardial infarction. Because CTF1 stimulates sarcomeric units in cardiomyocytes using the gp130 signalling pathway, it causes myocardial cell hypertrophy. Infarction intervals of 39.8-50.3% were observed in infarcted coronary artery ligation tissues. All groups had higher CTF1 and gp130 mRNA and protein levels than the control. (Aoyama et al., 2000) In another study on CTF1 and the closure of infarcts and heart remodelling after MI, it was investigated whether mechanical stretch resulting from MI activates the Janus kinase (JAK) / signal transducers and activators of transcription (STAT) pathway in cardiomyocytes. It has also been discovered that calcium (Ca^{2+}) levels are important in this activation. (Pan et al., 1999) Moreover, in another study designed to examine how Cardiotrophin-1 (CTF1) and its receptor complex, the gp130/leukaemia inhibitory factor receptor system, patients with end-stage heart failure due to ischemic cardiomyopathy and dilated cardiomyopathy were used as the experimental group. CTF1 mRNA and protein levels increased by 142% and 68% in the left ventricles of individuals with heart failure, and immunohistochemistry confirmed that this increase occurred specifically in cardiac myocytes. gp130 expression increased by 91%, while the protein level decreased by 34%. At the same time, contrary to previous studies, the phosphorylated STAT3/ total STAT3 ratio was similar in patients with heart failure and the control group. The researchers think in the article that while CTF1 levels increase, the decrease in gp130 protein levels may prevent excessive gp130 signal activation, and this system has developed a mechanism to maintain balance in heart failure. This mechanism can protect the heart from further damage. (Zolk et al., 2002) There are also publications mentioning that CTF1 can also be used in treating patients who have had an MI before. Although treating the wound opened after MI with cell transplantation is a method with

great potential, the rate of transplanted cells settling in the wound tissue is quite low. The study aimed to determine cytokines that could improve mesenchymal stromal cells (MSCs) adhesion to the heart. To understand that, cytokine library screening was performed, and the cytokine library was transferred to MSCs produced from bone marrow. Later, these MSCs were injected into the hearts of normal and MI-experienced mice. Three weeks later, DNA sequencing was performed on the cells that adhered to the heart to determine which cytokines increased the survival of MSCs. The most potent effective molecule was found to be CTF1, and it was observed that MSCs pre-treated with CTF1 preserved heart function and reduced the size of the infarct area, and these cells continued to exist in the heart for at least two months after injection. It has also been reported that this protective effect of CTF1 occurs by increasing the adhesive properties of MSCs via focal adhesion kinase (FAK) and focal adhesion complex via STAT3. (Bortolotti et al., 2017) Finally, publications show that CTF1 can be used as a biomarker to diagnose MI-based diseases. CTF1 levels were significantly higher in patients who died or had heart failure compared to survivors. NT-proBNP levels were significantly higher in this group of patients. As a result of ROC (receiver operating characteristic) curve analysis found that the combined use provided better predictive power than using both markers separately. In other words, this study emphasises the clinical importance of CTF1 and shows that using both markers together may provide superiority in diagnosis and risk assessment. (Khan et al., 2006)

1.3.1.4 CTF1 and Cardiac Fibrosis

Cardiac fibrosis is a critical problem correlated with various heart diseases, especially leading to heart failure due to disruption of the contraction cycle of the heart. Cardiac fibrosis is characterised by accumulating extracellular matrix components (ECM). When injury occurs, cardiac fibroblasts transform into myofibroblasts and contribute to cardiac fibrosis. Understanding the mechanisms behind this phenomenon is crucial to developing new strategies for detecting and treating cardiac fibrosis. (Martínez-Martínez et al., 2017) The hardening of vascular tissue and fibrosis characterise arterial fibrosis. This event leads to arteriosclerosis, which can lead to other cardiovascular diseases as people age. The CTF1 molecule is thought to be a protein that plays a role in affecting both cardiac fibrosis and arterial fibrosis. (López-Andrés et al., 2013) Previous studies have shown that the CTF1 protein may have a role in the aldosterone-dependent mechanism. Thus, mRNA and protein levels of CTF1 increase depending on time and

dose under the influence of Aldo, and eventually this event increases hypertrophy in cardiomyocytes. (López-Andrés et al., 2008) In a study examining the effects of molecules that trigger heart fibrosis (Aldosterone, Galectin-3 and Cardiotrophin-1) on human heart fibroblasts, Aldo, Gal-3 and CTF1 were applied to human heart fibroblasts, respectively, and the changes in protein were examined by proteomic analysis. In the Aldo group, 30 proteins, in the Gal-3 group, 17 proteins, and in the CTF1 group, 89 proteins are changed. The "Reticulocalbin (RCN)" family stands out among the proteins these three molecules interact with. After applying recombinant RCN-3 protein, collagen production is decreased due to activation of the AKT protein. Recombinant RCN-3 prevented not only Aldo, Gal-3 and CTF1-induced fibrosis but also Angiotensin II-induced fibrosis. Researchers stated that RCN-3 may be a novel negative regulator that suppresses cardiac fibrosis, and Aldo, Gal-3 and CTF1 may increase cardiac fibrosis by decreasing RCN-3 levels. (Martínez-Martínez et al., 2017) In another study conducted to treat cardiac fibrosis, the antifibrotic effects of Astragaloside IV (AsIV) on isoprenaline (ISO)-induced cardiac fibrosis and elucidate whether this effect is associated with the ROS and CTF1 relationship. It was observed that CTF1 levels increased in cardiac fibroblasts stimulated with ISO, and when CTF1 was knocked out, fibroblast proliferation decreased, and collagen I production also decreased. Regarding the relationship between ROS and CTF1, it was stated that ROS production was associated with overexpression of CTF1, but the opposite was not true. This study shows that the antifibrotic effect of AsIV is related to ROS and CTF1 and may be a new therapeutic agent that can be used to reduce cardiac fibrosis. (Jia et al., 2017) At the same time, CTF1 null mice have lower vascular wall thickness, arterial fibrosis, apoptosis levels, senescence markers, telomere-associated proteins, DNA repair proteins, and antioxidant enzyme activities. It is also known in the literature that CTF1 null mice have a 5-month longer lifespan. (López-Andrés et al., 2013) Finally, when the relationship between circulating fibrosis-related biomarkers and cardiac fibrosis assessed by magnetic resonance (MRI) in patients with dilated cardiomyopathy (DCM) was investigated, circulating fibrosis markers (Cardiotrophin-1, GDF-15, PDGF, etc.) were not found to be associated with fibrosis measured by MRI in DCM patients. In contrast, cardiac-specific biomarkers such as NT-proBNP and hs-TnT were related to the presence of fibrosis. Circulating fibrosis markers do not appear to help diagnose and monitor fibrosis in DCM patients. These results suggest that using the CTF1 protein as a biomarker in cardiac fibrosis is currently unlikely. (Rubiś et al., 2021)

1.4 CTF1 and embryonic development

1.4.1 In bone development

Bone remodelling under normal conditions or in response to bone fracture, inflammation, or trauma depends on the balance and activity between osteoblast and osteoclast cells, which absorb mineralised bone matrix. The activation, reabsorption, proper functioning and differentiation of these cells depend on various cytokines, hormones and growth factors. Multiple factors affect bone absorption, like parathyroid hormone (PTH), 1,25-dihydroxy vitamin D-3 (1,25-d3) and prostaglandin E2 (PGE2), or cytokines like Interleukin-α, even tumor necrosis factor α and β (TNF-α, TNF-β). Studies revealed that mOSM, LIF and CTF1 were strongly increased dose-dependently by osteoclast formation and lytic action by D. Pennica. These factors caused osteoclasts to create larger and more resorptive pits in the bone. Dexamethasone (DEX, corticosteroid) synergistically potentiates the osteoclast-enhancing effects of these factors. These results indicate that these cytokines may play an important role in osteoporosis caused by high levels of corticosteroids. (Richards et al., 2000) It is known that CTF1 is an osteoblastic cytokine that is secreted from osteoclasts. (Watt et al., 2018) In CTF1 $^{-/-}$ newborn mice, low bone mass, decreased osteoblast numbers, increased osteoclast numbers, and excess cartilage residue in the bone were found. These discoveries are an indication that bone destruction is not occurring properly. In bone marrow cell cultures from CTF1 $^{-/-}$ mice, it was found that larger osteoclasts were produced compared to normal mice, but poor mineralisation occurred. In CTF1 $^{-/-}$ mice, although the osteoblast deficiency disappeared as they aged, bone destruction was still observed to be uneven. (Walker et al., 2008) Another factor that plays a role in bone absorption by increasing osteoclast formation is HIF-1α. Osteoclasts migrate from the high-oxygen bone marrow to the low-oxygen bone lesions. The effect of HIF-1α was investigated after mandibular osteotomy (jaw bone incision) using an osteoclast-specific HIF-1α-conditional knockout mouse model, and primary osteoclasts were used to examine the expression of HIF-1α and CTF1 at mRNA and protein levels. The osteogenesis capacity of BMMSCs (bone marrow mesenchymal stem cells) was tested with the conditional culture medium obtained from HIF-1α knockout osteoclasts. As a result, HIF-1α increased osteoclastogenesis (formation of new osteoclasts) and bone resorption. In osteoclast-specific HIF-1α-conditional knockout mice, bone repair was delayed relative to normal mice. HIF-1α-knockout osteoclasts suppressed bone

resorption and reduced CTF1 expression. It was also observed that HIF-1α and CTF1 expression were correlated, and CTF1 gene expression or protein levels were decreased in the HIF-1α conditioned knockout group. However, it was stated that recombinant CTF1 application stimulated osteogenic differentiation in BMSCs. These results prove that HIF-1α plays a critical role in bone resorption by increasing osteoclast formation, and this process supports the bone healing process by secreting CTF1. (Y. Tian et al., 2022)

1.4.2 In neuron development

Motor neurons in the development process need trophic factors from their target tissue, the muscle tissue, to complete this process healthily. In 2001, D. Pennica et al. discovered that CTF1 is a crucial neurotrophic factor for motor neuron survival and was first identified as an essential neurotrophic factor secreted by skeletal muscles. In CTF1-deficient (CTF1 $^{-/-}$) mice, motor neuron death was significantly increased in the spinal cord and brainstem between embryonic day 14 (E14) and the first postnatal week. However, no additional motor neuron loss was observed in the postnatal period. (Oppenheim et al., 2001) It is also found that in IGR-mediated (ionotropic glutamate receptors) cell death, CTF1 acts as a neurotrophic factor to support survival of motor neurons at a basal level, but not against ecotoxicity. (Fryer et al., 2000) Various mouse models have been established to examine CTF1 regulation of motor neuron survival during embryonic development. Using these models, it has been discovered that fewer astrocytes were found in the cortex of CTF1 $^{-/-}$ neonatal mice. That means newly born neurons produce CTF1, which instructs multipotent cortical precursors to generate astrocytes, thereby ensuring that gliogenesis does not occur until complete neurogenesis. In double knock-out LIFR and CTF1 mice models, the development of PSNs (preganglionic sympathetic neurons) and their effects on the adrenal medulla were investigated. In LIFR $^{-/-}$ and CTF1 $^{-/-}$ mice, the number of PSNs decreased by approximately 20%. This loss was more pronounced in PSNs projecting to the adrenal medulla, reaching 55%. (Oberle et al., 2006)

1.5 Protective role of Cardiotrophin-1

1.5.1 In cardiomyocytes

The survival of cardiac muscle cells is essential for preserving the heart's normal condition and cardiac development. The survival of cardiac muscle cells is vital to

preserving the heart's normal condition and cardiac development. Since adult cardiac muscle cells are terminally differentiated, they can no longer proliferate. Unlike skeletal muscle, the myocardium lacks satellite heart muscle cells, and irreparable heart damage causes scarring and ultimately declines overall cardiac function. The adult myocardium initiates an adaptive hypertrophic response to mechanical stimuli and hemodynamic stress. This response is typified by an increase in myocardial cell size without a corresponding rise in myocyte number. CTF1 is a well-known hypertrophic inducer protein highly expressed in both human and mouse heart tissue. In the literature, it has been stated that CTF1 has an anti-apoptotic effect both in adult and neonatal rat cardiomyocytes. Anti-apoptotic effect of CTF1 occurs via p44/p42 MAPK signalling pathway. (Latchman, 1999) When MEK inhibitor is used, the protective effect of CTF1 in myocardial cells is diminished. Additionally, CTF1 activates STAT3 via JAK/STAT pathway, but the protective role of CTF1 is mediated through the p44/p42 MAPK pathway, not the JAK/STAT pathway. (Sheng et al., 1997) Moreover, CTF1 also increases phosphorylation of AKT, which eventually activates the PI3K signalling pathway, increasing the activation of the pro-apoptotic factor BAD. The application of PI3K inhibitor LY2940042 and Wortmannin reduced these effects. (Kuwahara et al., 2000) these results suggest that CTF1 promotes cell survival via PI3K and p44/p42 MAPK pathway. Furthermore, CTF1 increases heat-shock protein 70 (hsp70) and heat shock 90 (hsp90) expression in neonatal cardiomyocytes for protecting cells from stress (Stephanou et al., 1998). Still, this increase is not at the mRNA or RNA synthesis level, perhaps due to post-transcriptional modifications. (Railson et al., 2001) In disease models, CTF1 has a cardiomyocyte protective role in both *in vivo* and *in vitro* ischemia models. The cardiomyocyte protective role of CTF1 was inhibited by MAPK inhibitor in both conditions: ischemia/reoxygenation application, then CTF1 treatment or ischemia/reoxygenation application after CTF1 treatment. (B. Brar, 2001; Liao, 2002) CTF1 also activates PI3K, p44/p42 MAPK pathway under ischemia conditions, decreasing apoptosis or total cell death. (B. K. Brar et al., 2001; N. López et al., 2005) In another disease model, which is the myocardial infarction model, it has been observed that CTF1 increases left ventricular pressure and arterial pressure and decreases left ventricular end-diastolic pressure. Also, CTF1 treatment inhibited pro-apoptotic proteins p53, Fas, Bax and increased the expression of Bcl2. (Yin et al., 2004) In Valsatran and Spironolactone treatment, commonly used drugs to treat heart failure, CTF1 protein and mRNA levels are decreased in hypertrophy conditions. (Al-Mazroua

et al., 2013) Additionally, in hypertrophy conditions, CTF1 increases the expression of the GATA4 mRNA and binds to the cardiomyocytes. ERK1/2 negatively regulates this expression. (He-nan et al., 2009) In hypoxia conditions, CTF1 levels are elevated both *in vivo* and *in vitro,* and this increase occurs when HIF-1α transcription factor binds to the CTF1 promoter site. (Robador et al., 2011)

1.5.2 Hepatocytes

The survival of hepatocytes is essential for continuing the liver's normal function and resistance against liver damage. One of the pro-survival molecules for hepatocyte survival is CFT1. CTF1 is highly expressed in the liver and increases liver regeneration via suppressing apoptosis by inhibiting caspase 3, activating phosphorylation of STAT3, ERK1/2 and AKT during serum starvation and TGF-β treatment. The survival rate of rats after subtotal hepatectomy increased 54% when CTF1 was applied as a treatment. (Bustos et al., 2003) Another group of hepatocyte protective molecules are prostaglandins. Prostaglandins protect hepatocytes by increasing the expression of COX2. The rats that received partial hepatectomy and were given COX2 inhibitor NS-398 treatment had downregulation of CTF1 and COX1 levels. After treating hepatocytes with CTF1 and COX2 inhibitor, the expression of COX1, VEGF and prostaglandin was restored to the basal level. Notably, giving CTF1 treatment to the primary hepatocytes isolated from rats receiving partial hepatectomy increased the expression of COX1, COX2 and VEGF. (Beraza et al., 2005) When a double dose of CTF1 was applied to the rats that underwent hepatectomy again with different techniques, liver functions were increased, enlarged the volume of liver remnant, upregulated the expression of von Willebrand factor and increased the number of $BrdU^+$ or Ki-67^+ hepatocytes. Application of CTF1 increased expression of CTF1 nuclear factor-kB (p65), CyclinD1, VEGF, p42/p44 in remnant liver and diseased hepatocytes; however, these effects of CTF1 were blocked by VEGF inhibitor PTK787. (Yang et al., 2008) Hypoxia/reoxygenation (H/R) is one of the stress conditions that induces apoptosis and an increase in reactive oxygen species (ROS) also in the liver. After creating an H/R in vitro model of the primary hepatocytes, CTF1 was applied. CTF1 increased activation of STAT3, which induced Manganese Superoxide Dismutase (Mn-SOD) levels at the mRNA and protein levels. (Terui et al., 2004) After extended ischemia, blood flow is restored, which results in ischemia-reperfusion (I/R) liver injury. Through unclear processes, ischemic preconditioning [IP], a temporary disruption of blood flow, develops tolerance to later persistent ischemia. It has been

discovered that CTF1-null mice are more sensitive to the I/R liver injury. IP decreased transaminase levels significantly and stopped the activation of caspase-3 and c-Jun–NH2-terminal kinase during I/R in normal mice, but not in CTF1-null mice. After CTF1 neutralizing antibody application, the protective effect of IP reduced. Oxidative stress is an important mechanism for IP-induced hepatocyte protection. This mechanism induces CTF1 release from hepatocytes. CTF1 null animals failed to activate STAT3 and provoked marked hypertransaminasemia. (Iñiguez et al., 2006) Another liver injury model was constructed using D-galactosamine in rats to create a fulminant hepatic failure model. In these studies, it has been found that CTF1 treatment increased survival of hepatic rats at 12 and 18th hours. CTF1 treatment decreased shortening of activated clotting time, reduced bilirubin and alanine aminotransferase (ALT) levels in serum. Additionally, CTF1 treatment decreased apoptotic cells through reduced caspase 3, DNA fragmentation and calpain activity but increased p-STAT3, AKT, Ki-67^{+} and calpastatin activity, a calpain inhibitor. Besides, CTF1 treatment increased gp130, CyclinD1 and hsp90 levels. (Herencia et al., 2015; Ho, 2006) Moreover, the genetically engineered endothelial progenitor cells that overexpress CTF1 enhance hepatocyte protection against lethal fulminant hepatitis liver injury. (Fernandez-Ruiz et al., 2011) Furthermore, the study indicates that CTF1-/- mice died faster when Fas agonist Jo-2 was applied at a lethal dose. At sub-lethal doses, CTF1-/- mice had extensive hepatocyte apoptosis and 50% death occurred within the first 24 hours. CTF1-/- and wild-type mice liver transcriptome analysis revealed that 9 genes are associated with cell survival and death. Four of them are downregulated at CTF1-/- mice, which are IGFBP1, Peroxiredoxin3, TNFR1 and calpastatin. Treatment of $CTF1^{-/-}$ mice with the calpain inhibitor MDL28170 protected against Fas-induced liver injury. (Marquès et al., 2007) Lastly, CTF1 levels are increased at the mRNA and protein levels in biopsies from patients with pediatric cholestatic liver disease (PCLD). CTF1 is expressed predominantly in biliary epithelial cells. According to *in vitro* research, LX-2 cells preconditioned with CTF1 showed significant increases in extracellular matrix component formation and proliferation and positive regulation of the STAT3 and p38MAPK pathways. (Hua et al., 2015) In conclusion, CTF1 has a hepatoprotective effect and can be used as a potential therapeutic agent against several liver diseases.

In neurons:

LIF and CNTF, the two members of the IL6 family cytokines, are well-known trophic factors that have a role in the survival of motor neurons. CTF1 is closely related to

CNTF and has a role in not just cardiomyocyte or hepatocyte, but also motor neuron survival. CTF1 is highly expressed in embryonic limb buds and differentially in myotubes. In vitro studies revealed that CTF1 treatment prolonged the 43% survival time of primer E14 neonatal rat motor neurons for 2 weeks. In vivo studies established that CTF1 protect neonatal sciatic motor neurons against the axotomy effect. (Pennica, Arce, et al., 1996) For central motor neuron survival, synergistic expression of multiple neurotrophic factors is required, but the secretion of numerous neurotrophins must occur with different cell types. GNDF (Glial cell line-derived neurotrophic factor) and CTF1 are needed for synergistic secretion. *gndf* mRNA transcripts mainly in Schwann cell lines; conversely, myoblasts express CTF1 mRNA principally. GDNF neutralising antibody reduced the trophic activity of Schwann cells by 75%, while CTF1 antibody reduced myotube-directed activity by 46%. CTF1 and GNDF together increase motorneuron survival in *in vitro* studies. (Arce et al., 1998) For the motor neuron survival process, LIFRβ is also needed. (Arce et al., 1999) Adenoviral delivery of CTF1 to newborn progressive motor neuropathy (pmn) model mice, sustained expression observed in muscle and bloodstream of the animal. Moreover, more prolonged survival and improved motor functions were observed. CTF1-treated pmn mice exhibited less degradation of facial motorneuron cytoskeletons and phrenic nerve myelinated axons. The terminal innervation of skeletal muscle, which was severely disrupted in untreated pmn mice, was almost entirely intact in CTF1-treated pmn animals. (Bordet et al., 1999) In the chick embryo oculomotor system, it was demonstrated in vivo that CTF1 and IGF-I caused neurite outgrowth and retrograde transport from muscle to nerve. It was also observed that injection of CTF1 or IGF-I into the eye muscles increased motor neuron survival by 20-30%. (Rind & Von Bartheld, 2002) However, CTF1 mRNA levels didn't change significantly before or after crush and transfection injury in adult peripheral neurons. (Ito et al., 2000) Additionally, CTF1 couldn't protect adult motor neurons after facial nerve avulsion. (Sakamoto et al., 2003) In the literature, it has been stated that the effect of CTF1 may be related to axonal transport from other sources (e.g., muscle) rather than local production of its mRNA in the distal nerve, and CTF1 can be transported to the nerve retrogradely. (Rind & Von Bartheld, 2002) Also, in the literature, many studies indicate that CTF1 supports motor neuron survival, but in CTF1 KO mice,, there is no significant result in neuron degeneration. (Oppenheim et al., 2001) Furthermore, CTF1 receptor component gp130, a critical element for CTF1 signal transduction, is downregulated in adult mice. This means that CTF1 doesn't support

adult motor neuron survival. (Sakamoto et al., 2003) Although few studies indicate that in spinal cord injury to adult rats and huCTF1 treated adenovirally from C3-4 lateral funiculus hemisection cavity, CTF1 expression was sustained and increased the survival of neurons by 20%. It provided regeneration of 1.2% of rubrospinal neurons. Behavioural tests showed recovery in limb usage. (Zhang et al., 2003) In addition, preconditioning with moderate oxidative stress can help photoreceptors deal with more lethal doses of oxidative stress and induce retina tissue changes like ischemic preconditioning in heart tissue. It has been discovered that CTF1 and p-STAT3 expression increase with other IL-6 family cytokines when using bright light for a moderate oxidative stress model. When LIFR inhibitor (LIF05) is applied, these effects are diminished. These results indicate that this mechanism depends on LIFR. (Chollangi et al., 2009)

1.5.3 In the renal system

Many studies explain CTF1's role in myofibroblasts, hepatocytes, and motor neurons and it has a protective factor on these cell types related diseases. There are also a few studies about CTF1's role in renal system-related diseases. CTF1 treatment on Wistar rats didn't change serum creatinine level. Still, it increased urinary, neutrophil gelatinase-associated lipocalin (NGAL) or microalbuminuria/creatinineuria ratio, common biomarkers for detecting chronic kidney disease (CKD). (López-Andrés et al. 2012) CKD is a severe condition that eventually leads to irreversible kidney damage. CKD is usually associated with cardiac apoptosis or cardiac hypertrophy. In the doxorubicin-induced CKD model, rats were challenged with 60 60-minute running or 60 60-minute swimming session. In the end, in healthy groups CTF1, IL6, LIFR and gp130 was upregulated but JAK and STAT were downregulated. In contrast, CTF1, IL6 and gp130 in exercised challenged groups were downregulated, but JAK and STAT were downregulated interestingly. These results indicate that exercise saved CKD by decreasing cardiac hypertrophy through the CTF1 activation of the STAT3 pathway. (Chen et al., 2014) It is also known that CKD is characterised by tubulointerstitial fibrosis, which involves inflammation, fibroblast proliferation, extracellular matrix accumulation, and tubular apoptosis. Unilateral ureteral obstruction induced a tubulointerstitial fibrosis model applied in $CTF1^{-/-}$ rats. In the early stage, it has been observed that high inflammation markers (IL-1β, Cd68, ICAM-1, COX-2 and iNOs), high NF-κB activation, high myofibroblasts, increased apoptosis and high tubular damage. In the late stage, it has been seen that high fibrosis is present in the kidneys.

CTF1 treatment at $CTF1^{-/-}$ fibrosis model rats and $CTF1^{+/+}$ fibrosis model rats decreases fibrosis levels. *In vitro* studies revealed that primary renal myofibroblasts have higher Collagen 1, fibronectin and NF-κB activation. (Perretta-Tejedor et al., 2019) CKD patients with LVH have higher CTF1 levels when compared to the non-LVH CKD patients additionally. (Cottone et al., 2007) Moreover, CTF1 has a protective role in chronic kidney disease and acute kidney injury (AKI). In the the gentamycin-induced AKI model, CTF1 treatment reduced kidney damage markers (NAG, NGAL, KIM-1, t-gelsolin, CD68, iNOS, TNF-α, IL6, plasma creatinine level) and increased creatinine clearance. Furthermore, for renal transplantation, ischaemia/ reperfusion is a significant problem. In IRI-induced rats with CTF1 treatment, rats have a prolonged survival rate, prevented IRI-induced glomerular filtration rate, reduced oxygen-radical production, neutrophil and macrophage infiltration, expression of adhesion molecules and plasma levels of proinflammatory cytokines (TNF-α, IL-1α, IFN-γ). Inducible nitric oxide synthase expression, NF-κB activation, and apoptosis were reduced. (Garcia-Cenador et al., 2013) Also, one of the significant problems among ischemia injuries is cold ischemia reperfusion injury (CIRI). CTF1 administration in CIRI modelled rats reduced the oxidative stress markers (superoxide anion and inducible nitric oxide synthase), inflammation markers (NF-κB and tumor necrosis factor-α), and vascular damage (vascular cell adhesion molecule-1), renal damage markers, activated LIFR and STAT3, increased renal functions and improved overall animal survival. (García-Cenador et al., 2018) Lastly, CTF1 has a protective role in contrast-induced nephropathy (CIN). CIN usually occurs when there is a contrast media toxicity, which generally leads to longer hospitalisation time, higher cardiovascular disease, dialysis necessitates and high mortality rate. CTF1 treatment in CIN rats resulted in almost complete prevention of renal tissue damage with decreased expression of tissue damage markers (NAG, NGAL, KIM-1), reduced caspase 3 and oxidative stress levels and increased expression of cell proliferation. (Quiros et al., 2013)

1.6 CTF1s role in adipocyte development

In vitro studies indicate that CTF1 treatment at 3T3-L1 adipocytes activates STAT1, STAT3, STAT5A, STAT5B and ERK1/2 signaling pathways, resulting in translocation to the nucleus. CTF1 expression in adipocytes increases progressively along differentiation from pre-adipocytes to adipocytes (Natal et al. 2008), but CTF1 is not involved in adipocyte differentiation. In acute CTF1 application, an increase in SOCS-3 mRNA in adipocytes and a decrease in PPAR mRNA, which temporarily binds to

STAT1, were observed. The effect of CTF1 on SOCS-3 and PPAR mRNA is independent of the MAPK signalling pathway. Moreover, CTF1 expression in white adipose tissue directly involves PPARα and PPARγ. (Carneros et al., 2020) Although chronic CTF1 application showed that fatty acid synthesis and insulin substrate receptor 1 (ISR1) protein levels decreased in adipocytes, other proteins were unaffected. In addition, when insulin-dependent glucose uptake was examined, it was found that adipocytes developed insulin resistance. (Zvonic et al., 2004) Another study points out that LIF and CTF1 treatment of the 3T3-L1 adipocytes increased SOCS3 expression but didn't affect the IRS-1 degradation. (He & Stephens, 2006) Furthermore, CTF1 pre-treatment affects blocking other IL-6 family member cytokines, even itself, in 3T3-L1 adipocytes. This inhibition effect was measured with STAT3, ERK1/2 activation and SOCS3 mRNA induction. Moreover, this inhibiting cross-talk dependent on degradation of LIFR. CTF1 pre-treatment on 3T3-L1 cells resulted in LIFR degradation; this degradation is proteosome- and lysosome-dependent. When lysosome inhibitors (leupeptin and chloroquine) were used, both basal and CTF-1-induced LIFR degradation was found to be blocked. LIF-induced SOCS3 mRNA levels are also decreased. (Zvonic et al., 2005) Moreover, some studies reveal CTF1's role in diabetes, obesity and other metabolic diseases. CTF1 KO mice developed obesity, insulin resistance, and higher cholesterol levels despite reducing calorie intake. Acute CTF1 administration reduced glucose uptake in muscles in an insulin-independent manner and resulted in AKT phosphorylation. These changes are associated with fatty acid synthesis, which were not observed in AMPKα2 mice, proving that these changes are also AMPK dependent. In chronic CTF1 treatment, it has been perceived that increased energy expense, increased expression of lipolysis genes, fatty acid oxidation, increased mitochondrial biogenesis, reduced body weight and corrected insulin resistance. (Moreno-Aliaga et al., 2011) CTF1 treatment on 3T3-L1 adipocytes also increased glycerol secretion, increased cAMP levels, protein kinase (PK)A-mediated phosphorylation of perilipin and hormone-sensitive lipase (HSL) at Ser660. Knockdown of PK and HSL also resulted in a decrease in the CTF1-mediated lipolysis activity. Acute CTF1 administration to the obese mice also increased PKA-associated peripilin phosphorylation and adipose triglyceride lipase. These results demonstrate that CTF1 can affect the main lipase activity *in vivo* and *in vitro*, having an anti-obesity effect. (López-Yoldi et al., 2014) Additionally, CTF1 protected MIN6B1 pancreatic beta cells and murine islets against apoptosis stimulated by serum deprivation. CTF1 also

increases insulin secretion stimulated by glucose in MIN6B1, and a phospholipase C inhibitor inhibits insulin secretion. CTF1 KO mice are more likely to develop diabetes, and their glucose tolerance test results in impaired glucose clearance. (Jiménez-González et al., 2013) Moreover, CTF1 administration decreased the expression of leptin, resistin and visfatin in 3T3-L1 adipocytes. Still, it increased the mRNA and protein expression of apelin, but apelin expression decreased when a PI3K inhibitor was applied. These results show that apelin production can mediate this pathway. CTF1 administration to the obese mice significantly downregulated leptin and resistin but didn't modify the apelin or visfatin production in adipose tissue at mRNA or protein level. (López-Yoldi et al., 2017) In addition, in vivo and in vitro studies imply that CTF1 treatment at everted intestinal rings in both long- and short-term treatments, α-Methyl-D-glucoside levels are significantly decreased, paralleled with a significant decrease of SGLT-1 protein expression. CTF1 enhanced the expression of phosphorylated STAT3 and STAT5 but decreased the expression of AMPK. JAK/STAT inhibitor and AMPK activator reversed these effects. They corrected α-Methyl-D-glucoside uptake and SGLT-1 levels (López-Yoldi et al., 2016). In obese insulin-resistant mice treated with pterostilbene for glycaemic control and different doses, GLUT4 expression, AKT expression and CTF1 expression also increased in the higher dose group (Gómez-Zorita et al., 2015). Moreover, CTF1 has intriguing involvement in the relationship between Type 2 diabetes and neuromuscular disorders (Rende et al., 2013), and human SNP rs8046707 has been discovered to be associated with insulin sensitivity. (Lutz et al., 2014) It has been found that the patients who have impaired glucose tolerance (IGT) and newly diagnosed diabetes (NDD) have higher CTF1 levels, along with higher CTF1 levels in non-obese NDD patients compared with obese NDD patients. IGT and NDD are positively associated with obesity, which is negatively associated with CTF1. (Hung et al., 2013) It was also discovered that in the Chinese population, subjects who are obese or overweight have significantly lower CTF1 levels. (Hung et al., 2015) CTF1 mRNA expression have higher levels in subcutaneous abdominal (scABD) than femoral (scFEM) depot in obese individuals. scFEM CTF1 expression negatively correlated with visceral adiposity and intrahepatic lipid but positively correlated with insulin sensitivity in obese women.(Stephens et al., 2019) On the other hand, a study suggests that CTF1 is not associated with obesity (body mass index or waist circumference level). (Jung et al., 2008) Some studies also imply the importance of CTF1 in metabolic diseases. Metabolic syndrome (MS) presents at least

three of the following five medical conditions: abdominal obesity, high blood pressure, high blood sugar, elevated serum triglycerides, and low serum high-density lipoprotein. (Rh et al., 2024) Therefore, serum CTF1 levels of the MS patients are much higher than those of the control group, as well as those of patients who have hyperglycemia and obesity.(Natal et al., 2008) Additionally, obese children who underwent a 10-week weight loss program had higher CTF1 levels compared to the children who had lost less weight at the end of the weight loss program. CTF1 levels are associated with reduced cholesterol levels and the development of metabolic syndrome. (Rendo-Urteaga et al., 2013) Lastly, not only were serum FFA levels of fasting CTF1 KO mice significantly lower than those of controls, but also HSL phosphorylation in the adipose tissue of CTF1 KO mice was significantly reduced in fasting model animals. (Carneros et al., 2020) Moreover, in the cohort of women with PCOS, the groups were separated according to whether they had metabolic syndrome (MetS+) or did not have metabolic syndrome (MetS-). The women who are MetS+ are waist-hip ratio (WHR), systolic and diastolic blood pressure, triglyceride, total cholesterol, insulin resistance (HOMA-IR), free androgen index (FAI), Ferriman-Gallwey scores (FGS, hirsutism measurement) and CT-1 levels were found to be higher. In contrast, HDL cholesterol levels were found to be lower. CTF1 levels were positively correlated with diastolic blood pressure, triglyceride level and FGS (hirsutism degree). In women with PCOS, CTF1 levels are elevated in the presence of metabolic syndrome. CTF1 is linked to metabolic disorders and clinical symptoms (hypertension, dyslipidemia, hirsutism).

Therefore, CTF1 may be a novel metabolic biomarker and could be used to predict long-term health risks (e.g., cardiovascular disease, metabolic syndrome) in women with PCOS. (Anik Ilhan et al., 2018) These results explain that CTF1 has a role in cellular energy status and is associated with metabolic disorders.

CTF1 and cancer

Even though cytokines' involvement in cancer development and tumorigenesis is well established, CTF1's role in cancer is not illuminated. Several gene expression and bioinformatic analyses discovered that CTF1 is a differentially expressed gene in many types of cancer. TCGA and GTEx database analyses revealed that CTF1 expression increased in GBM and decreased in colon adenocarcinoma. (Cai et al., 2025) They analysed GBM data further and discovered that high levels of CTF1 are associated with

worse prognosis. Additionally, they silenced CTF1 using RNAi and saw loss of CTF1 expression resulted with suppressed proliferation and induced apoptosis in GBM cell lines. (Cai et al., 2025) CTF1 levels are also significantly associated with high-grade glioma, drug response and immune filtration in TCGA and GTEx data sets. (He et al.,2024 kaynakça!) Also, in Hepatocellular carcinoma CTF1 is a differentially expressed gene by methylation regulation. When CTF1 is hypermetilated, it is negatively associated with overall survival of HCC patients. In addition 353 HCC patients divided as low and high according to methylation status, gender, T stage of the tumor is significantly correlated. (Liang et al., 2021) In patients with gastroentero-pancratic and bronchial neuroendocrine tumors, serum CTF1 levels were significantly decreased compared to healthy individuals. These results support CTF1's capacity as a biomarker in cancer.

Non-coding RNAs, miRNA, and lncRNA have been excessively studied in cancer before, but the role in these mechanisms remains uncovered. In the literature, ceRNA network analysis in lung adenocarcinoma, it is discovered that CTF1 is one of the prognostic markers for lung adenocarcinoma. (Gao & Zhang, 2021) A similar study was conducted in gastric cancer, still CTF1 was in the top five mRNAs, which has good prediction and diagnostic capacity. (Ding et al., 2022) When fluorouracil-resistant or sensitive cell lines and patients who have received fluorouracil-based chemotherapeutic treatment, or not combined with BTN3A3, were investigated, CTF1 was reported as a differentially expressed gene. It explained that CTF1 has a prognostic value to predict the survival of gastric cancer patients with chemotherapy based on fluorouracil. (Pan et al., 2019) In addition, CTF1 is not only associated with prognostic and diagnostic biomarker capacity, but also has a role in different stages of cancer; cancer stemness, cancer cell signalling, migration, invasion, cell proliferation, metastasis and drug resistance. Human mammary epithelial cells (HMEC) were treated with OSM. They activated the STAT3/SMAD3 pathway while undergoing EMT and generated Cancer Stem Cells (CSCs). Parallel to OSM, CTF1 increased the cancer stem cell population in the same experiment setup. (Junk et al., 2017) Furthermore, CTF1 induced ovarian cancer cell proliferation in a dose-dependent manner and induced cell proliferation in many of the Ewing sarcoma cell lines that they used. (Scoles et al., 2010) In 2023, Akkoç et al. published that for the first time, CTF1 is derived from breast cancer cells and it is potent regulator of autophagy in fibroblasts leads to CAF differentiation. They provide evidence that CTF1 regulates autophagy dependent cancer cell migration and

invasion. This evidence is supported by patient-derived breast tumour samples. In these samples, it has been discovered that CTF1 expression significantly correlated with lymph node metastasis. (Akkoc et al., 2023) In another study, breast cancer patient cohort who had neo-adjuvant chemotherapy divided groups as sensitive and resistant. Among other genes, CTF1 is a downregulated gene in the resistant and lower overall survival group. (Barrón-Gallardo et al., 2022) In ovarian cancer, it has been found that CTF1 is increased with oxidised LDL treatment, and this effect is reversed by nuclear liver X receptor (LXR) agonist in ovarian cancer cell lines (SKOV3 and CAOV3). (Scoles et al., 2010)

Lastly, CTF1's role in immunity and inflammation has been studied from various perspectives. CTF1 is associated with secreting acute-phase proteins. For example, CTF1-treated hepatocytes secrete acute-phase proteins in a dose-dependent manner. (Richards et al., 1996) Treating mice with ulcerative colitis using CTF1 prevented colon deterioration and decreased both systemic and colonic levels of tumor necrosis factor α (TNF-α). At the same time, CTF1 null mice exhibited more severe colon damage and ulcerative colitis compared to wild-type mice. (Prieto-Vicente et al., 2018) These studies indicated that CTF1 could have both pro-inflammatory and anti-inflammatory roles depending on the context. It was linked to T and NK cell-mediated tumor immunity in the colorectal cancer tumor engraftment model. The authors demonstrated that colorectal carcinoma cells formed tumors when injected subcutaneously into wild-type mice. However, the same cells did not develop tumors when engrafted into the liver of *Ctf1* null mice. Reducing CTF1 levels through systemic neutralizing antibody administration mimics the phenotype seen in Ctf1 null mice within wild-type animals. Additionally, similar resistance was not observed when other cancer cells, such as pancreatic carcinoma and melanoma, were engrafted, indicating a colorectal cancer-specific response in liver engraftment. Notably, the cytotoxic effect of liver lymphocytes from a CTF1 null animal was comparable to that from a wild-type animal, supporting the idea that both local and systemic CTF1 effects contribute to cancer immunity. (Bustos et al., 2012)

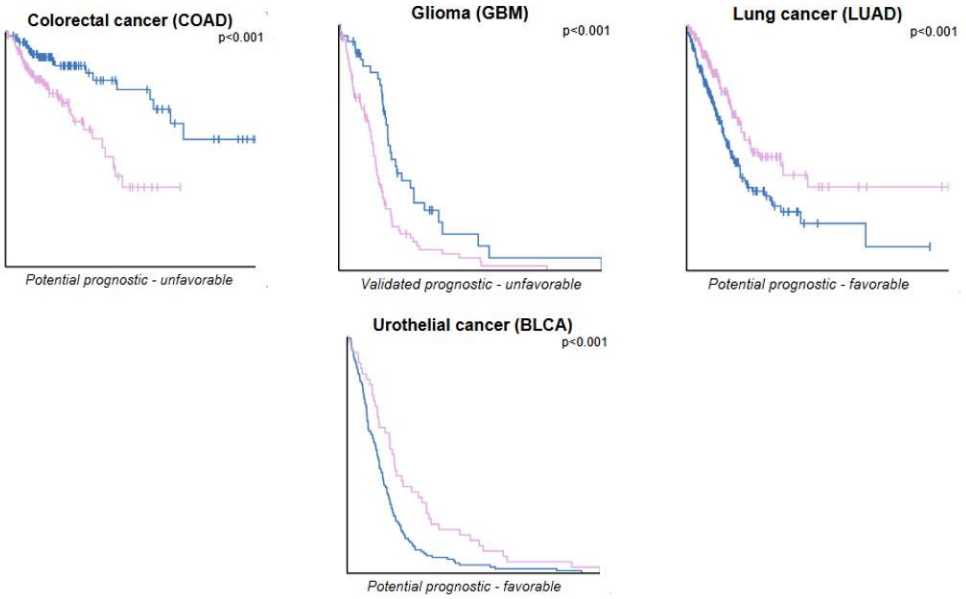

Figure 1.7 CTF1s correlation with cancer types. According to Human Protein Atlas data, CTF1 correlates with different cancer survival types and can be used as a

1.7 CTF1 and tumor microenvironment

Macroautophagy, also known as autophagy, is a cellular stress response mechanism that has been conserved throughout evolution. Autophagy is a double-edged sword in cancer. Moreover, autophagy induction in tumor stroma supports tumor microenvironment. In TME, cancer cells and fibroblasts both have high levels of autophagy. Akkoç et al. discovered that CTF1 activates autophagy in fibroblasts and CAFs. It has been stated that STAT3 is phosphorylated and translocated into the nuclei by CTF1; in this way, transcriptional activation of essential autophagy proteins starts. AMPK and ULK1 were activated after CTF1 treatment. When CTF1 is applied to the fibroblast cells, they activate, produce more stress fibers, and accumulate ACTA2/α-SMA. Moreover, a relationship is discovered in breast cancer tumors between CTF1 expression. In breast cancer patients with lymph node metastasis, CTF1 expression is elevated. Although the cancer cells themselves do not express gp130 and LIFR — which are key for CTF1 signalling — fibroblasts and CAFs do have CTF1 receptors on their surfaces. This leads to a one-way interaction driven by CTF1. Additionally, when CTF1 activates fibroblasts, it further promotes tumor growth by triggering the secretion of signalling molecules and inducing autophagy. This mechanism establishes a positive feedback loop, akin to other cytokines within the same family.(Akkoc et al., 2023)

2 Antibodies

Antibodies are also known as immunoglobulins (Ig). The immune system uses large, Y-shaped antibodies to identify and neutralise antigens from viruses, bacteria, or disease-causing organisms. Each antibody recognizes one or more specific antigens. The term antigen means “antibody generator,” so the presence of an antigen causes the formation of an antigen-specific antibody. Each Y-shaped antibody chain contains paratopes that bind specifically to the antigen paratope. They can identify non-self-molecules or pathogens, leading to their destruction or removal. For example, antibody binding inactivates viruses and microbial toxins (neutralization) by preventing them from binding to host cell receptors.(Chiu et al., 2019) They also tag invading pathogens for destruction (opsonization), primarily by making it easier for phagocytic cells of the innate immune system to ingest them. Antibodies can be attached to the surface of an immune cell, like in a B cell receptor, or they can be secreted freely into the extracellular space. (Daëron, 1997) Usually, the term 'antibody' refers to the secreted form, while 'immunoglobulin' can describe both the surface-bound and free forms. (Yu & Lieber, 2019) Moreover, artificial antibodies can be designed and produced *in vitro* conditions and used for therapeutic or diagnostic approaches—for example, specific monoclonal antibodies produced using the hybridoma technique developed by Köhler and Milstein in 1975. Since then, antibody-based drugs have played a massive role in cancer and other disease diagnostics and treatments. (Leavy, 2016)

2.1 Antibody structure

Antibodies are heavy, approximately 150 kDa proteins about 10 nm in size. They have three globular regions that form a Y shape. In humans and most other mammals, an antibody contains four polypeptide chains: two identical light chains and two identical heavy chains. Disulfide bonds link these chains. Each chain also contains domains; the light chain has one variable domain (V_L) and one constant domain (C_L), while the heavy chain contains one variable domain (V_H) and three to four constant domains (C_H1, C_H2).(Chiu et al., 2019) There are two antibody light chains in mammals: lambda (λ) and kappa (κ). Kappa and lambda light chain ratios differ among species. In humans, the kappa/lambda ratio is 60:40, but in mice, it's 95:5. (Popov et al., 1999) It is a known fact that there is no functional difference between these two chains, but many articles suggest that in multiple myeloma, cancer cells produce more free light chains than

control group and associated with lower overall survival. Free light chain amount can be biomarker in some diseases. (Singh & Xu, 2021) Different types of light chains, such as iota (ι), are found in other vertebrates like sharks (Chondrichthyes) or bony fishes. (Teleostei). (Lefranc & Lefranc, 2022)

As a structure, an antibody also includes two antigen-binding fragments, the Fab region. Fab region contains one VL, VH, CL and CH1 domain. The subregion of the Fab region, which includes variable domains, is essential specifically for antigen binding. Each variable domain includes three hypervariable regions containing amino acids that cause antibody variability. When the antibody protein folds, these regions lead to three β-strand loops. These loops are often referred to as complementary determining regions (CDRs). Four relatively conserved sequences called framework regions (FR1-FR4) exist between each CDR. These regions help maintain the three-dimensional structure of the V-domains. The three CDRs of each VH and VL chain form loop structures resembling fingers extending from the variable domain. These three heavy and light chains loops come together to create an antigen-binding site. Variations in the sequences of the CDRs among different antibodies lead to unique interaction surfaces, which determine the specificities of each antibody.

The antibody's Fc region (crystallizable fragment) contains constant domains of the heavy chains. It regulates immune cell activity. Effector molecules bind to this region and trigger many effects after the antigen binds to the Fab region of the antibody. The Fc region also selects and distributes different antibody classes. (Chiu et al., 2019)

2.2 Antibody diversity

In 1970, Kabat and Wu gave the first real view of antibody diversity. They assembled existing amino acid sequences of Ig chains and analysed the variability of 77 light chains. Discovered that the number of evolutionarily conserved light chain residues in mice differs from that in humans. Additionally, they created a metric for variability at each amino acid residue position (Variability = number of different amino acids at the position/frequency of the most common amino acid at the position). Later, they applied this variability across 207 light chain variable region residues. They discovered that residues 24-34, 89-97, and 50-56 are essential for the light chain diversity. Moreover, Kabat and Wu also suggested that CDRs are encoded by small DNA sequences called

episomes. An extensive repertoire of episomes exists for each CDR. (T. T. Wu & Kabat, 1970)

Many mechanisms cause antibody diversity in mammals. Before and after antigen stimulation, two steps result in immense antigen diversity. Multiple germ-line gene segments and combinatorial V-(D)-J joining are the first causes of diversity. In germ-line, numerous copies of variable (V), diversity (D), and joining (J) gene segments are encoded for immunoglobulin proteins, known as V, D, and J segments, respectively. In humans, there are 134 VH, 13 DH, 4 JH, 85 Vκ, 4 Jκ, 2 Vλ, and 3 Jλ gene segments. The random rearrangement of V, D, and J segments for heavy chains and V and J for light chains initially generates the antibody variable region diversity. VDJ recombination is the genetic rearrangement mechanism that acts in B or T cells to create more diverse antibodies, with the random joining of two gene fragments and adding or deleting new nucleotides. Random V, D and J genes are joined to create an antibody gene during this mechanism. The same principles are applied in T cells while creating unique T cell receptors. The light chain contains only V and J. Therefore, the possible number of combinations between heavy and light chains is about 2.41×10^6. P nucleotide and non-templated (N) nucleotide addition also contains antibody diversity via asymmetric cleavage of DNA hairpin forming at the coding joint, which is subsequently repaired by recombination activation gene 1 and 2 (RAG1/2). Later, recombinase fills a palindromic sequence or P nucleotides. In non-templated (N)-nucleotide addition, N-nucleotides are added by terminal deoxynucleotidyl transferase (TdT) activity to the coding joint again. Furthermore, Exonuclease trimming commonly occurs at a heavy chain's V-D and D-J junctions, leading to the unintended loss of coding joint nucleotides. Lastly, somatic hypermutation is the most essential mechanism that leads to antibody diversity. This process occurs in the germinal centre after a mature B cell is exposed to an antigen. During proliferation in response to the antigen, the genes encoding the variable regions of the heavy and light chains undergo rapid point mutations. Somatic hypermutation enhances the diversity of the antibody's variable domains and can alter their affinity for the antigen. Only B cells with high-affinity receptors are selected for survival. This process of producing antibodies with improved binding strengths is known as affinity maturation. (Briney & Jr., 2013) The actual combinatorial diversity is usually lower than what calculations suggest. These calculations indicate that the human antibody repertoire can reach a diversity of 10^{15} -

10^{18}, which leads to the concept of an "infinite repertoire". This is biologically impossible because not all V gene segments are used equally; some are common in antibodies, while others are rare. Additionally, not every heavy chain can pair with every light chain, as certain VH and VL combinations will not produce a stable molecule. Suppose heavy and light chains fail to pair properly within cells. Further light-chain gene rearrangement may occur until a compatible chain is formed, or the molecules will be eliminated. Despite these limitations, it is generally believed that most heavy and light chains can pair successfully, and this combinatorial diversity plays a crucial role in creating an immunoglobulin repertoire with broad specificities. Moreover, having a physical naive repertoire of 10^{15} independent B cell clones in the human body is unfeasible. This figure would surpass the total number of cells in the body by 100 times and the circulating B cells by 1 million times. (Rees, 2020)

2.3 Recombinant Antibodies

Due to their production method, antibodies can be polyclonal, monoclonal or recombinant. All of the antibody types have their advantages and disadvantages. In 1975, Kohler and Milstein established hybridoma technology and introduced the concept of producing specific antibodies at a large scale in the laboratory. Since their first production, monoclonal antibodies have played a massive role in treating cancer and other diseases and in diagnosis. (Leavy, 2016) Monoclonal antibodies are specific antibodies that can only be produced from a single B cell clone and are specific to only one antigen epitope. An animal (usually a mouse) is immunised with a particular antigen to produce monoclonal antibodies. After some time, the mouse spleen was harvested and collected B cells. Later, B and myeloma cells fused with a fusion reaction using PEG or electrofusion. Moreover, they selected a selection medium called HAT (Hypoxanthine-Aminopterin-Thymidine). Only hybridomas can survive; B cells and non-fused myeloma cells will die. Eventually, each clone will produce the same antibody.

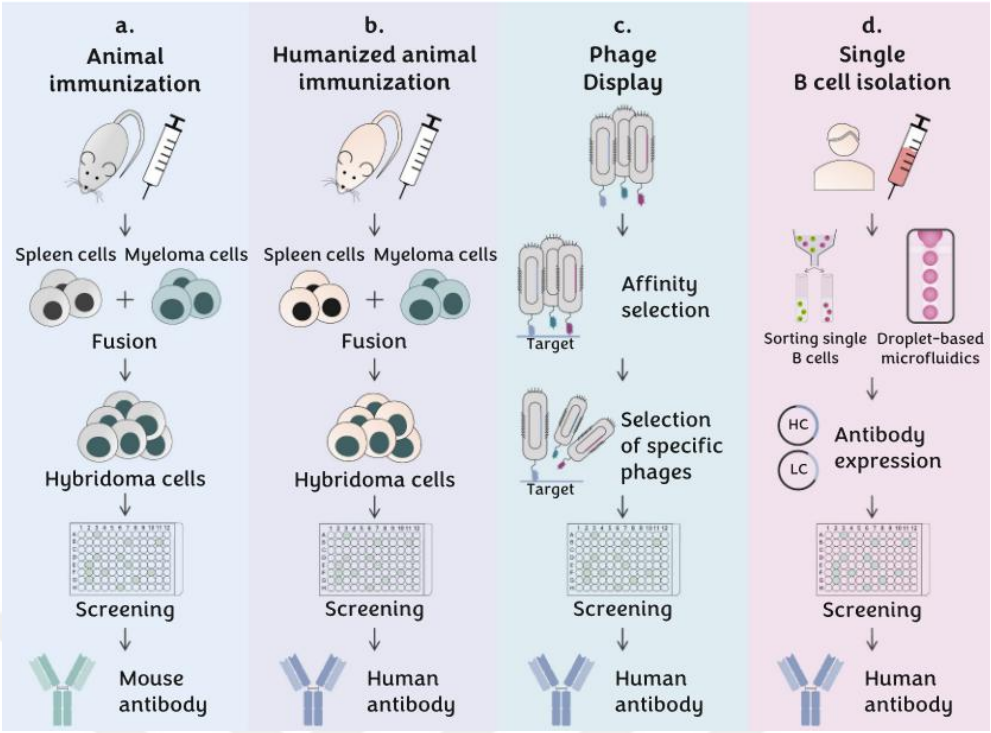

Figure 2.3 Obtaining monoclonal antibody methods. (Istomina et al., 2024) Copyright © 2024 Polina V. Istomina et al. This is an open access article distributed under the Creative Commons Attribution License, which permits unrestricted use, distribution, and reproduction in any medium, provided the original work is properly cited.

Monoclonal antibodies faced several disadvantages along the disease treatment journey.(J. K. H. Liu, 2014) One of the disadvantages of monoclonal antibodies is the human anti-mouse antibody (HAMA) across the monoclonal application in patients. The creation of HAMA seriously limits the clinical applications of disease treatment. To get over this limitation, monoclonal antibodies should be humanised. Additionally, monoclonal antibody production is expensive, long and needs expertise. Additionally, disadvantages include the instability of aneuploid cell lines, the inability to produce human antibodies, the low efficiency of B lymphocyte fusion with myeloma cells, low tissue penetration into the solid tumors, and the use of immunised experimental animals. (Rodríguez-Nava et al., 2023) Because of these problems, researchers started to investigate new recombinant antibody structures. These antibody structures include Fab fragments, Fv fragments, scFv (single chain fragment variable), nanobodies or diabodies. Compared to full-sized antibodies, these antibodies have better tumor tissue penetration, more rapid blood clearance, reduced immunogenicity, and lower retention times in non-target tissue. They are much cheaper and easier to produce than full-sized antibodies. (Ahmad et al., 2012)

Table 1 Advantages and disadvantages of different antibody obtaining methods.

	Source	Technique	Advantages	Disadvantages	Immunogenity	Cost	Time
Hybrdoma technology	Mouse B cells from spleen and myeloma cells	Starts with animal immunisation, continues with B cell and myeloma cell fusion and ends with hybdroma cloning	High-purity, specific antibodies. Theoretically, it can produce an unlimited number of antibodies. Many clinically approved drugs are available.	Time-consuming and low efficiency in cell fusion.	High. Needs a humanisation process.	High	Months
Phage display	Antibody fragments from human or animal.	The antibody library is expressed on the bacteriophage surface. Using a biopanning strategy to select	Animal immunisation is optional. Human antibodies can be produced. CDR regions can be redesigned to	In the beginning, library preparation and system is expensive and long.	Low, it can produce fully human antibodies.	Low	Much faster

		target antigen.	increase affinity. Fast selection steps.				
B cell sorting	Human blood or B cells from lymphoid tissue	Single B cells are isolated using FACS or magnetic beads. Gene amplifies with RT-PCR— clones into the mammalian expression vector.	Direct human source, matched VH-VL antibodies. No need for animal immunisation. It can produce very fast and highly specific antibodies.	Equipment is very expensive and requires expertise. In some species, B-cell markers are not available.	Very low because it comes from natural human B cells.	Very high	Fast

2.3 Single chain fragment variable (scFV)

2.3.1 Structure of scFv:

A scFV antibody contains one heavy (VH) and one light chain (VL), which are joined with a flexible linker peptide. This antibody form can be expressed in functional form in E. coli, which can be easily modified to improve the abilities of scFV, like increasing solubility, affinity, or even specificity. The average molecular weight of the scFvs is 27 kDa.

The DNA linker's length is critical for the correct folding of the scFV. The peptide linker should be approximately 3.5 nm (35 Å) between the carboxy and amino termini

of the antibody's light and heavy chain domains. Besides the length of the linker, amino acid composition also plays a considerable role in successful scFVs. They must have a hydrophilic sequence to avoid the intercalation of the linker sequence between light and heavy chain domains through protein folding. (Argos, 1990) Currently, the most common linker design contains Gly for flexibility and Ser for solubility (G4S)n. On the other hand, there are other linker sequences that contain Gly and Lys to add more solubility.(Huston et al., 1991) Some studies showed that if the linker is longer than 12 amino acid residues, it causes a sufficient distance between the heavy and light chain domains. (Atwell et al., 1999) It should be considered that repeated sequences carry problems in PCR experiments and are more likely to be immunogenic, also showing less stability than non-repetitive linkers. (Arslan et al., 2022) Additionally, longer linkers promote proteolysis of the domains. If it's shorter, it prevents physical annealing of two antibody domains. This strategy is commonly used when creating multimers like diabodies, tribodies, and bispecific antibodies. (Atwell et al., 1999)

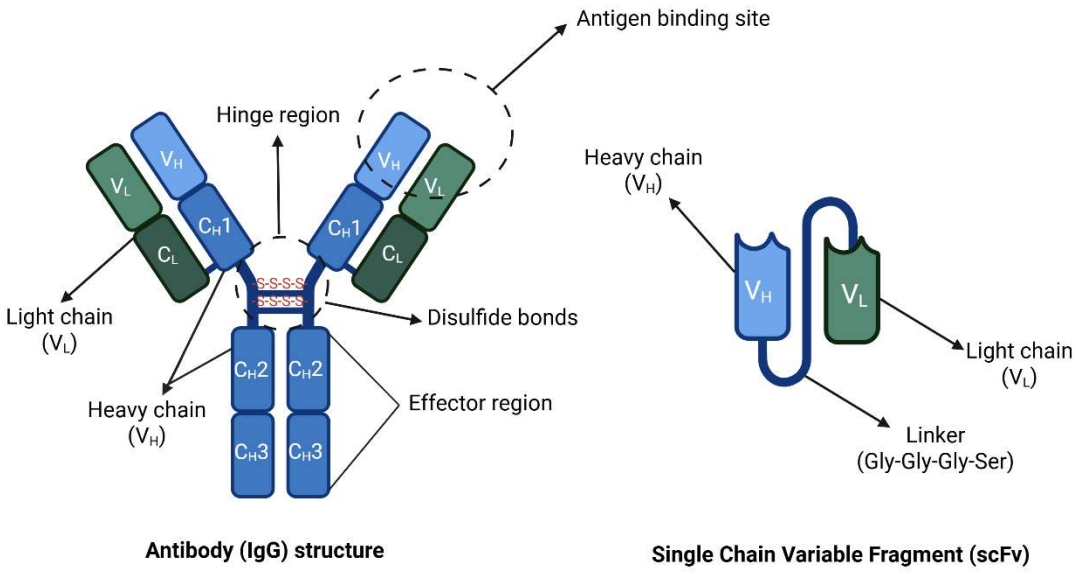

Figure 2.4.1 Structure of classical antibody (IgG) and Single Chain Variable Fragment (scFv). Created with BioRender.

Currently, there are three main scFv-based drug formats in the literature or clinical trials: bispesific T cell engager (BiTE), dual-affinity re-targeting proteins (DARTs), and Tandem diabodies (TandAbs). (Mallender & Voss, 1994) BiTE molecules have been commonly used in cancer immunotherapy to target T cells or re-target tumor-associated cells in the tumor microenvironment. Structure is based on two scFV joined with a linker, but these antibodies target two antigens. The short, flexible linker connecting the

two scFvs allows the arms to rotate freely, essential for flexible engagement with target receptors on two opposing cell membranes—such as a cytotoxic T-cell and a tumor cell—and for triggering T-cell activation. One of the successful BiTE drugs is blinatumomab (Blincyto, DrugBank entry DB09052). Blinatumomab contains anti-CD19 scFV in the VL-VH orientation linked with a GGGGS linker. It is commonly used in the clinic for treating B-cell precursor acute lymphoblastic leukaemia (ALL). According to small size, blinatumomab reaches close site of the T-cell and targets cell membrane but also cleans and eliminates rapidly in the patient body. Notably, blinatumomab has some problems with aggregation and decreased protein stability. (Klinger et al., 2012) Additionally, there are dual-affinity re-targeting proteins, which are short for DARTs. DARTs contain two Fv fragments again, with two unique antigen binding sites formed when these Fv fragments heterodimerize. Specifically, Fv1 is composed of a VH from antibody A and a VL from antibody B, whereas Fv2 includes a VH from antibody B and a VL from antibody A. Unlike BiTE antibodies, which are linked by a polypeptide chain, this combination enables DART to replicate the natural interaction in an IgG molecule. (Holliger et al., 1993) Furthermore, there are also Tandem antibodies (TandAbs). In Tandem antibody structure two binding sites for each antigen is present to increase binding affinity. Furthermore, TandAbs molecular weight is bigger (around 105 kDa) than other types: 55 kDa for BiTE, 50 kDa for DART. In clinical trials, there are two TandAb format drug for testing: AFM13 (CD30 X CD16 for NK cell recruitment and AFM11 (CD19 X CD3) for T cell recruitment. (Reusch et al., 2014) Finally, there are other scFV based drugs which is approved by FDA which is stated in the table below.

Table 2 scFv-based drugs that are approved by the FDA.

Drug name	**Format**	**Target molecule**	**Target disease**	**Brand name**	**Approved year**	**Reference**
Blincyto® (Blinatumomab)	Bispesific	CD19 and CD3	Philadelphia chromosome-negative relapsed	Amgen Inc.	December 2014	(Klinger et al., 2012)

			or refractory B-cell precursor acute lymphoblastic leukemia			
Beovu (Brolucizumab)	Humanized scFv	VEGF-A	Diabetic macular edema	Novartis	October 8, 2019	(FDA,2022)
Abecma (Idecabtagene vicleucel)	CAR-T cell	B cell maturation antigen	Multiple myeloma	Bristol Myers Squibb	March 26, 2021	(Research, 2024b)
Tecartus (Brexucabtagene autoleucel)	CAR-T cell	CD19 and B cell maturation antigen	Relapsed or refractory B cell precursor acute lymphoblastic leukemia	Kite Pharmaceuticals, Inc.	October 1, 2021	(Research, 2024g)
Kimmtrak (Tebentafusp)	Bispesific	gp100 and CD3	Metastatic uveal melanoma	Immunocore	January 25, 2022	(Research, 2024d)
Vabysmo (Faricimab)	Bispesific	VEGF-A and Ang-2	Diametic macular edema and neuvascular age-related	Genentech	January 28, 2022	(Medscape, 2022)

			macular degeneration			
Carvykti (ciltacabtagene autoleucel/cilta-cel)	CAR-T cell	B cell maturation antigen	Multiple myeloma	Johnson & Johnson	March 30, 2022	(Research, 2024f)
Yescarta (Axicabtagene ciloleucel)	CAR-T cell	CD19 expressing cancer cells	Large B cell lmyphoma	Kite, a Gilead Company	April 1, 2022	(Research, 2024a)
Kymriah (Tisagenlecleucel)	CAR-T cell	CD19 expressing B cells	Relapsed or refractory follicular lymphoma	Novartis Pharmaceuticals Corporation	May 27, 2022	(Research, 2024e)
Breyanzi (Lisocabtagene maraleucel)	CAR-T cell	CD19 expressing cancer cells	Large B cell lymphoma	Bristol Myers Squibb	June 24, 2022	(Research, 2024c)

2.3.2 Generation of ScFv

scFV antibodies are generally produced from spleen cells of the immunized mice or B lymphocytes from humans. As explained before, scFV contains the light and heavy chains of the antibody. To generate this structure, the mRNA from the host should be isolated. Then, continue with the cDNA conversion step to use as a template for PCR amplification. To create a cDNA library for the scFV selection process, many PCR reactions with different primer sequences should be made. After this, the PCR reactions are isolated from the agarose gel and continue with another PCR reaction called SOE-PCR (splicing by overlap extension). In this PCR reaction, the light and heavy chain

PCR products will amplify due to overlapping regions of the PCR product. This structure will be cloned into the phage display vector called phagemids. After cloning, the library is transformed into E. coli cells such as XL1-Blue, TG1, and ER2537, either through electroporation or chemical competency. To release the desired segment's cloning vector, these competent bacteria are infected with helper phages like VCSM13 or M13KO7. From these, antibody variable domain libraries are created and screened to identify antibodies with high affinity for specific targets such as enzymes, other antibodies, or cell surface receptors. This in vitro process for selecting peptides of interest is known as biopanning. The step-by-step process involves incubating the display library with ligands attached to a solid support, such as beads or membranes. Unbound phages are then washed away, and the bound phages are eluted. These are subsequently used to infect *E. coli* cells. This method results in a library where each phage displays a single antibody fragment on its surface. Multiple cycles of binding (usually four to six) and amplification are performed to isolate antigen-specific phages that tightly bind to the target molecule. Lastly, each clone is identified through DNA sequencing, which uncovers its unique CDR regions.(Clackson et al., 1991; X. Liu et

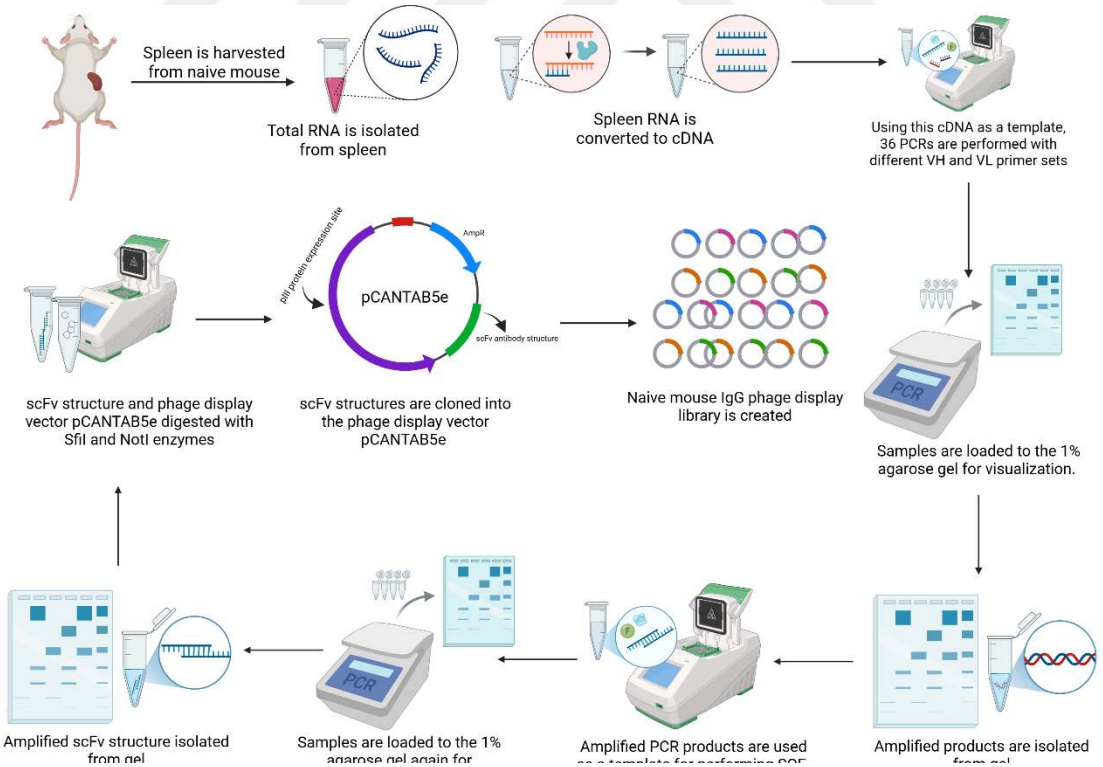

Figure 2.4.2 Workflow for generating a naive mouse phage display library. Created with BioRender.

al., 2022; Xia et al., 2006)

2.3.3 ScFv library types

2.3.3.1 Immune library

Immune libraries are constructed from B cells derived from different animals: mouse (Okamoto et al., 2004), camel (Rahbarizadeh et al., 2004), sheep (Charlton et al., 2001), chicken (Okada et al., 2006) and humans (Xia et al., 2006)In these libraries, animals are immunised against the antigen of interest. According to in vitro affinity maturation of the antibodies, immune libraries always result in a significant number of positive clones and higher binding affinity. But a new library should be constructed for each antigen against which you want to produce an antibody. For example, a rabbit phage display library screens against microcytin-LR, the most common biotoxin that pollutes water and agricultural products. (Xu et al., 2019) Furthermore, another mouse phage display immune library was constructed against porcine aminopeptidase N, cellular receptor for swine transmissible gastroenteritis virus (TGEV) and porcine epidemic diarrhea virus (PEDV). (Sun et al., 2012) Finally, the ovarian tumor library was amplified using lymphocytes of ovarian tumor patients. (Xia et al., 2006)

2.3.3.2 Naïve library

Naïve libraries are derived from animal B cells, but in this case, these animals are not immunised against any antigen. Eventually, generating a new library for each interested antigen is unnecessary. However, the number of positive clones is much lower than that of the immune libraries. Moreover, the affinity of antibodies excessively depends on the library size, so large naïve libraries should be generated while doing biopanning against the target antigen. (Sheets et al., 1998) The affinity of the small library, containing approximately 3×10^7 antibody clones, ranges from 10^6 to 10^7 M^{-1}, while the large library, with 10^{10} clones, ranges from 10^8 to 10^{10} M^{-1}. (Hu et al., 2013)

2.3.3.3 Synthetic library

Synthetic libraries also originate from non-immune sources, enabling the synthetic combination of germ-line sequences and complementary determining regions (CDRs). Most human synthetic antibody libraries focus on randomising the CDR3

regions, as they tend to be the most diverse and critical for antigen recognition. Consequently, these libraries are widely selected to develop high-affinity monoclonal antibodies. (Knappik, n.d.)

2.3.4 Advantages of ScFv

scFvs have several advantages over full-sized mAbs. Small size, low immunogenic effects, high expression, ease of production, rapid blood clearance and great tissue penetration give scFvs many more advantages than full-sized antibodies. Furthermore, low production costs provide more opportunities for researching new drug candidates. scFv molecules are less immunogenic because they lack the Fc domain responsible for activating antibody effector functions. They can be stored at 4 ^{o}C for several years. Finally, because they are easy to modify, it can be easily modified to improve activity, stability, or affinity to bind target molecules. (Ahmad et al., 2012)

2.3.5 Limitations of ScFv antibodies

The lack of an Fc domain in the scFv antibody makes it less thermostable than the parental mAb, and without FcRn-mediated recycling, these molecules tend to have a short circulation half-life. Additionally, the small size of the biologic increases the tendency for aggregation, which can raise immunogenicity risks. Its rapid clearance from the bloodstream necessitates higher and repeated doses. Although fusion methods, such as attaching scFv to bovine serum albumin (BSA) or polyethylene glycol (PEG), aim to improve half-life, they can diminish the advantages of scFv over mAbs due to increased size and higher costs. (De Aguiar et al., 2021)
Developing full recombinant antibodies involves challenges similar to those faced by small antibody fragments, including bioengineering, expression, purification, safety, and stability issues. Phage display technology, used to create fully human or humanized scFv antibodies, remains complex, time-consuming, and expensive. Using transgenic animals with integrated human immunoglobulin loci also involves tedious procedures for gene integration. Expression systems further limit proper folding and functional yield of scFv antibodies: prokaryotic systems lack glycosylation and can produce endotoxins that are hard to remove, while eukaryotic single-cell systems often encounter protein misfolding within the endoplasmic reticulum (ER). Additionally, purifying scFv antibodies is more complicated due to

the absence of the Fc domain. Affinity tags are fused with scFv antibody for the selective capture and efficient purification. Still, proteolytic cleavage at the end may not completely remove the full tags and leave some residual amino acids that lead to aggregation and/or misfolding of scFv antibodies and even enhance their immunogenicity.

2.4 Phage display

In 1985, George Smith established early studies of phage display, which was later awarded a Nobel prize in 2018. Filamentous phages are recombinantly engineered during phage display to display a peptide or an antibody on the surface. Due to insertion of random oligonucleotides sequences into the N-terminal of pIII or pVIII gene into the phagemids, it results with expression of billions of random peptide or antibody sequences. For achieving this, randomly synthesised oligonucleotides are amplified using PCR, later purified and restrictionally cloned into the M13 vector system. After the ligation reaction, vector is transferred to E.coli through electroporation or other transformation methods, this step is especially necessary to obtain large and diverse libraries. In the end of the library creation process, biopanning process starts, which is a key step for phage display.(Barderas & Benito-Peña, 2019) Biopanning basically is an affinity selection process. In first step, recombinant phage library is constructed. Secondly, this library is incubated with target molecule to allow the peptides or antibodies to bind. In third step, low affinity, unbound phages are removed using a detergent-containing buffer. In the fourth step, binding high-affinity phages are eluted with low pH buffer or sometimes competitive elution performed. Lastly, in fifth step, eluted positive phages are used to infect E.coli again for the amplification of phages. New amplified library is used again for next round to achieve more high affinity binding phages. In this system, both phagemid and helper phage are used together; the phagemid vector contains genes of VH and VL to create a scFv or Fab structure, meanwhile the helper vector contains encoding genes of coat proteins to display the library on the phage surface.

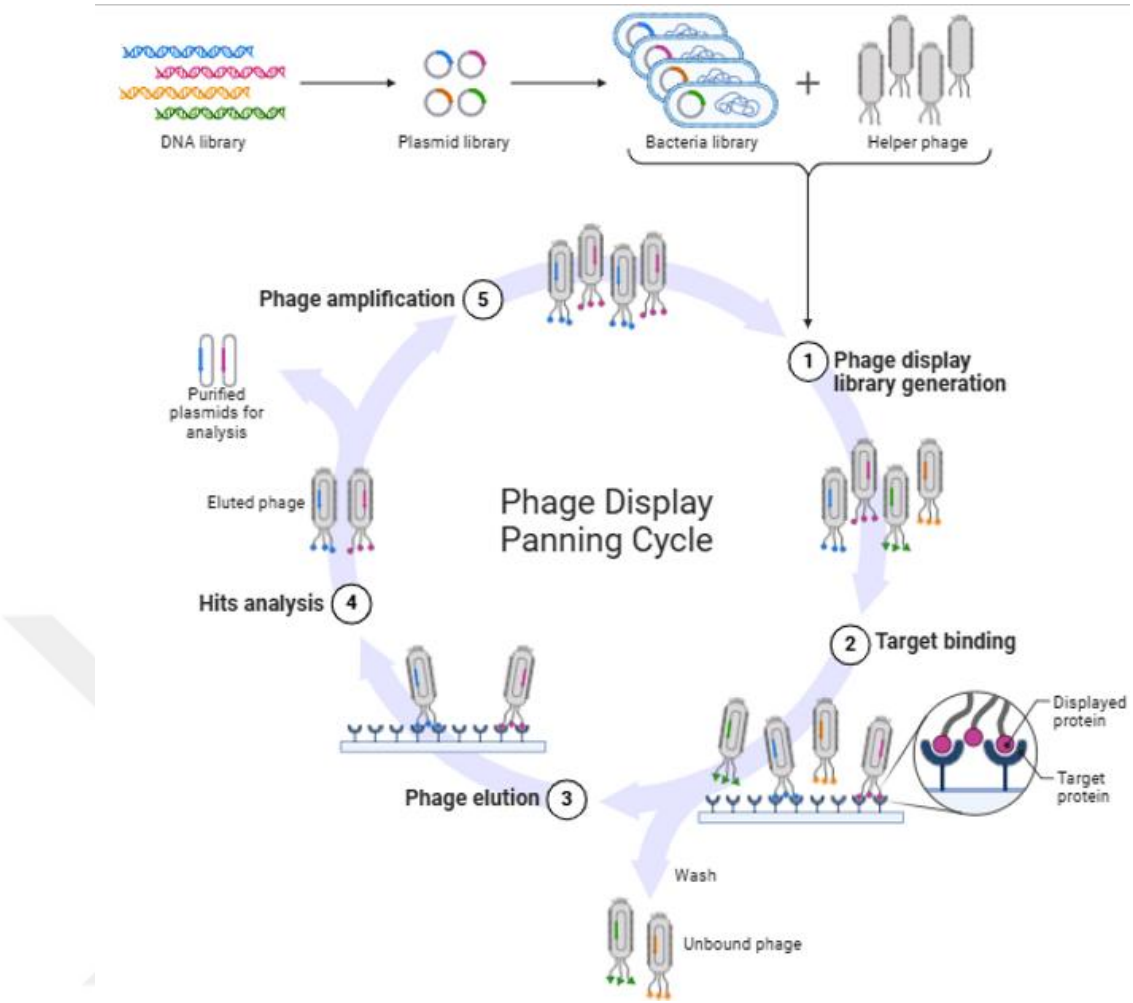

Figure 2.5 Biopanning cycle of phage display. Created with BioRender.

The most common helper phage is M13K07, which includes an antibiotic resistance gene and the P15A ORF. One of the advantages of the M13 helper phage system is that it has a low efficiency in antibody display capacity. Moreover, hyper-phage, which is another phage system, is utilized to display an enhanced number of scFv on the filamentous phage. In this system, helper phage lacks the pIII gene for pIII-antibody polyvalent display, so the phage only expresses the pIII- antibody gene of the phagemid. (S et al., 2001) M13 and fd filamentous phages are the most commonly used vectors in phage display. Filamentous phages infect only Gram-negative bacteria by attaching to bacterial F-pili through the pIII protein. N1 and N2 domains of pIII protein play a role in this interaction. After attaching the F-pilus, the N1 domain interacts with the bacterial TolA receptor. These receptor forms are complex with TolQ and ToIR. The Tol protein complex (Q,R and A) mediates incorporation of phage coat proteins (pIII and pVIII) into the cytoplasmic membrane. Later translocates of the single-stranded DNA (ssDNA). (Armstrong et

al., 1983) Bacteria replicate and express phage coat proteins, which later form phage proteins, which are pI, pXI and pIV. The first phage display study is conducted with M13 bacteriophage by George Smith. M13 bacteriophage has 6.4 kb ssDNA genome with the size 800 nm in length, 6.6 nm in width. M13 genome is well defined with five capsid proteins (pIII, pVI, pVII, pVIII, pIX). M13 virus has a high replication capacity and able to embrace foreign large DNAs, additionally infects bacteria non-lytically.(R et al., 2017) Due to it is non-infective to the humans, it is very useful to work in research. Other bacteriophages are also used including bacteriophage T7, T4 or λ with different advantages or disadvantages. For example, M13 undergoes a lysogenic life cycle that does not kill the host bacteria during infection. In contrast, T7 and T4 viruses follow a lytic life cycle. Additionally, T7 can express large peptides and proteins at a high level, whereas M13 shows a lower capacity for expressing large peptides or proteins. Phage display technology enables the presentation of vast libraries that are randomly generated and re-engineered recombinantly. Various biomolecules are used as delivery agents to specifically target tumor components for therapeutic and diagnostic applications. (T et al., 2012)

Chapter 2:

AIM OF THE THESIS

Cytokines have a key role in tumor-stroma crosstalk. This thesis aims to develop systems for generating antibody-based drugs that target cytokines in the tumor microenvironment using PCR-based technologies. We previously explained that cancer-secreted factors, such as cytokines, influence tumor progression by modulating stromal autophagy and cancer-stroma signaling. One of the crucial cytokines in the tumor microenvironment is CTF1. Due to these results, this thesis's objectives can be listed as:

- Cloning of the CTF1 gene into the bacterial protein expression vector
- Producing recombinant CTF1 protein for use in animal immunization, affinity selection process
- Designing primer sets to cover the mouse IgG repertoire
- Optimization of antibody high and heavy chain fragment primers to generate phage display library
- Optimization of creating scFv structure
- Generation of naïve mouse phage display library

Eventually, this thesis could lead to the generation of new therapeutic antibody-based drugs that can be used clinically.

Chapter 3:

MATERIALS AND METHODS

3.1 Preparation of Competent DH5α and BL21 (DE3) Cells

The Escherichia coli (E.coli) strains BL21(DE3) were prepared with Calcium Chloride treatment. These steps were performed with ice-cold pipette tips, serological tips and Falcon tubes. Due to this technique, bacterial cells can take foreign DNA from outside the cell. To prepare competent E. coli cells, grow the bacteria in LB medium (nzytech, MB14501) until the optical density (OD) at 600 nm reaches 0.3. Then, the bacterial pellet was incubated on ice for 20 minutes, suspended in a cold 100 mM $MgCl_2$ solution, and incubated again for 30 minutes on ice. $MgCl_2$-treated bacterial cells were centrifuged and pelleted, and this pellet was resuspended with 100 mM $CaCl_2$ and 20% (v/v) glycerol-containing solution and quickly frozen to -80 ºC. Aliquots were stored at -80 ºC.

3.2 Cloning of CTF1 protein into the bacterial expression vector

Firstly, the CTF1 gene is amplified using PCR according to the protocol, which is stated below:

Table 3 CTF1 conventional PCR cycle

95 ºC	**95 ºC**	**58 ºC**	**72 ºC**	**72 ºC**	**4 ºC**
5 min.	30 sec.	30 sec.	30 sec.	10 min.	∞
	30X				

Table 4 CTF1 conventional PCR protocol

	Stock concentration	**Amount**
pCMVSPORT6 (Thermo Fisher Scientific, MAN0000443) plasmid (Template DNA)	25 ng	1 µl

dNTP	10 nM	0.5 µl
$MgCI_2$ (Finnzymes, P510M)	10 nM	0.66 µl
Forward primer	10 nM	0.66 µl
Reverse primer	10 nM	0.66 µl
Q5 Reaction Buffer 5x (New England Biolabs, M0491S)	5x	4 µl
Q5 GC enhancer 5x (New England Biolabs, M0491S)	5x	4 µl
Q5 High Fidelity DNA Polymerase (New England Biolabs, M0491S)	100 U	0.3 µl
Nuclease Free Water	Completed till	20 ul

Table 5 Primers used for CTF1 amplification

Name	Sequence
EcorATGCTF1 FWD	AGCAGAATTCATGAGCCGGAGGGAGGG
EcorCTF FWD	AGCAGAATTCAGCCGGAGGGAGGGAAG
SalIATGCTF1 REV	ATTAGTCGACTCAGGCCGAGCCCCCG

After PCR reaction, pGEX-4T-1-3xFLAG bacterial expression vector, pGEX4T2 and CTF1 PCR product were digested with EcoRI (Thermo Fisher Scientific, #ER0271, 00022097) and SalI (Thermo Fisher Scientific, #ER0641,00599758) enzymes. 1 ug plasmid DNA was incubated at 37°C for 2 hours in O buffer (Thermo Fisher Scientific, #BO5, 00040007) with EcorI and SalI. Then, the digested sample was run on 1% agarose (ISOLAB, MB3217002ARW) gel at 100V for 45 mins. According to the manufacturer's protocol, the digested plasmid DNA and PCR product were extracted with an agarose gel extraction kit (Macherey-Nagel, NucleoSpin, Gel and PCR Clean-up, REF 740609.50, LOT 2101/004).

After digesting the gel products, a ligation reaction was performed. The vector plasmid and PCR products were ligated with T4 DNA Ligase (Thermo Fisher Scientific,

EL0011) in 1:3 ligation ratio overnight at 16°C. The new plasmid sequence was verified with Sanger sequencing.

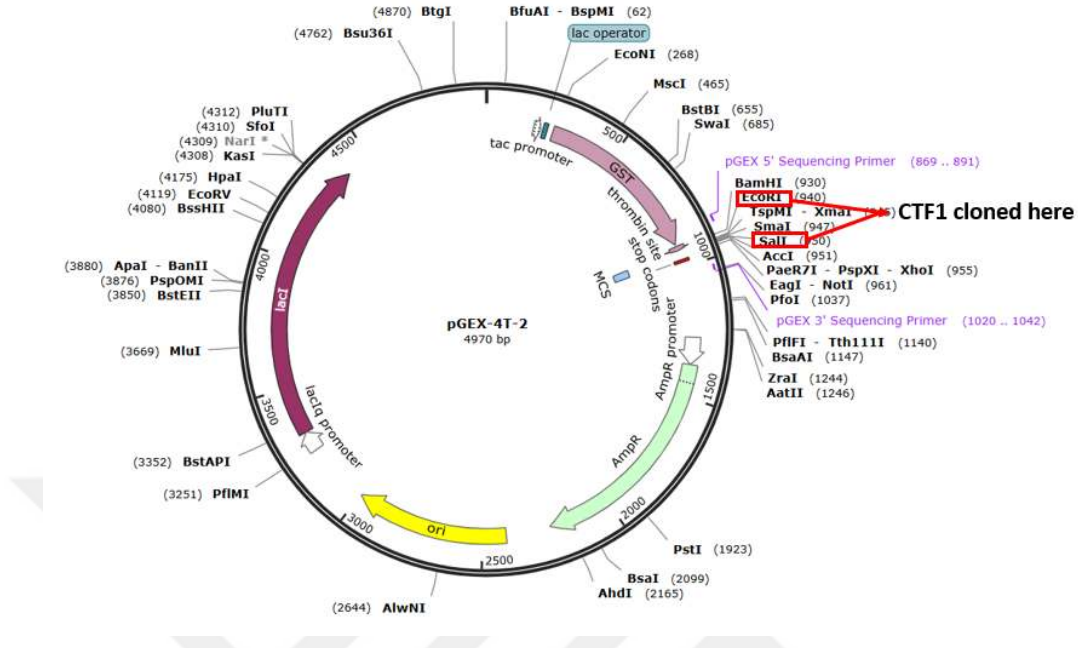

Figure 3 Cloning strategy of CTF1 into the pGEX-4T-2

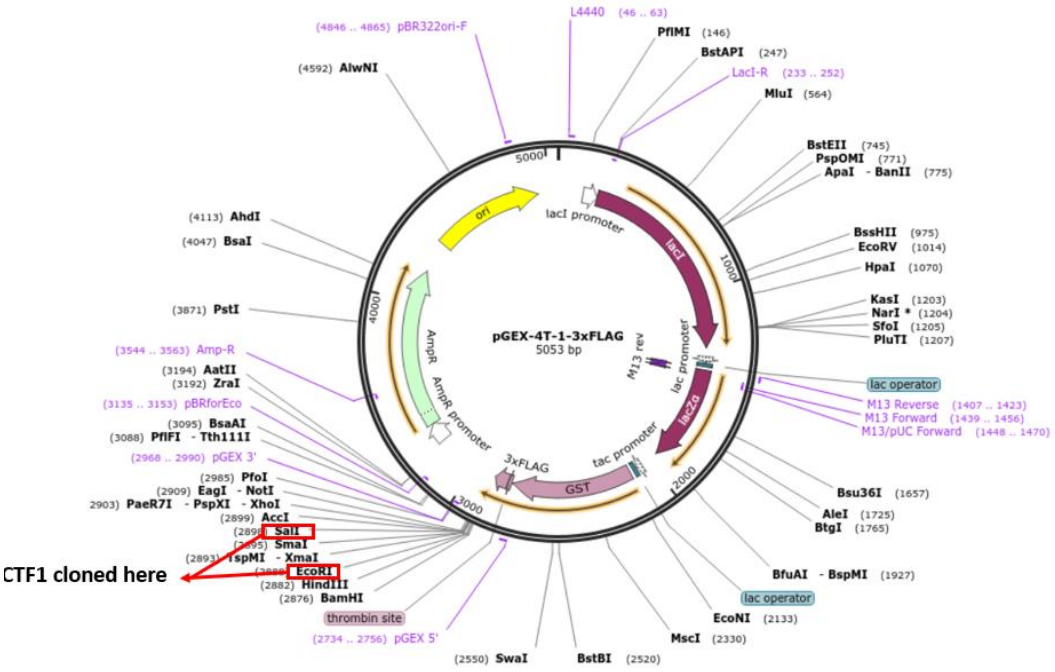

Figure 7 Cloning strategy of CTF1 into the pGEX-4T-1-3xFLAG

3.3 Production of Recombinant CTF1 protein

After verifying the new sequence, the plasmid vector encoding CTF1 was transformed into BL21 cells for recombinant GST-CTF1 protein production. The BL21 strain was also transformed with the original pGEX 4T-1-3xFLAG vector as a control. Competent bacteria was incubated with ligation reaction for 25 minutes on ice. Heat-shock was applied to the bacteria in 42 ºC for 90 seconds and 2-3 minutes on ice again. Transformed bacteria was recovered in 2 ml plain LB for 1.5 hour, 37 ºC bacteria shaker. After the recovery process, bacteria were centrifuged in 2000 rpm for 2 minutes. Pellet was dissolved in 1 ml ampicillin positive LB and spread to the ampicillin plate. Following overnight incubation at 37°C on ampicillin-containing agar plates, single colonies were picked and grown in LB broth. Once the culture reached an optical density corresponding to a bacteria suspension of approximately 0.3, it was divided into two Erlenmeyer flasks. 0.2 mM isopropyl β-d-1 thiogalactopyranoside (IPTG) (Invitrogen, #15529-019) was added to induce GST-fusion protein expression, and bacteria were incubated at 20°C for 16 hours. After protein production, bacteria were centrifuged, and the pellets were resuspended in an appropriate volume of lysis buffer (containing 500 mM NaCl, 50 mM Tris-HCl ph 8.0, 2 mM EDTA, protease and phosphatase inhibitors) with 1% Sarcosyl. The lysates were sonicated for 4 minutes at 37% amplitude (2 seconds on, 5 seconds off), then centrifuged at 3000G for 1 hour at 4°C. The supernatant, containing recombinant proteins, was mixed with 3X loading dye, while the pellets were resuspended in 1X loading dye. Equal volumes of supernatant and pellet were denatured at 95°C for 10 minutes and loaded onto a 12% polyacrylamide gel. The gel was fixed in a solution of 50% methanol (ISOLAB, LR0902111ARQ) and 10% glacial acetic acid (Merck, K39159956 835), then stained with Coomassie Brilliant Blue (C.T 42655,43016763) to visualise the protein bands.

3.4 Preparation of Coomassie gel solutions

Fixation solution: %40 MetOH, %10 glacial asetic acid and %40 dH2O water were mixed together. Final volume is 50 ml. 12% SDS-PAGE gel was fixed for 10 minutes at room temperature.

Coomassie brilliant blue staining: 0.25 g of Coomassie Brilliant blue R-250 was weighed and dissolved with 10% glacial acetic acid and 45% methanol. After the fixation process, the gel was dyed with Coomassie Brilliant blue R-250 for 5 minutes.

Destaining solution: For preparing the destaining solution, 10% glacial acetic acid, 40% methanol, and 50% water were mixed together. After the dying process, the gel was washed with the destaining solution for 20 minutes. At the end of 20 minutes, the gel was put into the water and left in RT on the shaker overnight.

3.5 Purification of CTF1 protein

After identifying proteins in the Coomassie gel for CTF1 protein purification, glutathione Sepharose 4B (GE Healthcare, 17-0756-01) beads were used. A 20 µl bead solution was washed with bacteria lysis buffer containing protease inhibitor and PMSF to remove the storage solution and equilibrate the beads. Next, bacterial lysate was loaded onto the beads and incubated overnight at 4 °c on a rotator. Beads coupled with GST and GST-tagged protein were then incubated with an appropriate amount of pull-down buffer (20 mM L-Reduced Glutathione [Fluka Analytical, 49750], 50 mM Tris-HCl, pH 8.0, 5% glycerol, final ph 8.0) at RT for 15 minutes on a rotator. The samples were subsequently run on a 12% polyacrylamide gel and stained with Coomassie Blue to confirm successful purification and elution.

3.6 RNA isolation and cDNA conversion

Total RNA was extracted from naïve mouse spleen using TRIzol reagent (Invitrogen, 15596018) according to the manufacturer's instructions. Cells were lysed with TRIzol, and nucleic acids were separated by adding 200 µL of chloroform (Sigma-Aldrich, LOT K53823345). After vortexing until the lysate turns pink, incubate at room temperature for 3-5 minutes. Lysates centrifuged at 12.000 g for 15 minutes at 4 °C. The RNA-containing phase was transferred to new tubes and precipitated with a 1:1 ratio of isopropanol (Sigma-Aldrich, STBH3504). The supernatant was discarded, and 0.75 ml of 70% ice-cold ethanol was added to wash the RNA pellet. After vortexing the solution, the samples were centrifuged at 12.000 g for 5 minutes at 4°C. The resulting RNA pellet was resuspended in an appropriate volume of DEPC water. The concentration and purity of the RNA samples were measured using a Nanodrop. The RNA samples were kept in -80 °C until the following experiment.

Table 6 cDNA conversion protocol 1

	Stock concentration	**Amount**
RNA stock	1 ug	-

DNase I buffer with $MgCI_2$ (Thermo Fisher Scientific, B43)	10X	2 µl
DNase I (1 U/ul RNase Free (Thermo Fisher Scientific, EN0521)	1000 U	1 µl
DEPC water	Completed till	9 µl

The reaction mixture was incubated at 37 °c for 30 minutes. Subsequently, 1 µl of 25 mM EDTA was added, and the mixture was incubated at 75 °c for 10 minutes. To synthesize cDNA from RNA via reverse transcription, the master mix was prepared according to the protocol below, and 10 µl of this master mix was added to each PCR tube containing DNase I-treated RNA samples.

Table 7 cDNA conversion protocol 2

	Concentration	Amount
Random hexamer (Invitrogen, P/N58875, LOT1153658)	300 ug	2 µl
dNTP mix	10 nM	0.5 µl
RT buffer (Thermo Fisher Scientific,3037603)	5X	4 µl
Ribolock enzyme (Thermo Fisher Scientific, EO0381)	40 U	0.2 µl
RT (reverse transcriptase) enzyme (Thermo Fisher Scientific, EP0441)	200 U	0.1 µl
Water		4.2 µl

3.7 PCR amplification of light and heavy chain fragments

18 light chain fragments forward and reverse primers and 18 heavy chain fragments forward and reverse primers were used with naïve mouse spleen cDNA as a template while performing PCR. PCR reactions were optimized to find the most efficient way to

amplify these fragments. Because of that, each primer set has different annealing temperatures.

Table 8 Light Chain and Heavy Chain PCR protocol

	Concentration	**Amount**
Q5 Reaction Buffer (New England Biolabs, M0491S)	5X	4 µl
Q5 High Fidelity Polymerase (New England Biolabs, M0491S)	100 U	0.3 µl
Q5 GC enhancer (New England Biolabs, M0491S)	5X	4 µl
Template naïve mouse spleen cDNA	1 ug	2 µl
$MgCI_2$	10 nM	0.5 µl
Forward primers	10 nM	0.66 µl
Reverse primers	10 nM	0.66 µl
dNTP	10 nM	0.5 µl
NF water	Up to 20 µl	7.38 µl

Table 9 PCR cycle for amplifying 18 light chain fragments

95 °C	**95 °C**	**54 °C**	**72 °C**	**72 °C**	**4 °C**
3 min.	30 sec.	30 sec.	30 sec.	10 min.	∞
	35X				

Table 10 PCR cycle for amplifying 9 heavy chain (REV1) fragments

95 °C	**95 °C**	**55 °C**	**72 °C**	**95 °C**	**63 °C**	**72 °C**	**72 °C**	**4 °C**
3 min.	30 sec.	30 sec.	45 sec.	30 sec.	30 sec.	45 sec.	2 min.	∞
	5X			30X				

Table 11 PCR cycle for amplifying 9 heavy chain (REV2) fragments

95 ºC	**95 ºC**	**58 ºC**	**72 ºC**	**95 ºC**	**63 ºC**	**72 ºC**	**72 ºC**	**4 ºC**
3 min.	30 sec.	30 sec.	45 sec.	30 sec.	30 sec.	45 sec.	2 min.	∞
	5X			30X				

After PCR reactions, PCR products were loaded into a 1% agarose gel and run for 45 minutes at 100V. They were then isolated from the gel using a gel extraction kit (MN) and stored at 20°C.

3.8 Splicing by Overlap Extension (SOE) PCR

After the gel extraction step, the DNA concentration of VH and VL PCR products was measured. It was calculated as 100 ng for each VH and VL fragment to amplify. The final amplified DNA concentration to produce the scFv structure is 200 ng. SOE PCR is repeated to get the maximum DNA concentration for the cloning steps.

Table 12 Splicing by Overlap Extension (SOE) PCR protocol

	Concentration	**Amount**
Q5 Reaction Buffer (New England Biolabs, M0491S)	5x	4 ul
Q5 GC enhancer (New England Biolabs, M0491S)	5x	4 ul
Q5 High Fidelity Polymerase (New England Biolabs, M0491S)	100U	0.3 ul
mscFV FWD primer (added at the second step)	10 nM	0.66 ul
mscFV REV primer (added at the second step)	10 nM	0.66 ul
$MgCI_2$ (Finnzymes, P510M)	10 nM	0.66 ul
dNTP	10 nM	0.5 ul
Template DNA (volumes will be determined		-

according to gel isolation concentration)

In the first SOE PCR step, primers were not added to enhance the joining reaction.

Table 13 First step of SOE-PCR without primers

94 ºC	**63 ºC**	**68 ºC**	**4ºC**
60 sec.	60 sec.	2 min.	∞
	10x		

Table 14 Second step of SOE PCR with primers

95 ºC	**95 ºC**	**55 ºC**	**72 ºC**	**72 ºC**
5 min.	1 min.	1 min.	1 min.	10 min.
	35X			

After the second PCR cycle, the PCR products were loaded onto a 1% agarose gel. A heavy and light chain fragment mix was also loaded as a control condition.

3.9 Cloning of scFv structure into the phage display pCANTAB5e vector

SOE PCR products were isolated from gel using agarose gel extraction kit (Macherey-Nagel, NucleoSpin, Gel and PCR Clean-up, REF 740609.50, LOT 2101/004) protocol. After that, the phage display vector pCANTAB5e and the SOE PCR product were digested with the SfiI and NotI restriction enzymes. First, the PCR product and vector were digested for 1 hour at 50 ºC with the SfiI enzyme in the G buffer. Later, they were digested with NotI at 37 °C and then again with G buffer. After that, the digested products were visualised and digested from gel using the same agarose gel extraction kit (Macherey-Nagel, NucleoSpin, Gel and PCR Clean-up, REF 740609.50, LOT 2101/004) with the same protocol. Finally, the ligation reaction was set to ligate the scFv structure and pCANTAB5e using T4 DNA Ligase (Thermo Fisher Scientific,

EL0011) in a 1:8 ligation ratio overnight at 16°C. The new plasmid sequence was verified with Sanger sequencing.

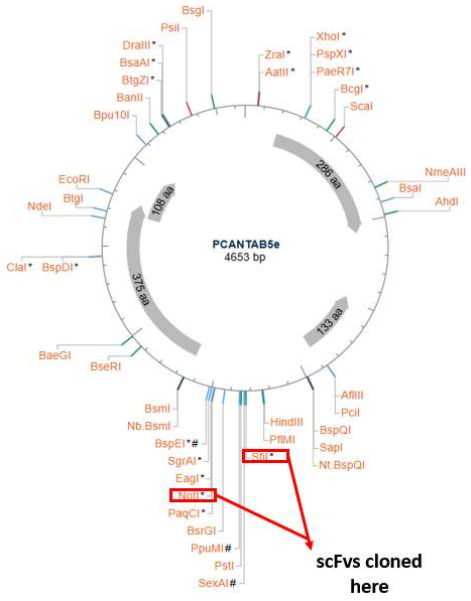

Figure 6 Cloning strategy of scFvs into the pCANTAB5e. Created with NebCutter^{TM} v3.0

3.10 Immunoblotting and Antibodies

Protein was loaded, separated in 12% SDS-polyacrylamide gel, and then transferred to NC membranes. Following blocking with 5% (w/v) non-fat milk powder (Biorad, 1706404) in 1X PBS-T (PBS and 0.05% Tween 20, pH 7.4) or 3% BSA (w/v) (Sigma-Aldrich, A3059) in 1X TBS-T (TBS and 0.05% Tween 20, pH 7.4) for phosphorylated proteins, membranes were incubated overnight at a cold room with 3% BSA PBST containing primary antibodies. After three washing, the membranes were treated for one hour at room temperature with suitable secondary antibodies in blocking solution. Protein bands were observed with ChemiDoc MP Imaging equipment (Bio-Rad). Band intensity was quantified using ImageLab software and standardized to intensities of ß-actin bands (phosphorylated proteins were normalized to total levels of the interesting protein).Following primary antibodies were used :Anti-CTF1 (Boster Bio, # A08056, 1:1000) , Anti-GST (CST, #2622S, 1:1000)

Table 15 All primer sequences that are used in creating a naive mouse phage display library

Name	Sequence
VL1 FWD	CGTCGGCCCAGCCGGCCCGATGTTTTGATGACCCAAACT
VL2 FWD	CGTCGGCCCAGCCGGCCCGATATTGTGATGACGCAGGCT
VL3 FWD	CGTCGGCCCAGCCGGCCCGATATTGTGATAACCCAG
VL4 FWD	CGTCGGCCCAGCCGGCCCGACATTGTGCTGACCCAATCT
VL5 FWD	CGTCGGCCCAGCCGGCCCGACATTGTGATGACCCAGTCT
VL6 FWD	CGTCGGCCCAGCCGGCCCGATATTGTGCTAACTCAGTCT
VL7 FWD	CGTCGGCCCAGCCGGCCCGATATCCAGATGACACAGACT
VL8 FWD	CGTCGGCCCAGCCGGCCCGACATCCAGCTGACTCAGTCT
VL9 FWD	CGTCGGCCCAGCCGGCCCCAAATTGTTCTCACCCAGTCT
VL REV 1	GGATCCGCCGCCGCCAGAACCACCACCACCCCGTTTCAGCTCCAG CTTG
VL REV 2	CCTAGGGCCGCCGCCAGAACCACCACCACCCCGTTTTATTTCCAGC TTGGT
VH1 FWD	GGTGGTGGTGGTTCTGGCGGCGGCGGATCCCAGGTGCAGCTGAAG GAGTC
VH2 FWD	GGTGGTGGTGGTTCTGGCGGCGGCGGATCCCAGGTGCAGCTGAAG GAGTC

VH3 FWD	GGTGGTGGTGGTTCTGGCGGCGGCGGATCCCAGGTGCAGCTGAAG CAGTC
VH4 FWD	GGTGGTGGTGGTTCTGGCGGCGGCGGATCCCAGGTTACTCTGAAA GAGTC
VH5 FWD	GGTGGTGGTGGTTCTGGCGGCGGCGGATCCGAGGTCCAGCTGCAA CAATCT
VH6 FWD	GGTGGTGGTGGTTCTGGCGGCGGCGGATCCGAGGAGGTCCAGCTG CAGCAGTC
VH7 FWD	GGTGGTGGTGGTTCTGGCGGCGGCGGATCCCAGGAGGTCCAACTG CAGCAGCCT
VH8 FWD	GGTGGTGGTGGTTCTGGCGGCGGCGGATCCGAGGTGAAGCTGGTG GAGTC
VH9 FWD	GGTGGTGGTGGTTCTGGCGGCGGCGGATCCGAGGTGAAGCTGCTG GAATC
VH REV 1	TTCTATGCGCGCGGCCGCTTATGCAGAGAGAGTGACCAGAGT
VH REV 2	TTCTATGCGCGCGGCCGCTTATGAGGAGACTGTGAGAGTGGT
MscFv FWD	CGTCGGCCCAGCCGGCCC
MscFv REV	TTCTATGCGCGCGGCCGCTTA

Chapter 4:

RESULTS

4.1 Recombinant CTF1 protein production

4.1.1 Cloning of CTF1 ATG (+) gene into the pGEX4T-2 vector

4.1.1.1 CTF1 ATG (+) gene amplification with PCR

CTF1 gene encodes 606 base pairs. CTF1 gene amplification performed by PCR with normal PCR conditions at the annealing temperature of 58 ºC. In this PCR, EcorI ATG CTF1 FWD and SalI REV primers are used. Results are showed in figure 4.1.1

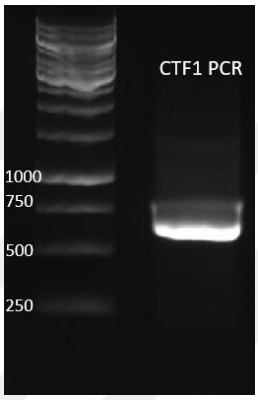

Figure 4.1.1 Agarose gel electrophoresis result of CTF1 PCR amplification. Results are visualized with 1% agarose gel.

After performing CTF1 PCR, the amplicon was isolated from the gel using the MN kit manuals. pGEX4T2 and CTF1 PCR product was digested with EcorI and SalI using O buffer at 37 ºC. Results are shown in figure 4.1.1.2

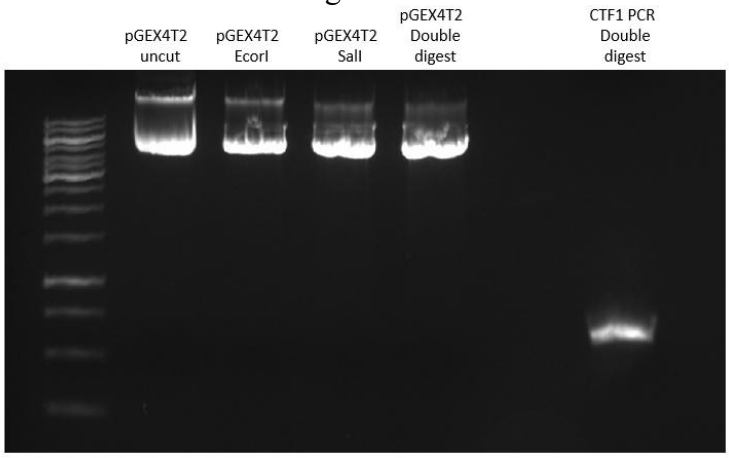

Figure 4.1.1.2 pGEX4T2 vector and CTF1 PCR product enzyme digestion using EcorI and SalI with O buffer at 37 ºC. Results are visualized with 1% agarose gel.

Digested vector and PCR product were isolated from agarose gel again using MN kit manufacturer protocols. After the isolation, DNA concentration were measured using nanodrop and ligated using T4 ligase enzyme and ligase buffer in a 1:3 ligation ratio, 16 ^{o}C overnight. Next day, ligation reaction is transformed to the *Dh5α* E.coli bacteria using heat-shock method. After the transformation process, bacteria are recovered in plain LB for 1.5 hours, and bacteria are spread to the ampicillin-containing agar plate. Next morning, 10 colonies were picked for cloning verification. Colonies left overnight in ampicillin containing LB for growing. After that, colonies are isolated using home-made mini prep kit and digested with EcorI and SalI using O buffer at 37^{o}C again for cloning verification. The colonies that have 606 bp CTF1 PCR product when enzyme digestion performed are positive. Result are showed in figure 4.1.1.3

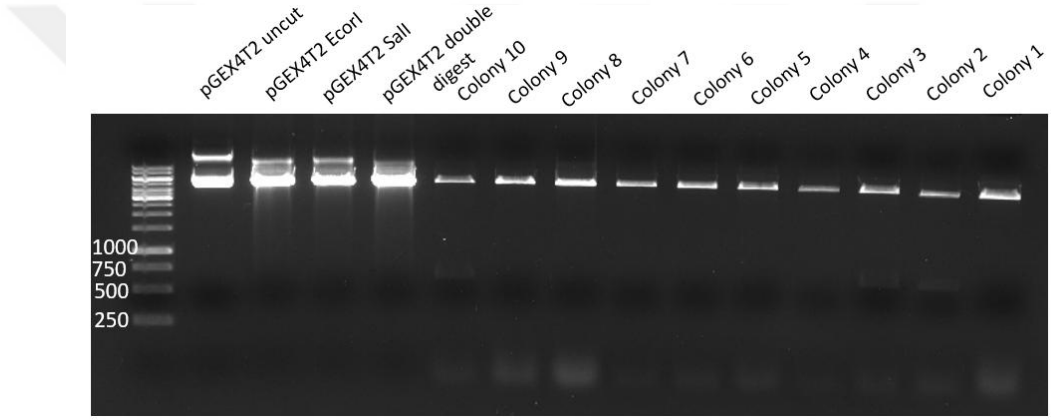

Figure 4.1.1.3 Agarose gel electrophoresis of pGEX4T2-CTF1 ATG (+) cloning. Empty vector, single EcorI digested, single SalI digested, and double digested pGEX4T2 vector loaded to the gel as a digestion control. Colonies were digested with both EcorI and SalI enzymes in O buffer, 37 ^{o}C for 2 hours. Colony 10, Colony 2 and Colony 3 are positive. Results are visualized with 1% agarose gel.

4.1.1.4 Purification of pGEX4T-2 CTF1 ATG (+) protein

After verifying the pGEX4T2-CTF1 ATG (+) vector construct, colonies 2,3 and 10 are transformed to the *BL21* E. coli to start recombinant protein production using the same transformation protocol. After the transformation and bacteria recovery process, bacteria are spread to ampicillin-containing agar plates and incubated overnight. The Figure 4.1.1.5 GST-CTF1 protein expression in BL21(DE3) bacteria with 0.2 mM IPTG at 20 °C was controlled by Coomassie staining. Using loading dye, bacteria was directly lysed at 95°C. There isn't any difference between ATG (+) colonies either. Results are visualised with a western blot.

next morning, bacterial colonies are picked in 1 mL of ampicillin-positive LB and incubated for several hours at 37 ºC a bacterial shaker. When bacteria grow, they are incubated in 50 mL of ampicillin-positive LB at 37 ºC a bacterial shaker. Optical density (OD) is frequently checked via a plate reader at 600 nm until the bacteria's OD reach 0.3. When OD reached 0.3, 50 mL of the bacteria was aliquoted to the 25 mL flasks and 1mM IPTG was added or not. Bacteria were incubated at 20 ºC a bacterial shaker. After 16 hours, OD was rechecked, and 0.7 OD was noted. 1 ml of bacteria was aliquoted from each group, the rest of the bacteria was centrifuged at max rpm for 10 minutes, and the pellet was stored at -80 ºC until the following experiment. 1 ml of bacteria pellet was lysed with 1x loading dye with SDS at 95 °C. Loading dye volume was determined based on the OD value. After the bacteria lyse, supernatants are loaded to 12% SDS-PAGE gel. Results are shown in Figure 4.1.1.4

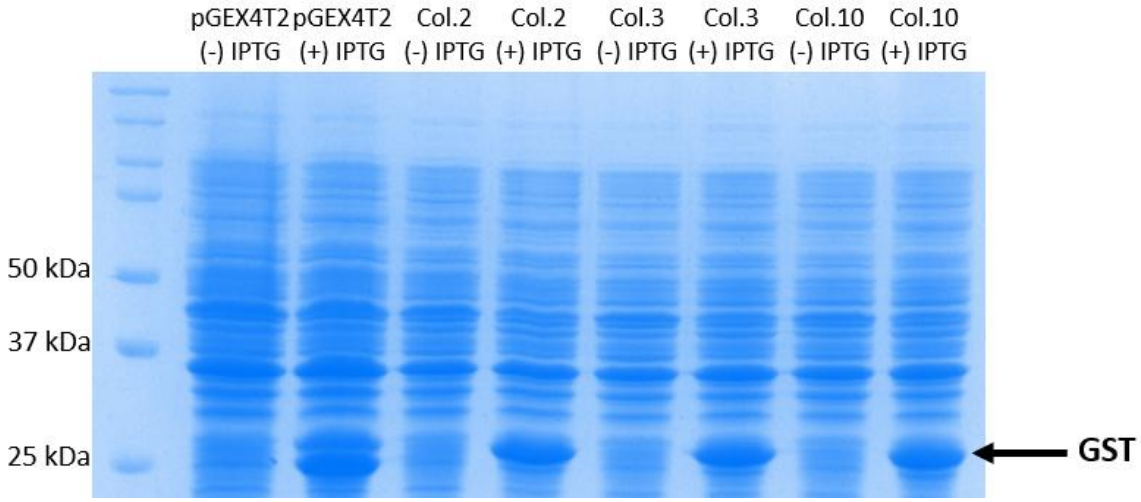

Figure 4.1.1.4 CTF1 and GST protein expression in Colony 2, 3 and 10. (A) CTF1 protein expression is observed in Colonies 2, 3, and 4 when BL21 E. coli bacteria are induced with IPTG. (B) GST protein expression is observed in Colonies 2, 3, and 10 when *BL21* E. coli bacteria are induced with IPTG.

When we saw there is no difference between IPTG (+) and IPTG (-) groups bacteria colonies were verified though western blot.

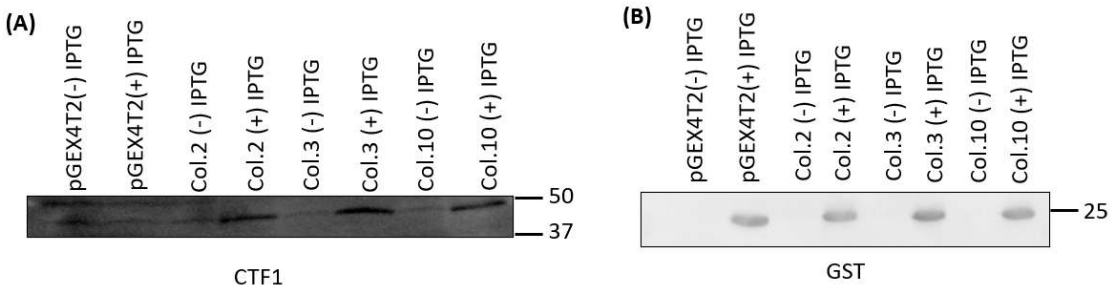

After colonies were verified for producing CTF1, bacteria were lysed through the lysis buffer with sonication, as stated in the materials and methods section. Pellet and supernatant loaded to the 12% SDS-PAGE gel again to check protein expression.

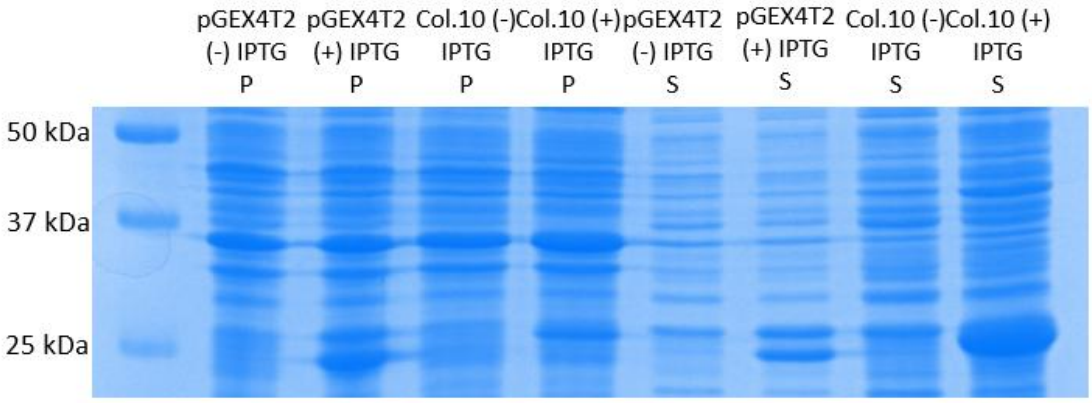

Figure 4.1.1.6 Purification of GST-CTF1 protein. After observed CTF1 and GST expression in Western Blot, ATG (+) pGEX-4T-2 colonies further purified with %2 sarcosyl contained lysis buffer. Bacterial pellet and supernatant were controlled by Coomassie Staining of SDS-PAGE gel. GST-CTF1 protein didn't observed at pellet or supernatant. Result are visualized with 12% SDS-PAGE gel coomassie staining

4.1.2 Cloning of CTF1 ATG (-) gene into the pGEX4T-2 vector

After the Coomassie gel results, another round of pGEX4T-2-CTF1 cloning was performed. This time, ATG (+) EcorI FWD and SalI REV primers were used for CTF1 PCR. Results are shown in figure 4.1.2.1

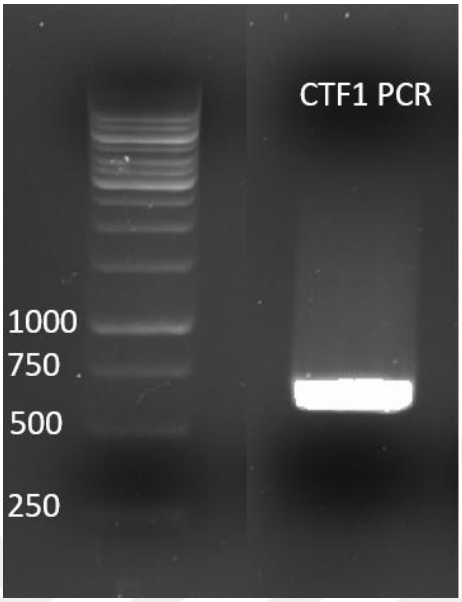

Figure 4.1.2.1 Agarose gel electrophoresis result of CTF1 PCR amplification. Results are visualized with 1% agarose gel.

After performing CTF1 PCR, the amplicon was extracted from the gel following the MN kit protocols. The pGEX4T2 plasmid and CTF1 PCR product were digested with EcorI and SalI enzymes in O buffer at 37°C. The digested vector and PCR product were isolated from an agarose gel using MN kit protocols. After isolation, DNA concentrations were measured with a nanodrop, then ligated with T4 ligase and ligase buffer at a 1:3 ratio overnight at 16°c. The following day, the ligation mixture was transformed into Dh5α E. coli cells via heat-shock. Post-transformation, bacteria were recovered in plain LB medium for 1.5 hours and then spread onto ampicillin-containing agar plates. The next morning, 10 colonies were selected for cloning verification. These colonies were incubated overnight in ampicillin LB for growth, then prepared using a homemade mini prep kit. The plasmids were digested with EcorI and SalI enzymes in O

buffer at 37 °c for verification. Colonies producing a 606 bp PCR product after enzyme digestion were identified as positive.

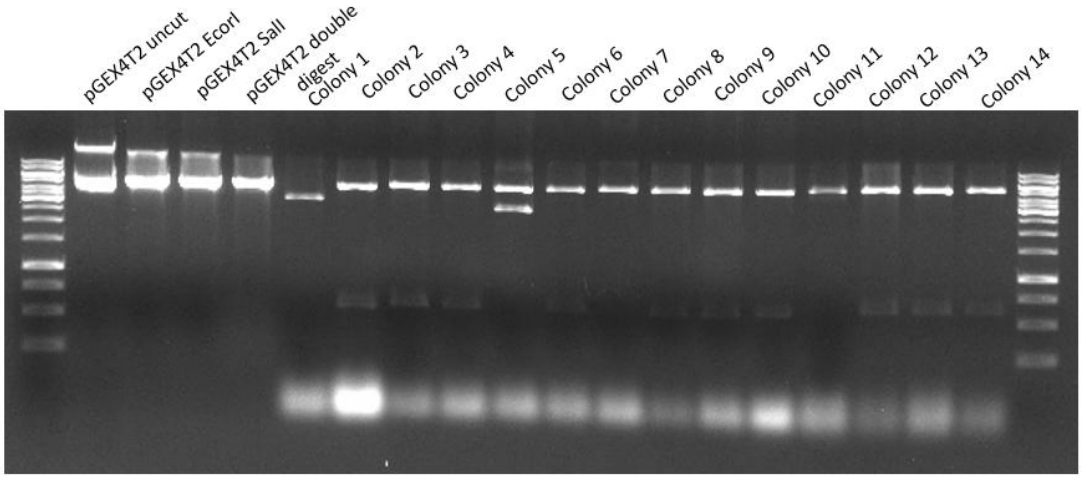

Figure 4.1.2.2 Agarose gel electrophoresis of pGEX4T2-CTF1 ATG (-) cloning. Empty vector, single EcorI digested, single SalI digested and double digested pGEX4T2 vector loaded to the gel as a digestion control. Colonies were digested with both EcorI and SalI enzymes in O buffer, 37 ºC for 2 hours. Except Colony 1, Colony 4, Colony 6 and Colony 10 rest of the colonies are positive. Results are visualized with 1% agarose gel

4.1.2.3 Purification of pGEX4T-2 CTF1 ATG (+) protein

After verifying the pGEX4T2-CTF1 ATG (-) vector construct, colonies 2, 3 and 10 were transformed into BL21 E. coli to initiate recombinant protein production using the same transformation protocol. After transformation and bacterial recovery, the bacteria were spread onto ampicillin-containing agar plates and incubated overnight. The following morning, bacterial colonies were picked into 1 mL of ampicillin-positive LB and incubated for several hours at 37 °c on a bacterial shaker. Once the bacteria grew, they were transferred into 50 mL of ampicillin-positive LB for incubation at 37 °c on a shaker. Optical density (OD) was regularly measured with a plate reader at 600 nm until the OD reached 0.3. When OD reached 0.3, 50 mL of bacteria was aliquoted into 25 mL flasks, with some flasks receiving 0.2 mm IPTG. The bacteria were then incubated at 20 °c on a shaker. After 16 hours, OD was remeasured and reached approximately 0.7. From each group, 1 ml of bacteria was aliquoted, while the remaining bacteria were centrifuged at maximum rpm for 10 minutes, with the pellet stored at- 80 °c for later use. The 1 ml of bacterial pellet was lysed with 1x SDS loading dye at 95°c. The

volume of loading dye was based on the OD. After lysis, the supernatants were loaded onto a 12% SDS-PAGE gel. The results are shown in the figure 4.1.2.3

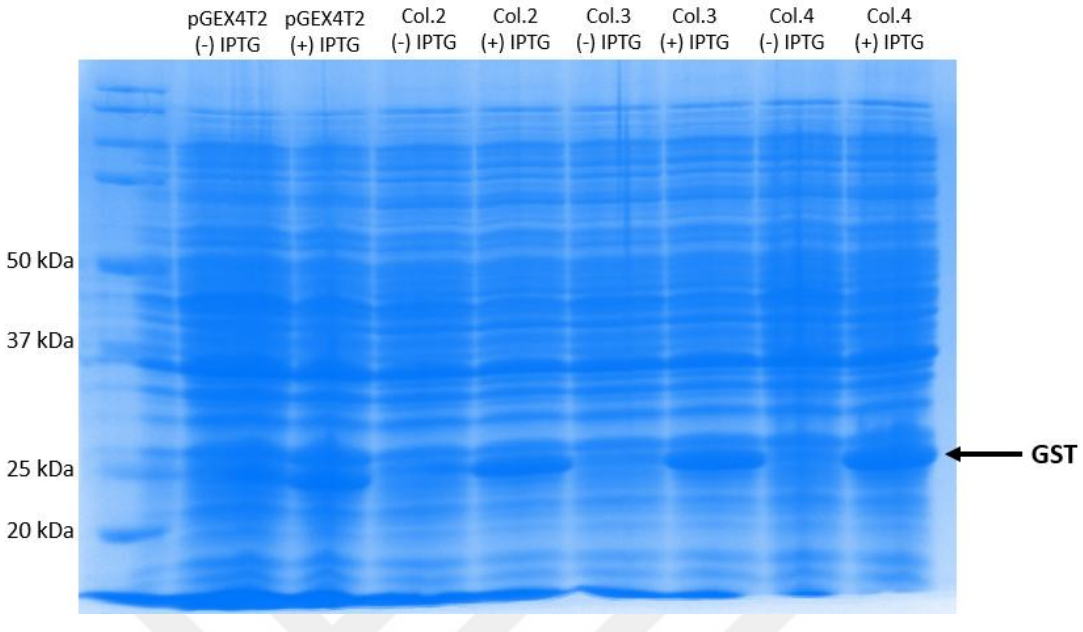

Figure 4.1.2.3 GST-CTF1 protein expression in BL21(DE3) bacteria with 1 mM IPTG at 20 °C was controlled by Coomassie staining. Using loading dye, bacteria was directly lysed at 95°C. There isn't any difference between ATG (-) colonies. Results are visualised with a 12% SDS-PAGE gel, Coomassie staining.

Moreover, because there is no difference between Colony 2, 3, and 10 in IPTG (+) groups in Coomassie staining, we decided to do a western blot to see protein expression. Bacteria lyse supernatants were loaded to a 12% SDS-PAGE gel again, and the gel was transferred to the NC membrane. The membrane was blocked with 5% milk and incubated with CTF1 and GST antibody overnight in a 4ºC shaker. Next day results are visualized. Results are shown in figure 4.1.2.4

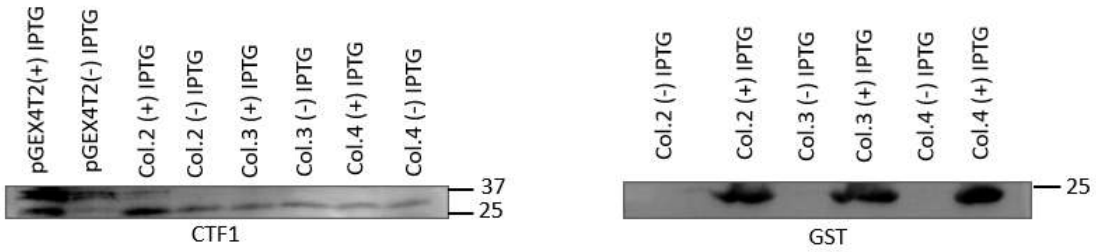

Figure 4.1.2.4 GST-CTF1 protein expression in BL21(DE3) bacteria with 0.2 mM IPTG at 20 °C was controlled by Coomassie staining. Using loading dye, bacteria was directly lysed at 95°C. There isn't any difference between ATG (+) colonies either. Results are visualised with a western blot.

After seeing the results of Western blot Colony 2, 3, and 10, we decided that CTF1 protein expression is valid but not enough to see on a Coomassie staining gel. Later, we picked colony 10 to continue with bacterial lysis with the lysis buffer using the same sonication protocol. Supernatant and pellet were loaded the 12% SDS-PAGE gel. Results are shown in figure

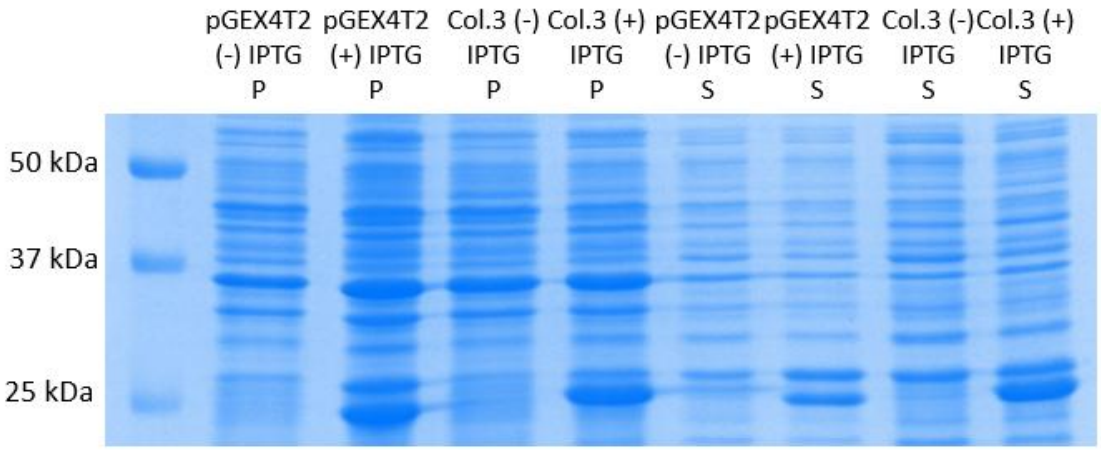

Figure 4.1.2.5 Purification of GST-CTF1 protein. After observed CTF1 and GST expression in Western Blot, ATG (+) pGEX-4T-2 colonies further purified with %2 sarcosyl contained lysis buffer. Bacterial pellet and supernatant were controlled by Coomassie Staining of SDS-PAGE gel. GST-CTF1 protein didn't observed at pellet or supernatant. Result are visualized with 12% SDS-PAGE gel coomassie staining.

4.1.3 Cloning of CTF1 ATG (+) gene into the pGEX4T-1- 3x-FLAG vector

In this moment, we decided to clone the CTF1 gene into the pGEX4T-1-3x-FLAG vector. The CTF1 gene was amplified using ATG (+) primers, EcorI ATG FWD and SalI REV. The PCR product and vector were digested with EcorI and SalI enzymes in O buffer at 37°c. After digestion, both were purified from an agarose gel using MN kit protocols. The DNA concentrations were measured with a Nanodrop, then ligated with T4 ligase and ligase buffer at a 1:3 ratio overnight at 16°c. The next day, the ligation mixture was transformed into Dh5α E. coli cells through heat-shock. Post-transformation, the bacteria were recovered in plain LB medium for 1.5 hours and then spread onto ampicillin-containing agar plates. The following morning, 10 colonies were selected for cloning verification. These colonies were incubated overnight in ampicillin LB, then prepared with a homemade mini prep kit. The plasmids were digested with

EcorI and SalI enzymes in O buffer at 37 °c for verification. Colonies that produced a 606 bp PCR product after digestion were identified as positive.

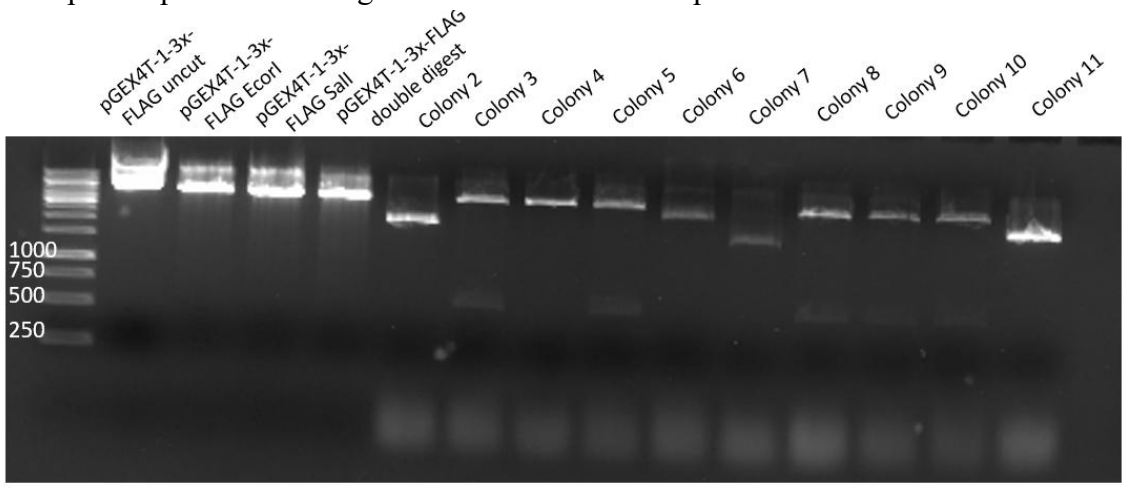

Figure 4.1.3.1 Agarose gel electrophoresis of pGEX4T-1-3x-FLAG-CTF1 ATG (+) cloning. Empty vector, single EcorI digested, single SalI digested and double digested pGEX4T-1-3x-FLAG vector loaded to the gel as a digestion control. Colonies were digested with EcorI and SalI enzymes in O buffer at 37 oC for 2 hours. Colony 3, colony 5, colony 8, colony 9 and colony 10 are positive. Results are visualised with 1% agarose gel.

After confirming the pGEX4T-1-3x-FLAG-CTF1 ATG (+) vector construct, colonies 5, 8, and 9 were transformed into BL21 E. coli to produce recombinant protein, following the same transformation protocol. Post-transformation and bacterial recovery, the bacteria were spread onto agar plates with ampicillin and incubated overnight. The next day, colonies were picked into 1 ml of ampicillin-containing LB and incubated at 37 °C on a shaker for several hours. Once grown, they were transferred into 50 mL of ampicillin-positive LB for further incubation at 37 °C on a shaker. Optical density (OD) was regularly measured at 600 nm until it reached 0.3. At this point, 50 mL of bacteria was aliquoted into 25 mL flasks, with some receiving 0.2 mm IPTG. The bacteria were then incubated at 20 °C on a shaker. After 16 hours, OD was remeasured; it reached approximately 0.7. From each group, 1 ml of bacteria was aliquoted, and the remaining bacteria were centrifuged at maximum rpm for 10 minutes, with the pellet stored at- 80 °C for later use. The 1 ml bacterial pellet was lysed with 1× SDS loading dye at 95°C. The volume of dye was based on OD. After lysis, supernatants were loaded onto a 12% SDS-PAGE gel. The results are shown in the figure 4.1.3.2

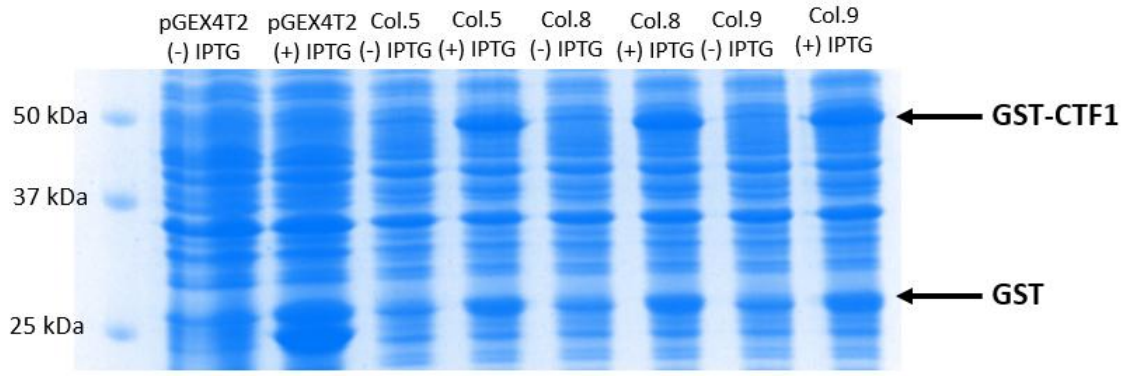

Figure 4.1.3.2 GST-CTF1 protein expression in BL21(DE3) bacteria with 0.2 mM IPTG at 20 °C was controlled by Coomassie staining. Using loading dye, bacterial dye was directly lysed at 95°C. Recombinant CTF1 protein is induced all of the ATG (+) pCMV-4T-1-3xFLAG colonies. Results are visualised with a 12% agarose gel Coomassie staining.

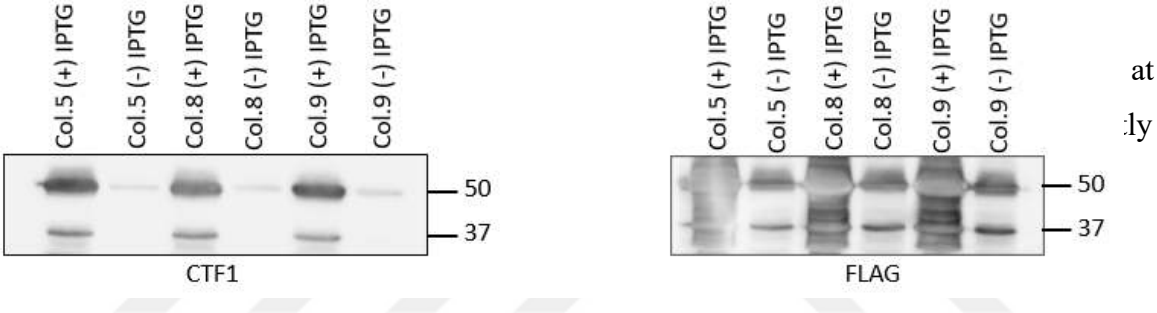

Figure 4.1.3.3 CTF1 and GST protein expression in Colonies 5, 8, and 9. (A) CTF1 protein expression is observed in Colonies 5, 8, and 9 when *BL21* E. coli bacteria are induced with IPTG. (B) GST protein expression is observed in Colonies 5, 8, and 9 when *BL21* E. coli bacteria are induced with IPTG.

After protein production results were verified via Coomassie staining and western blot, Col.8 was picked to continue protein purification. Bacteria were lysed through lysis buffer via sonication, as explained in the Materials and Methods section. After the sonication process, the pellet and supernatant were loaded onto the 12% SDS-PAGE gel again to see if the bacteria had been successfully lysed and if the protein of interest was in the supernatant.

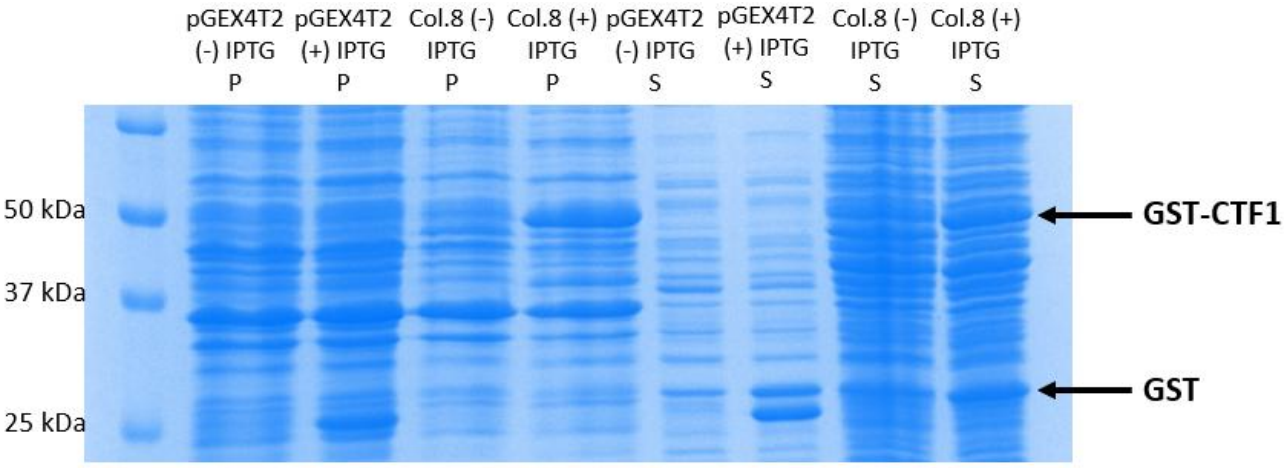

Figure 4.1.3.4 Purification of GST-CTF1 protein. After observing CTF1 and GST expression in Western Blot, ATG (+) pGEX-4T-1-3xFLAG colony 8 was further purified with 2% sarcosyl-containing lysis buffer. Coomassie Staining of SDS-PAGE gel controlled bacterial pellet and supernatant. GST-CTF1 protein was observed both in the bacterial pellet and the supernatant. Results are visualised with a 12% SDS-PAGE gel coomassie staining.

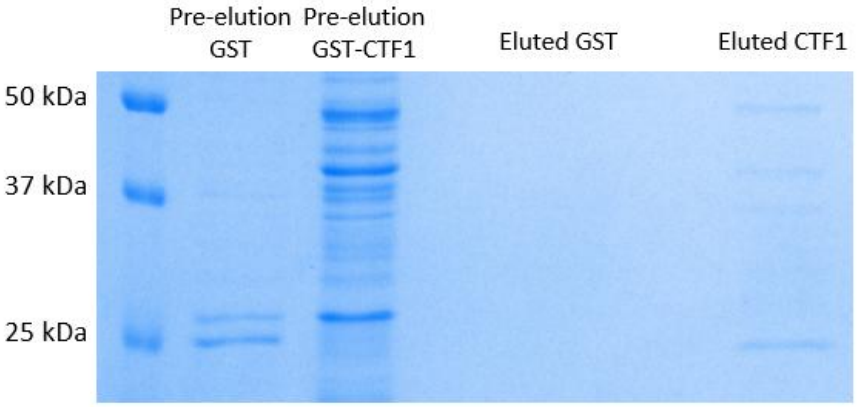

Figure 4.1.3.5 Elution of GST-CTF1 protein. After protein elution steps, the eluted proteins are loaded onto the 12% SDS-PAGE gel. CTF1 protein is not eluted correctly; it is still on the bead. Further optimisation is needed.

Colony 8 is eluted using glutathione Sepharose 4B beads. Results are shown in figure 4.1.3.5

4.2 Development of Naïve phage display library

4.2.1 Mouse spleen RNA isolation and cDNA conversion

Spleen was harvested from mouse and RNA isolated using Trizol protocol that is stated in the materials and methods section. The isolated product was 1 ug / µl. Isolated RNA was loaded to the agarose gel to visualize isolated product.

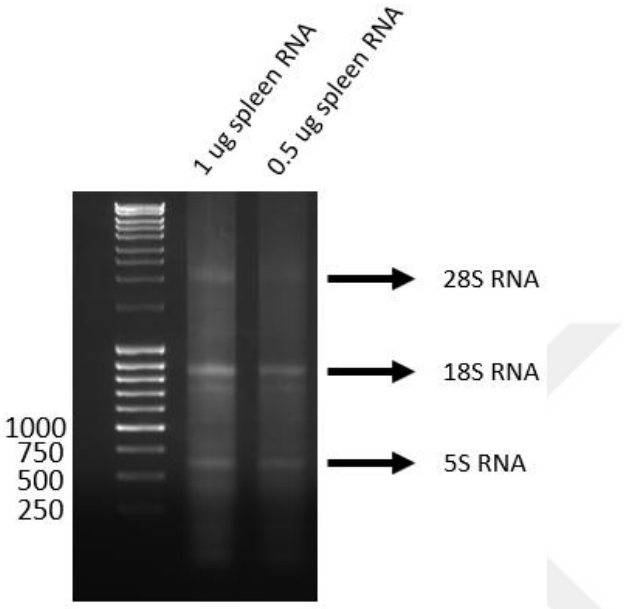

Figure 4.2.1 Agarose gel electrophoresis of 1 ug and 0.5 ug isolated RNA. Samples are loaded 1.5% agarose gel.

After the RNA isolation verification, RNA samples are converted to the cDNA. Because of the there is limited volume of spleen RNA, we decided to contininue our optimization process with B cell line, A20. RNA also isolated from A20 cell line, and converted to the cDNA. Later, cDNA is used as a template to amplify V_H and V_L primer sets. There are 9 V_L forward primers, 2 V_L reverse primers and 9 V_H forward primers, 2 V_H reverse primers with the SfiI / NotI restriction sites. These primers also consist overlap regions to amplify to each other to create scFv structure. To achieve this, firstly we started to optimize the primer working conditions for each set of PCR. In the beginning, all primers are anneal at 58-63 ºC. Results are shown in the figure 4.2.2

4.2.2 Optimization of primer sets

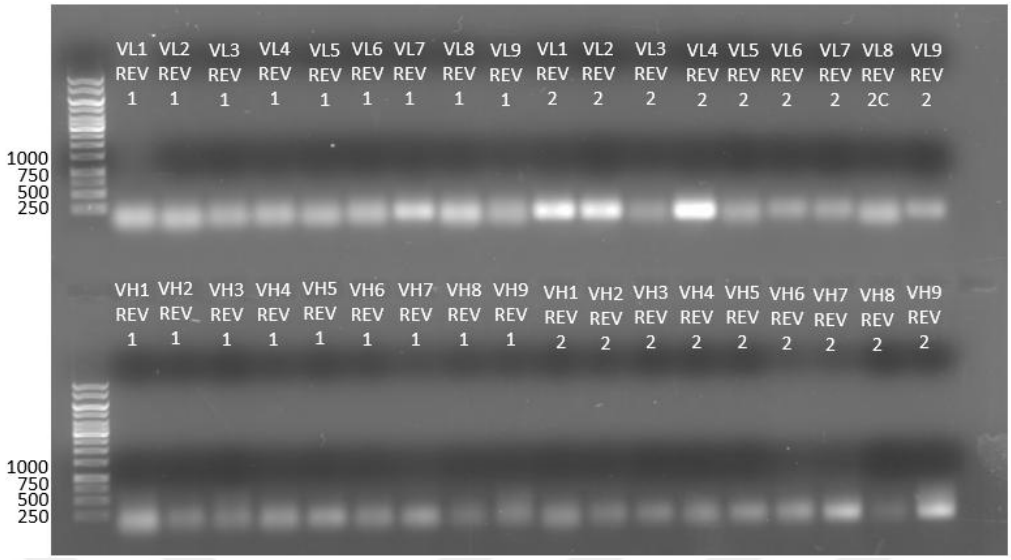

Figure 4.2.2 Agarose gel electrophoresis of all light chain and heavy chain primer sets. All primers are annealed at 55-63 ºC, using A20 B cell line cDNA as a template DNA for optimization. There isn't any successfully amplified PCR product. Results are visualized at 1% agarose gel.

After not getting any amplified PCR product, we start to study each primer set induvially. For this, we picked VL1-REV1 and VH1-REV1 for continue optimization. These primers are annealed 58-63 ºC again. Results are shown in the figure 4.2.3

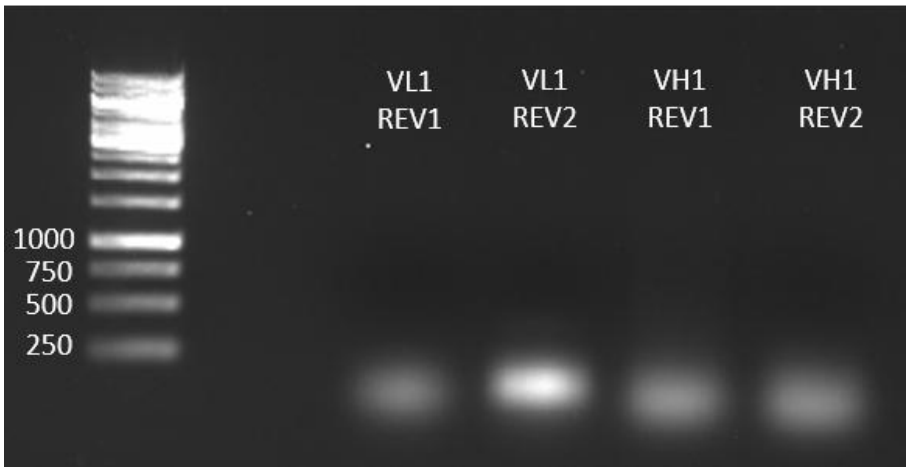

Figure 4.2.3 Agarose gel electrophoresis result of VL1-REV1, VL1-REV2, VH1-REV1, VH1-REV2 optimization. To begin optimization process of phage display antibody library, different primer pairs were picked from each primer set. 55-63 ºC annealing temperature were performed for PCR. There is a slight band at VL1-REV2. Results are visualized at 1% agarose gel.

We decided to try 55 oC annealing temperature in all primer sets. Results are shown in figure 4.2.4

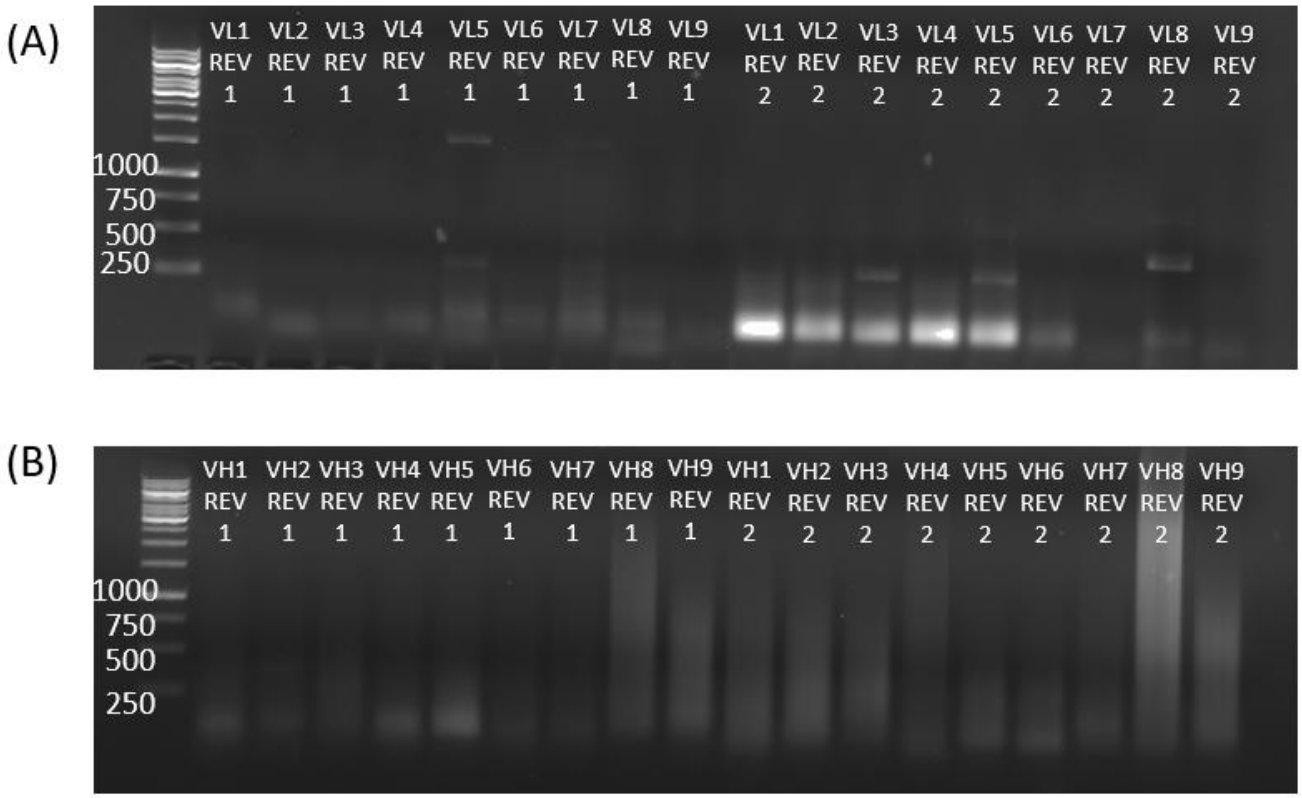

Figure 4.2.4 Agarose gel electrophoresis result of full set primers. (A) In 55 ºC annealing temperature PCR, VL1, VL5, VL7, VL3, VL5, and VL8 amplified. (B) In a 55 ºC annealing temperature of the full set of heavy chain primers, only VH2 amplified. Results are visualized at 1% agarose gel.

Moreover, we decided that for heavy chain primers, 55 ºC annealing temperature is not working because almost all of the results are smeared. Meaning that PCR reaction is not working at all. But when we look at the light chain primer set groups, there is amplification in VL1, VL5-REV1, VL7-REV1, VL3-REV2, VL5-REV2 and VL8-REV2. This could be mean that light chain PCRs annealing temperature is 55 ºC but it needs further optimization. So, we decided to continue more different methods like increasing template concentration or adding DMSO for primer-dimer inhibition.

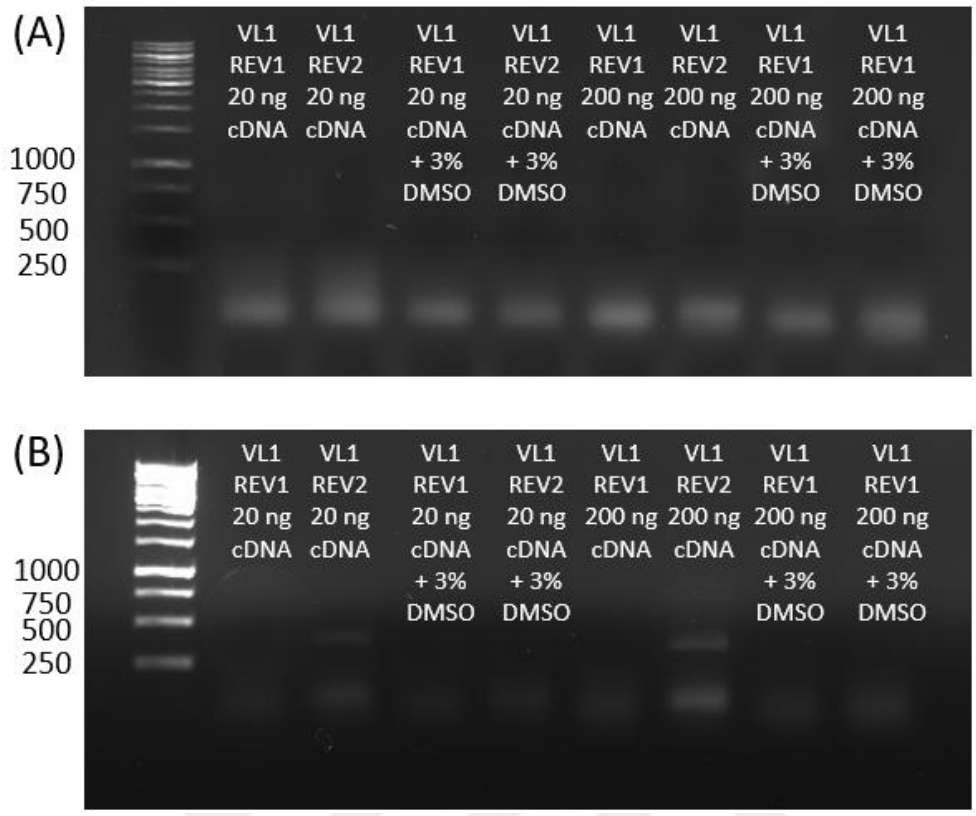

Figure 4.2.5 Agarose gel electrophoresis result of light chain primer optimization. PCR was performed with different conditions. (A) DMSO for decreaseing effect of primer dimerization was added with 20 ng template DNA, high concentration of template DNA and high concentration of template DNA and DMSO at 55-63 ºC annealing temperature. (B) DMSO for decreaseing effect of primer dimerization was added with 20 ng template DNA, high concentration of template DNA and high concentration of template DNA and DMSO at 55 ºC. It has been discovered that light chain primers are working at 55 oC annealing temperature with high concentrations of template DNA. Adding DMSO was decreased primer dimer formation but blocked PCR. Results are visualized at 1% agarose gel.

Same optimization process, increasing concentration of template DNA, adding DMSO for inhibiting primer-dimer formation, was conducted for heavy chain reverse 1 and 2 primer sets also. Results are shown in figure 4.2.6

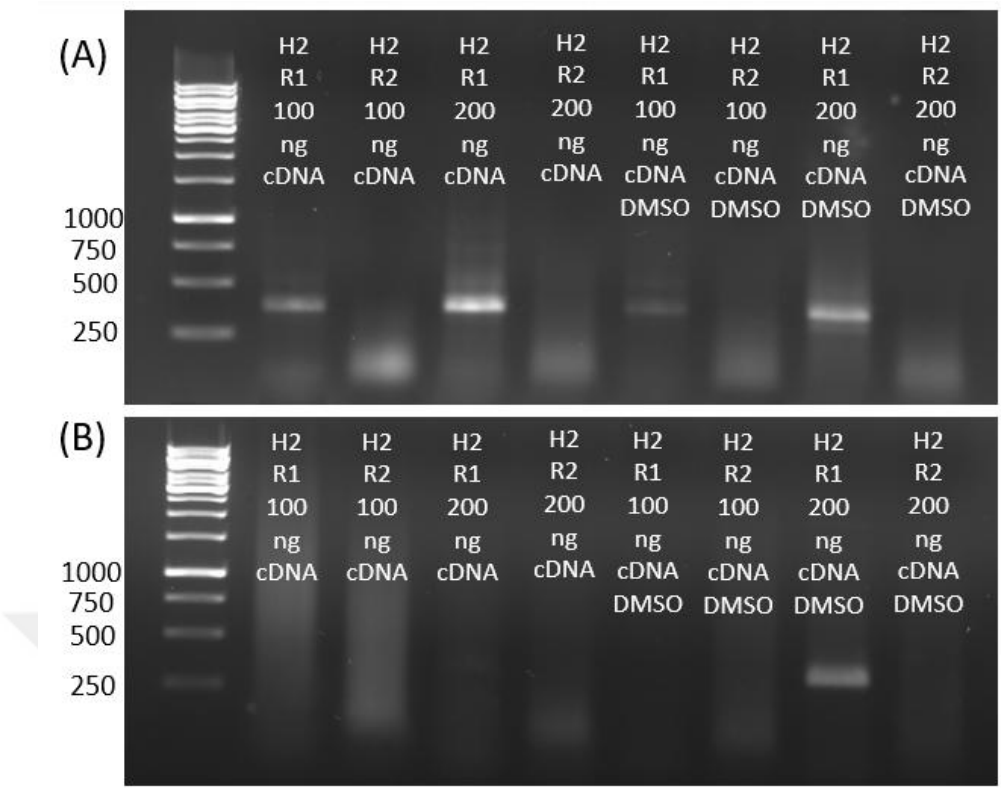

Figure 4.2.6 Agarose gel electrophoresis result of heavy chain primer optimization. PCR was performed with different conditions. (A) DMSO for decreaseing effect of primer dimerization was added with 20 ng template DNA, high concentration of template DNA and high concentration of template DNA and DMSO at 55-63 ºC annealing temperature. (B) DMSO was added to decreaseing the effect of primer dimerization with 20 ng template DNA, high concentration of template DNA and high concentration of template DNA and DMSO at 55 ºC. It has been discovered that heavy chain primers are amplifiying at 55-63 ºC annealing temperature with high concentrations of template DNA. Adding DMSO was decreased primer dimer formation but blocked PCR. Heavy chain reverse 2 primers still needed optimization. Results are visualized at 1% agarose gel.

Furthermore, we discovered that light chain primers are annealing at 55 oC, heavy chain reverse 1 primers are annealing at 55-63 oC, we performed a PCR again for all of the heavy chain primer sets again. Results are shown in the figure 4.2.7

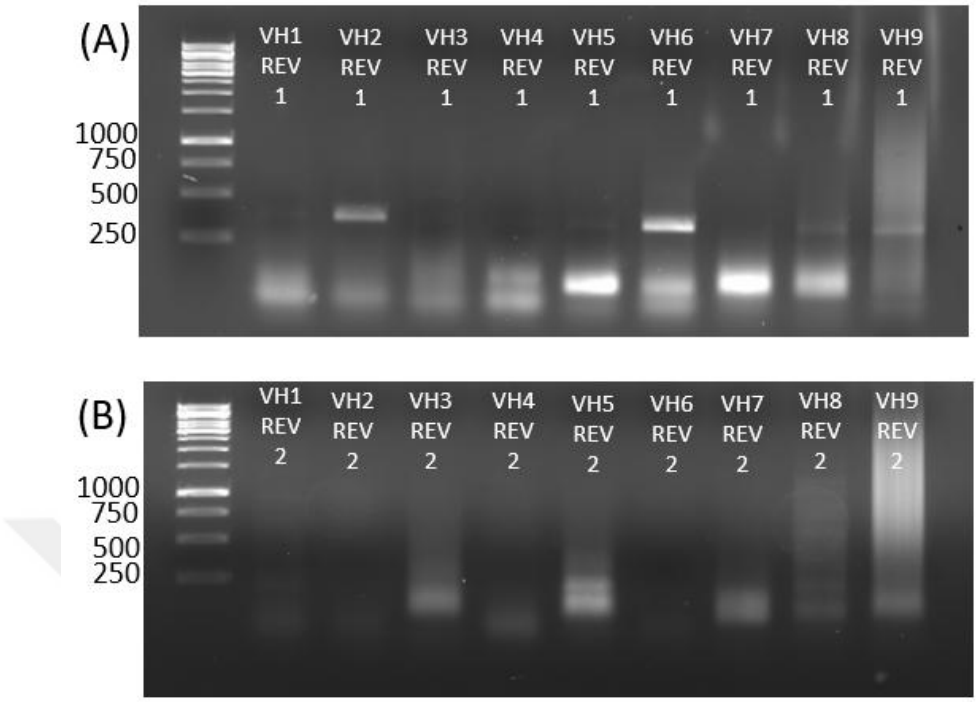

Figure 4.2.7 Agarose gel electrophoresis result of heavy chain primer sets. (A) Heavy chain reverse 1 primers annealed at 55-63 ºC using A20 B cell line. All of them worked at different efficiency levels. (B) Heavy chain reverse 2 primers annealed at 55-93 ºC using A20 B cell line. VH1 REV1, VH5 REV2, VH8 REV2 amplified with low efficiency. Results are visualized at 1% agarose gel.

Moreover, to find a correct annealing temperature of heavy chain reverse 2 primer set, we did Gradient PCR with a range of 62 ºC to 52 ºC. Results are shown in figure 4.2.8

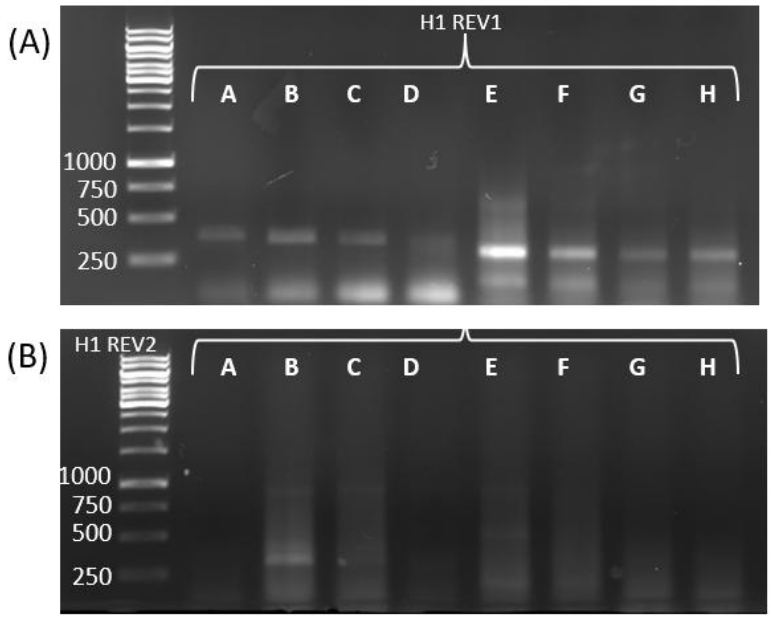

(C)

A	62 ºC
B	61.2 ºC
C	60 ºC
D	58.1 ºC
E	55.8 ºC
F	53.9 ºC
G	52.7 ºC
H	52 ºC

Figure 4.2.8 Agarose gel result of Heavy chain REV1 and REV2 primer optimization using Gradient PCR with A20 B cell line cDNA as a template DNA. (A) Heavy chain REV1 PCR annealed at different temperature ranges between 62 °C and 52 °C using the Gradient PCR technique. H1 REV1 amplified all the temperatures with varying levels of efficiency. (B) Heavy chain REV2 PCR annealed at different temperature ranges between 62 °C and 52 °C using the gradient PCR technique. H1 REV2 amplified at 61.2 °C. (C) Gradient PCR range table. Results are visualized at 1% agarose gel.

Furthermore, due to Gradient PCR result, heavy chain reverse 2 primers are annealed at 61 ºC. Results are shown in figure 4.2.9

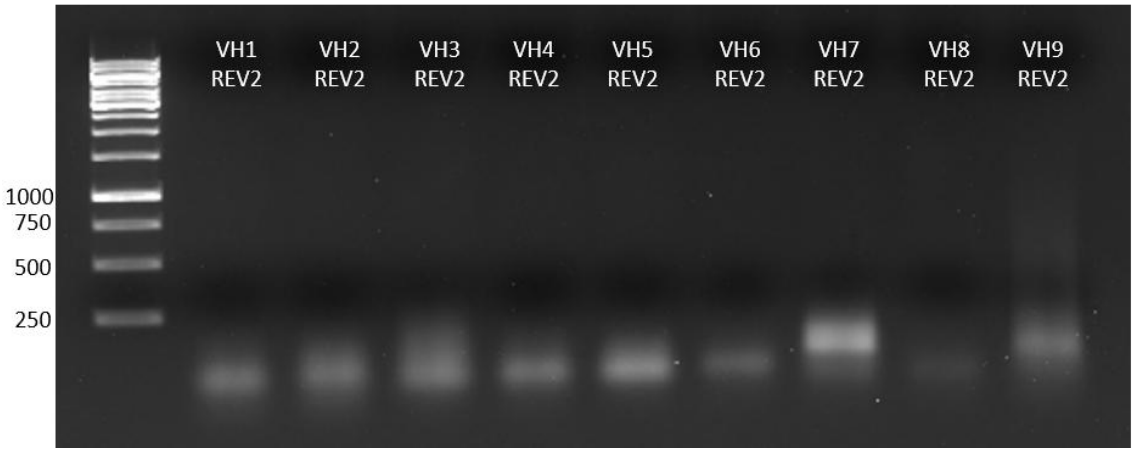

Figure 4.2.9 The agarose gel electrophoresis result of heavy chain reverse 2 was set at 61 ºC annealing temperature. The PCR was annealed at 61 ºC because of the previous gradient PCR result using A20 B cell line cDNA as a template. No PCR product was amplification. Results are visualized on 1% agarose gel.

Later, we decided to try heavy chain reverse 2 primer set in 58-63 ºC annealing temperature. Results are shown in figure 4.2.10

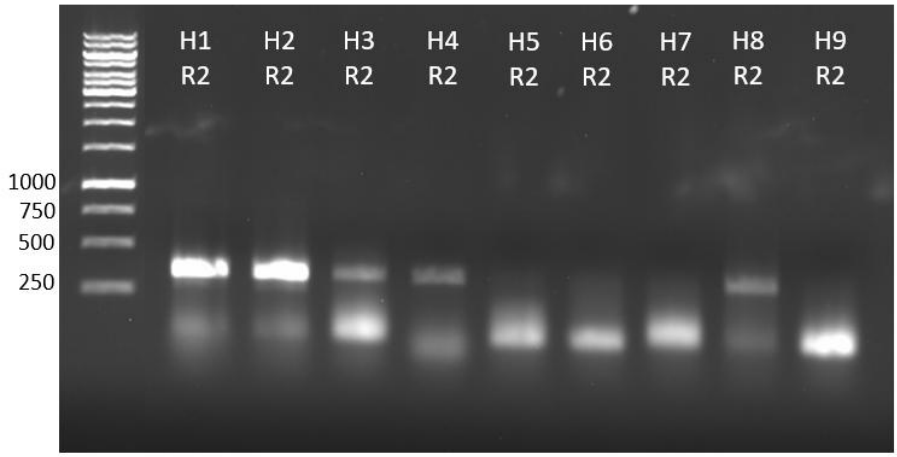

Figure 4.2.10 The agarose gel electrophoresis result of heavy chain reverse 2 was set at 58-63 ºC annealing temperature using A20 B cell line cDNA as a template. H1R1, H2R2, H3R2, H4R2 and H8R2 successfully amplified with different efficiencies. Results are visualized 1% agarose gel.

For the last part of the optimization of the VH and VL PCRs, we performed all PCR sets with naïve mouse spleen cDNA with most efficient PCR amplification conditions that we discovered earlier. Result are shown in figure 4.2.11

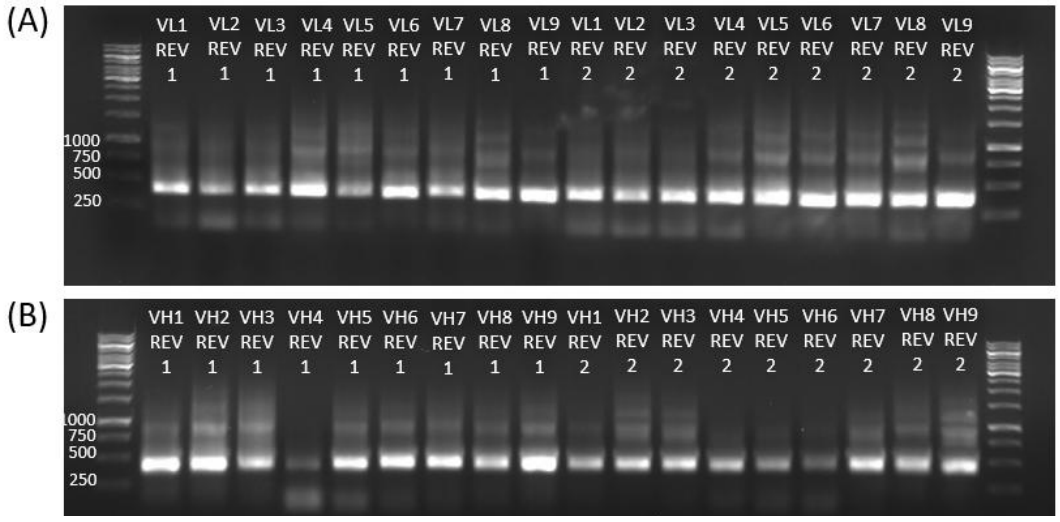

Figure 4.2.12 Agarose gel electrophoresis result of Light and Heavy chain fragments PCR set. (A) Light chain fragment set PCRs are performed at 55 ºC annealing temperature. All PCR products are amplified. Naive Mouse spleen is used as a cDNA template. (B) Heavy chain 1-9 REV1 PCRs performed at 55-63 ºC annealing temperature, Heavy chain 1-9 REV2 PCRs are performed at 58-63 oC temperature. Naive Mouse Spleen is used as a cDNA template. All PCR products were amplified. PCR products are visualized at 1% agarose gel.

4.2.12 SOE (splicing by overlap extension) PCR

After successfully annealed all PCR primer sets, its time to amplify each VL-VH pair together to create scFv structure via SOE PCR. Each primer set was isolated from gel using MN kit manufacturer protocol. 25 ng DNA was used from each set to combine PCR products, final concentration is 100 ng. Heavy chain and light chain PCR mix are loaded as control. Results shown in figure 4.2.12

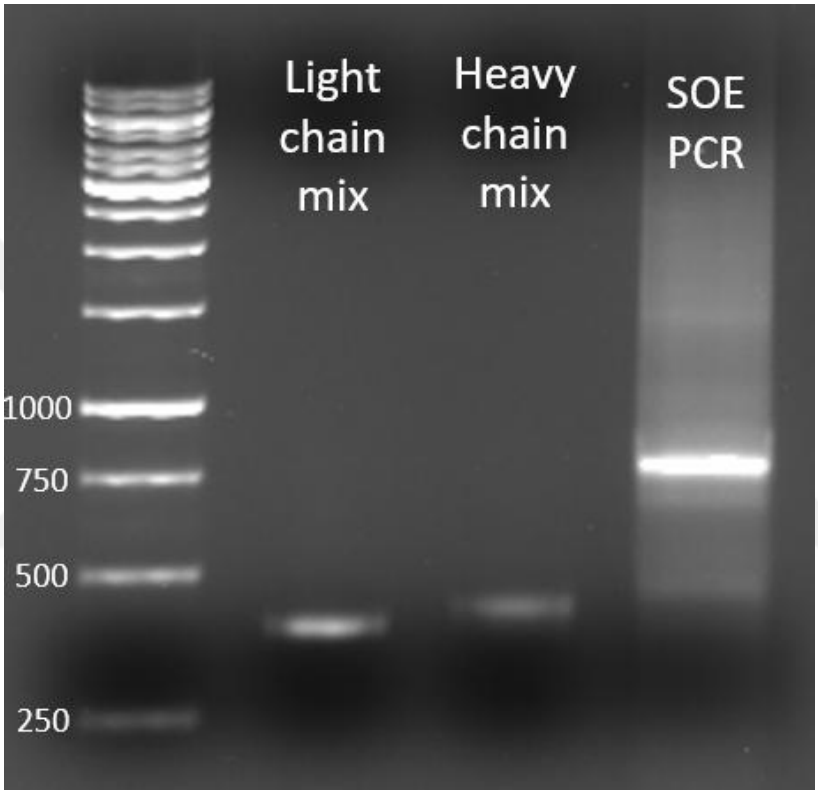

Figure 4.2.11 Agarose gel electrophoresis result of Splicing Overlap Extension PCR. Light and Heavy chain PCR products were amplified as 50 ng for each fragment. In first PCR cycle, primers didn't add for 20 cycles to enchance product amplification, later primers are added and continued for another 35 cycles. Light chain fragment mixture and heavy chain fragment mixture loaded as control. Results are visuailized at 1% agarose gel.

SOE PCR product was isolated from gel using MN NucleoSpin Gel Extraction kit, manufacturer protocols. We continue with cloning of the scFv product into the phage display vector, pCANTAB5e.

4.2.13 Cloning of scFv into the pCANTAB5e

SOE PCR product and pCANTAB5e vector were digested with SfiI restriction ezyme at 50 ºC in G buffer, 1 hour. After that, NotI restriction enzyme added and continued incubation at 37 ºC, 1 hour. Results are shown in figure 4.2.13

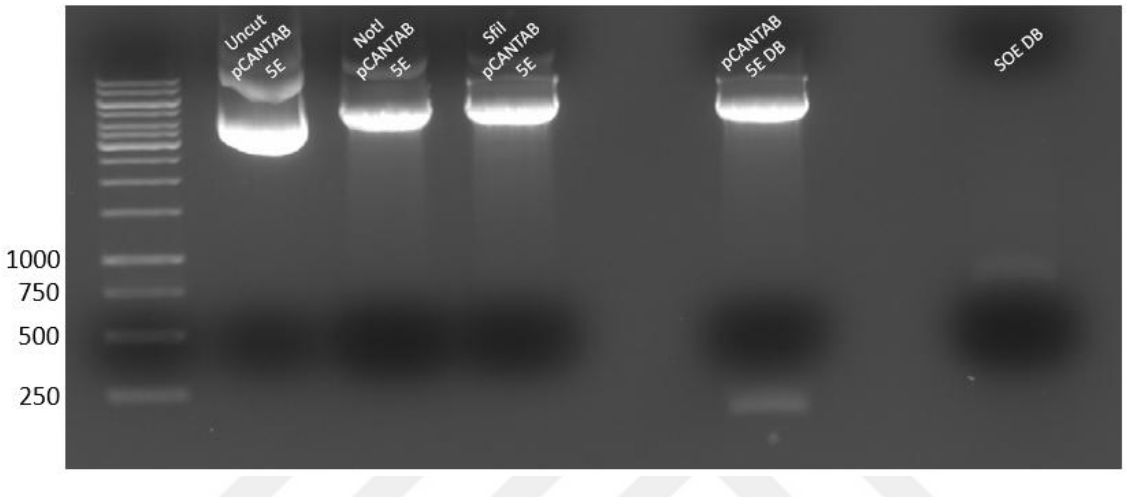

Figure 4.2.13 Agarose gel result of the pCANTAB5e and SOE PCR product enzyme digestion. Uncut pCANTAB5e, NotI single digest, SfiI single digest loaded as a digestion control. Vector successfully digested. Results are visualized in 1% agarose gel.

Finally, we isolated digested pCANTAB5e and scFv from gel and ligated these products performing normal ligation protocol in 1:8 ligation ratio, 16 oC overnight. The next day, the ligation reaction is transformed to the Dh5α E.coli, and spread to the Ampicillin agar plate. Colonies are picked overnight and mini-prep DNA extraction was performed to check cloning verification. Results are shown in the figure 4.2.14

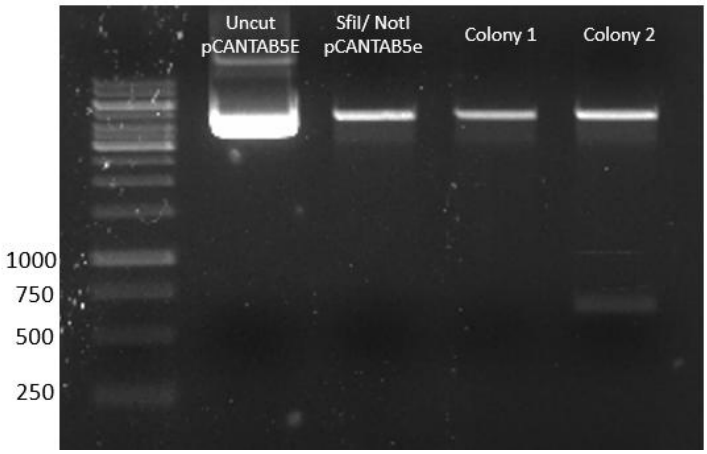

Figure 4.2.14 Agarose gel electrophoresis result of pCANTAB5e-scFv. Clones are verified trough enzyme digestion with SfiI and NotI. Colony 2 contains scFv structure.

Chapter 4

DISCUSSION

In the literature, many times it has been stated that Cardiotrophin 1 is associated with heart diseases; myocardial infarction, arterial stiffness, hypertension, etc. In addition, it is also associated with cell survival and acts as an anti-apoptotic factor that activates the STAT3 and PI3K-AMPK signalling pathways. Akkoç and colleagues discovered that CTF1 has a role in tumour-stroma interaction; it is secreted from breast cancer cells to the tumour stroma and alters the fibroblasts to carcinoma-associated fibroblasts. Moreover, this mechanism is autophagy-dependent. The effect of CTF1 is associated with the tumor stage, larger and lymph node metastatic tumors contain more CTF1 expression. But it is not associated with the hormone receptor levels. (Akkoc et al., 2023) Few factors promote CAF formation, like TGF-B, ROS, and LMP1, but CTF1 triggers a different mechanism than other cancer-derived factors that alter autophagy in CAFs. (Sari et al., 2024) It is important to discover new factors that might cause cancer invasion or migration to better treat or diagnose cancer. Many stroma-targeting drugs are still in clinical trials. These drugs target CAFs, which secrete TGF-B, called Fresolimumab, or target CAF-related proteins, which is an antibody-based drug called ABBV-085. (C. Wu et al., 2024) These discoveries make CTF1 is a potential drug target against breast cancer.

Since 2022, at least 111 antibody-based drugs are approved against many diseases, most of them are cancer. Because of the high specificity, powerful mechanisms of action, long half-life, and wide therapeutic application, they are very advantageous against several diseases. On the other hand, they faced many problems since Miller and Kühler introduced us with hybridoma technology. They are high cost, increased immunogenicity risk and need expertise to produce. In this case, phage display technologies appear. Phage display stands out due to low production cost, less immunogenicity, and better tissue penetration of antibodies than other antibody obtaining methods.

In this thesis, we aimed to develop a system to produce recombinant antibodies against CTF1 to target tumour-stroma crosstalk to inhibit breast cancer metastasis. For this matter, we produced recombinant CTF1 protein. This recombinant protein production was needed because even tough many companies are produces recombinant CTF1 protein but they are very expensive when is compared to the volume size and also have miscalculated concentrations of the protein. It is safer and more credible to generate our own recombinant proteins in the laboratory. To this matter we cloned CTF1 gene into the bacterial protein expression vector and induced with lactose analoge IPTG to echance recombinant target protein expression. After we saw appropriate amount of recombinant CTF1 on Coomassie gel, we continued with the bacteria's lyse. Bacteria were successfully lysed with detergent containing lysis solutions and eluted with agarose Sepharose GST beads. In the final parts of this chapter, we discovered that recombinant CTF1 protein is not eluted sufficiently, most of them are on glutathione Sepharose 4B (GE Healthcare, 17-0756-01) beads. Further optimization process is needed to elute CTF1 protein more efficiently. Many stragedies can be try; changing elution conditions like temperature or buffer conditions or try to elute by digesting GST tag using protease enzyme like Thrombin. In this way, we will use recombinant protein in other experiment currently conducted in our laboratory but also continue with animal immunization against CTF1 protein or to use in the biopanning process against CTF1 again.

In the second chapter of this thesis, we developed a system to create a naïve phage display library. In the first place, we designed 36 oligos from the KABAT-WU database, which represents the mouse IgG repertoire. Using this primer oligos, we conducted conventional PCR. To establish a system, they needed a further optimization process. We tried different annealing temperatures, increasing concentrations of template DNA or adding chemicals (DMSO etc.) to decrease the effect of primer-dimer formation. After discovering the most efficient PCR reaction condition, we continue amplifying these PCR products together. While creating a scFv, these recombinant antibodies have one light chain and one heavy chain, these chains are joined together with a Gly-Ser containing linker. After successfully amplifying these chains, we performed SOE PCR to join them together. SOE PCR needed optimization process also. We investigated correct annealing temperature; we try to enhance PCR product fusion. After that scFv structure is cloned to the phage display vector, a phagemid,

pCANTAB5e. In this way we created a naïve mouse library to use screening against target molecules. Naïve libraries are beneficial for screening against target molecules and producing recombinant antibodies against your target. But they have low positive clone numbers because they are not from an animal that was immunised against your antigen. Now, we will use our recombinant CTF1 protein to immunise the mouse against CTF1, harvest the spleen, conduct a phage display library using 36 oligos that we optimise in this thesis, and then perform a biopanning process using recombinant CTF1 protein and CTF1 phage display library. In this way, we will produce a recombinant antibody against CTF1 that can be used as a therapeutic agent that targets tumour stroma crosstalk against breast cancer invasion and migration.

Chapter 5

CONCLUSION AND FUTURE PROSPECTS

In this thesis, we attempted to create a technique for producing recombinant antibodies against CTF1 in order to target tumor-stroma crosstalk and limit breast cancer metastases. For this purpose, we created recombinant CTF1 protein. To this end, we cloned the CTF1 gene into a bacterial protein expression vector and stimulated it using the lactose analog IPTG to enhance recombinant target protein expression. In Chapter 2 of this thesis, we created a method to generate a naïve phage display library. First, we created 36 oligos using the KABAT-WU database, which contains the mouse IgG repertoire. We used these primer oligos to do conventional PCR. To develop a system, they needed to go through another optimization procedure. We experimented with different annealing temperatures, increasing template DNA concentrations, and adding chemicals (DMSO, etc.) to reduce the effect of primer-dimer formation. After determining the most efficient PCR reaction conditions, we continue to amplify these PCR products together. When producing a scFv, these recombinant antibodies have one light chain and one heavy chain that are connected together by a Gly-Ser linker. After successfully generating these chains, we used SOE PCR to connect them. In the final part of this thesis, we successfully cloned a scFv structure into the phage display vector. Our results indicates that we created a system to obtain recombinant antibodies against any target molecule. As discussed previously antibody-based drugs are effectively used in many diseases, but producing them are not so efficient; oftenly expensive. Having a system that can produce antibodies faster and cheaper can open a new way in cancer detection and therapy. In the future with using our system that develop in this thesis, we will now use our recombinant CTF1 protein to immunize the mouse against CTF1, extract the spleen, create a phage display library utilizing 36 oligos optimized in this thesis, and then perform a biopanning process with the recombinant CTF1 protein and CTF1 phage display library. In this method, we will create a recombinant antibody against CTF1 that can be employed as a therapeutic agent to combat tumor stroma interaction in breast cancer invasion and migration.

BIBLIOGRAPHY

Ahmad, Z. A., Yeap, S. K., Ali, A. M., Ho, W. Y., Alitheen, N. B. M., & Hamid, M. (2012). scFv Antibody: Principles and Clinical Application. *Clinical and Developmental Immunology*, *2012*, 1–15. https://doi.org/10.1155/2012/980250

Akkoc, Y., Dalci, K., Karakas, H. E., Erbil-Bilir, S., Yalav, O., Sakman, G., Celik, F., Arikan, S., Zeybek, U., Ergin, M., Akkiz, H., Dilege, E., Dengjel, J., Dogan-Ekici, A. I., & Gozuacik, D. (2023). Tumor-derived CTF1 (cardiotrophin 1) is a critical mediator of stroma-assisted and autophagy-dependent breast cancer cell migration, invasion and metastasis. *Autophagy*, *19*(1), 306–323. https://doi.org/10.1080/15548627.2022.2090693

Al-Mazroua, H. A., Al-Rasheed, N. M., & Korashy, H. M. (2013). Downregulation of the Cardiotrophin-1 Gene Expression by Valsartan and Spironolactone in Hypertrophied Heart Rats In Vivo and Rat Cardiomyocyte H9c2 Cell Line In Vitro: A Novel Mechanism of Cardioprotection. *Gene Expression*, *61*(4).

Anik Ilhan, G., Kanlioglu, C., Arslan, G., Yildizhan, B., & Pekin, T. (2018). Cardiotrophin-1 as a new metabolic biomarker in women with PCOS. *Gynecological Endocrinology*, *34*(9), 781–783. https://doi.org/10.1080/09513590.2018.1457637

Aoyama, T., Takimoto, Y., Pennica, D., Inoue, R., Shinoda, E., Hattori, R., Yui, Y., & Sasayama, S. (2000). Augmented Expression of Cardiotrophin-1 and its Receptor Component, gp130, in both Left and Right Ventricles after Myocardial Infarction in the Rat. *Journal of Molecular and Cellular Cardiology*, *32*(10), 1821–1830. https://doi.org/10.1006/jmcc.2000.1218

Arce, V., Garces, A., De Bovis, B., Filippi, P., Henderson, C., Pettmann, B., & deLapeyrière, O. (1999). Cardiotrophin-1 requires LIFRβ to promote survival of mouse motoneurons purified by a novel technique. *Journal of Neuroscience Research*, *55*(1), 119–126. https://doi.org/10.1002/(SICI)1097-4547(19990101)55:1<119::AID-JNR13>3.0.CO;2-6

Arce, V., Pollock, R. A., Philippe, J.-M., Pennica, D., Henderson, C. E., & deLapeyrière, O. (1998). Synergistic Effects of Schwann- and Muscle-Derived Factors on Motoneuron Survival Involve GDNF and Cardiotrophin-1 (CT-1). *The Journal of Neuroscience*, *18*(4), 1440–1448. https://doi.org/10.1523/JNEUROSCI.18-04-01440.1998

Argos, P. (1990). An investigation of oligopeptides linking domains in protein tertiary structures and possible candidates for general gene fusion. *Journal of Molecular Biology*, *211*(4), 943–958. https://doi.org/10.1016/0022-2836(90)90085-Z

Armstrong, J., Hewitt, J. A., & Perham, R. N. (1983). Chemical modification of the coat protein in bacteriophage fd and orientation of the virion during assembly and

disassembly. *The EMBO Journal*, *2*(10), 1641–1646. https://doi.org/10.1002/j.1460-2075.1983.tb01638.x

Arslan, M., Karadag, M., Onal, E., Gelinci, E., Cakan-Akdogan, G., & Kalyoncu, S. (2022). Effect of non-repetitive linker on in vitro and in vivo properties of an anti-VEGF scFv. *Scientific Reports*, *12*(1), 5449. https://doi.org/10.1038/s41598-022-09324-4

Atwell, J. L., Breheney, K. A., Lawrence, L. J., McCoy, A. J., Kortt, A. A., & Hudson, P. J. (1999). scFv multimers of the anti-neuraminidase antibody NC10: Length of the linker between VH and VL domains dictates precisely the transition between diabodies and triabodies. *Protein Engineering, Design and Selection*, *12*(7), 597–604. https://doi.org/10.1093/protein/12.7.597

Barderas, R., & Benito-Peña, E. (2019). The 2018 Nobel Prize in Chemistry: Phage display of peptides and antibodies. *Analytical and Bioanalytical Chemistry*, *411*(12), 2475–2479. https://doi.org/10.1007/s00216-019-01714-4

Barrón-Gallardo, C. A., Garcia-Chagollán, M., Morán-Mendoza, A. J., Delgadillo-Cristerna, R., Martínez-Silva, M. G., Aguilar-Lemarroy, A., & Jave-Suárez, L. F. (2022). Transcriptomic Analysis of Breast Cancer Patients Sensitive and Resistant to Chemotherapy: Looking for Overall Survival and Drug Resistance Biomarkers. *Technology in Cancer Research & Treatment*, *21*, 15330338211068965. https://doi.org/10.1177/15330338211068965

Beraza, N., Marqués, J. M., Martínez-Ansó, E., Iñiguez, M., Prieto, J., & Bustos, M. (2005). Interplay among cardiotrophin-1, prostaglandins, and vascular endothelial growth factor in rat liver regeneration†. *Hepatology*, *41*(3), 460–469. https://doi.org/10.1002/hep.20590

Bordet, T., Schmalbruch, H., Pettmann, B., Hagege, A., Castelnau-Ptakhine, L., Kahn, A., & Haase, G. (1999). Adenoviral cardiotrophin-1 gene transfer protects pmn mice from progressive motor neuronopathy. *Journal of Clinical Investigation*, *104*(8), 1077–1085. https://doi.org/10.1172/JCI6265

Bortolotti, F., Ruozi, G., Falcione, A., Doimo, S., Dal Ferro, M., Lesizza, P., Zentilin, L., Banks, L., Zacchigna, S., & Giacca, M. (2017). In Vivo Functional Selection Identifies Cardiotrophin-1 as a Cardiac Engraftment Factor for Mesenchymal Stromal Cells. *Circulation*, *136*(16), 1509–1524. https://doi.org/10.1161/CIRCULATIONAHA.117.029003

Brar, B. (2001). Cardiotrophin-1 can protect cardiac myocytes from injury when added both prior to simulated ischaemia and at reoxygenation. *Cardiovascular Research*, *51*(2), 265–274. https://doi.org/10.1016/S0008-6363(01)00294-2

Brar, B. K., Stephanou, A., Pennica, D., & Latchman, D. S. (2001). CT-1 MEDIATED CARDIOPROTECTION AGAINST ISCHAEMIC RE-OXYGENATION INJURY IS MEDIATED BY PI3 KINASE, Akt AND MEK1/2 PATHWAYS. *Cytokine*, *16*(3), 93–96. https://doi.org/10.1006/cyto.2001.0951

Briney, B. S., & Jr., J. E. C. (2013). Secondary mechanisms of diversification in the human antibody repertoire. *Frontiers in Immunology*, *4*. https://doi.org/10.3389/fimmu.2013.00042

Bustos, M., Beraza, N., Lasarte, J.-J., Baixeras, E., Alzuguren, P., Bordet, T., & Prieto, J. (2003). Protection against liver damage by cardiotrophin-1: A hepatocyte survival factor up-regulated in the regenerating liver in rats. *Gastroenterology*, *125*(1), 192–201. https://doi.org/10.1016/S0016-5085(03)00698-X

Bustos, M., Dubrot, J., Martinez-Anso, E., Larequi, E., Castaño, D., Palazon, A., Belza, I., Sanmamed, M. F., Perez-Gracia, J. L., Ortiz De Solorzano, C., Alfaro, C., & Melero, I. (2012). Cardiotrophin-1 determines liver engraftment of syngenic colon carcinoma cells through an immune system-mediated mechanism. *OncoImmunology*, *1*(9), 1527–1536. https://doi.org/10.4161/onci.22504

Cai, H., Tian, S., Liu, A., Xie, G., Zhang, H., Wu, X., Wan, J., & Li, S. (2025). Relationship between CTF1 gene expression and prognosis and tumor immune microenvironment in glioma. *European Journal of Medical Research*, *30*(1), 17. https://doi.org/10.1186/s40001-024-02192-w

Carneros, D., Medina-Gómez, G., Giralt, M., León-Camacho, M., Campbell, M., Moreno-Aliaga, M. J., Villarroya, F., & Bustos, M. (2020). Cardiotrophin-1 contributes to metabolic adaptations through the regulation of lipid metabolism and to the fasting-induced fatty acid mobilization. *The FASEB Journal*, *34*(12), 15875–15887. https://doi.org/10.1096/fj.202000109R

Charlton, K., Harris, W. J., & Porter, A. J. (2001). The isolation of super-sensitive anti-hapten antibodies from combinatorial antibody libraries derived from sheep. *Biosensors and Bioelectronics*, *16*(9–12), 639–646. https://doi.org/10.1016/S0956-5663(01)00192-0

Chen, K.-C., Hsieh, C.-L., Peng, C.-C., & Peng, R. Y. (2014). Exercise rescued chronic kidney disease by attenuating cardiac hypertrophy through the cardiotrophin-1 → LIFR/gp 130 → JAK/STAT3 pathway. *European Journal of Preventive Cardiology*, *21*(4), 507–520. https://doi.org/10.1177/2047487312462827

Chiu, M. L., Goulet, D. R., Teplyakov, A., & Gilliland, G. L. (2019). Antibody Structure and Function: The Basis for Engineering Therapeutics. *Antibodies*, *8*(4), 55. https://doi.org/10.3390/antib8040055

Chollangi, S., Wang, J., Martin, A., Quinn, J., & Ash, J. D. (2009). Preconditioning-induced protection from oxidative injury is mediated by leukemia inhibitory factor receptor (LIFR) and its ligands in the retina. *Neurobiology of Disease*, *34*(3), 535–544. https://doi.org/10.1016/j.nbd.2009.03.012

Clackson, T., Hoogenboom, H. R., Griffiths, A. D., & Winter, G. (1991). Making antibody fragments using phage display libraries. *Nature*, *352*(6336), 624–628. https://doi.org/10.1038/352624a0

Costa, A. da, Franco-Duarte, R., Machado, R., & Gomes, A. C. (2022). Uncovering the promiscuous activity of IL-6 proteins: A multi-dimensional analysis of phylogeny,

classification and residue conservation. *Protein Science*, *31*(11), e4469. https://doi.org/10.1002/pro.4469

Cottone, S., Nardi, E., Mulè, G., Vadalà, A., Lorito, M. C., Riccobene, R., Palermo, A., Arsena, R., Guarneri, M., & Cerasola, G. (2007). Association between biomarkers of inflammation and left ventricular hypertrophy in moderate chronic kidney disease. *Clinical Nephrology*, *67*(04), 209–216. https://doi.org/10.5414/CNP67209

Daëron, M. (1997). Fc RECEPTOR BIOLOGY. *Annual Review of Immunology*, *15*(Volume 15, 1997), 203–234. https://doi.org/10.1146/annurev.immunol.15.1.203

De Aguiar, R. B., Da Silva, T. D. A., Costa, B. A., Machado, M. F. M., Yamada, R. Y., Braggion, C., Perez, K. R., Mori, M. A. S., Oliveira, V., & De Moraes, J. Z. (2021). Generation and functional characterization of a single-chain variable fragment (scFv) of the anti-FGF2 3F12E7 monoclonal antibody. *Scientific Reports*, *11*(1), 1432. https://doi.org/10.1038/s41598-020-80746-8

Ding, W., Wu, L., Li, X., Chang, L., Liu, G., & Du, H. (2022). Comprehensive analysis of competitive endogenous RNAs network: Identification and validation of prediction model composed of mRNA signature and miRNA signature in gastric cancer. *Oncology Letters*, *23*(5), 150. https://doi.org/10.3892/ol.2022.13270

Dong, Z.-L., Wang, Y., Li, T.-F., Zheng, S.-J., Kong, Y.-Q., Lan, Y.-L., Guo, J.-L., & Fu, S.-G. (2014). P42/p44 mitogen-activated protein kinases inhibit atrial natriuretic peptide mRNA transcription in gp130-mediated hypertrophic ventricular myocytes. *Asian Pacific Journal of Tropical Medicine*, *7*(3), 216–220. https://doi.org/10.1016/S1995-7645(14)60024-9

Erdmann, J., Hassfeld, S., Kallisch, H., Fleck, E., & Regitz-Zagrosek, V. (1998). Cloning and Characterization of the 5′-Flanking Region of the Human Cardiotrophin-1 Gene. *Biochemical and Biophysical Research Communications*, *244*(2), 494–497. https://doi.org/10.1006/bbrc.1998.8311

FDA Approves Faricimab for nAMD and Diabetic Macular Edema. (n.d.). Medscape. Retrieved 25 August 2025, from https://www.medscape.com/viewarticle/967524

Fernandez-Ruiz, V., Kawa, M., Berasain, C., Iñiguez, M., Schmitz, V., Martinez-Ansó, E., Iñarrairaegui, M., Herrero, I., Sangro, B., D´Avola, D., Quiroga, J., Qian, C., & Prieto, J. (2011). Treatment of murine fulminant hepatitis with genetically engineered endothelial progenitor cells. *Journal of Hepatology*, *55*(4), 828–837. https://doi.org/10.1016/j.jhep.2011.01.036

Fritzenwanger, M., Meusel, K., Foerster, M., Kuethe, F., Krack, A., & Figulla, H.-R. (2007). Cardiotrophin-1 induces interleukin-6 synthesis in human monocytes. *Cytokine*, *38*(3), 137–144. https://doi.org/10.1016/j.cyto.2007.05.015

Fryer, H. J. L., Wolf, D. H., Knox, R. J., Strittmatter, S. M., Pennica, D., O'Leary, R. M., Russell, D. S., & Kalb, R. G. (2000). Brain-Derived Neurotrophic Factor Induces Excitotoxic Sensitivity in Cultured Embryonic Rat Spinal Motor Neurons Through Activation of the Phosphatidylinositol 3-Kinase Pathway. *Journal of Neurochemistry*, *74*(2), 582–595. https://doi.org/10.1046/j.1471-4159.2000.740582.x

Gao, L., & Zhang, L. (2021). Construction and comprehensive analysis of a ceRNA network to reveal potential prognostic biomarkers for lung adenocarcinoma. *BMC Cancer*, *21*(1), 849. https://doi.org/10.1186/s12885-021-08462-8

García-Cenador, B., Blanco-Gozalo, V., López-Montañés, D., Sanz Giménez-Rico, J. R., López-Novoa, J. M., & López-Hernández, F. J. (2018). Cardiotrophin-1 Improves Kidney Preservation, Graft Function, and Survival in Transplanted Rats. *Transplantation*, *102*(10), e404–e412. https://doi.org/10.1097/TP.0000000000002313

Garcia-Cenador, M. B., Lorenzo-Gomez, M. F., Herrero-Payo, J. J., Ruiz, J., Perez de Obanos, M. P., Pascual, J., Lopez-Novoa, J. M., & Garcia-Criado, F. J. (2013). Cardiotrophin-1 Administration Protects from Ischemia-Reperfusion Renal Injury and Inflammation. *Transplantation*, *96*(12), 1034. https://doi.org/10.1097/TP.0b013e3182a74db4

Gómez-Zorita, S., Fernández-Quintela, A., Aguirre, L., Macarulla, M. T., Rimando, A. M., & Portillo, M. P. (2015). Pterostilbene improves glycaemic control in rats fed an obesogenic diet: Involvement of skeletal muscle and liver. *Food & Function*, *6*(6), 1968–1976. https://doi.org/10.1039/C5FO00151J

González, A., López, B., Martín-Raymondi, D., Lozano, E., Varo, N., Barba, J., Serrano, M., & Díez, J. (2005). Usefulness of plasma cardiotrophin-1 in assessment of left ventricular hypertrophy regression in hypertensive patients. *Journal of Hypertension*, *23*(12), 2297–2304. https://doi.org/10.1097/01.hjh.0000184406.12634.f9

Hamanaka, I., Saito, Y., Yasukawa, H., Kishimoto, I., Kuwahara, K., Miyamoto, Y., Harada, M., Ogawa, E., Kajiyama, N., Takahashi, N., Izumi, T., Kawakami, R., Masuda, I., Yoshimura, A., & Nakao, K. (2001). Induction of JAB/SOCS-1/SSI-1 and CIS3/SOCS-3/SSI-3 Is Involved in gp130 Resistance in Cardiovascular System in Rat Treated With Cardiotrophin-1 In Vivo. *Circulation Research*, *88*(7), 727–732. https://doi.org/10.1161/hh0701.088512

Harrison, D. G., Coffman, T. M., & Wilcox, C. S. (2021). Pathophysiology of Hypertension – the Mosaic Theory and Beyond. *Circulation Research*, *128*(7), 847. https://doi.org/10.1161/CIRCRESAHA.121.318082

He, F., & Stephens, J. M. (2006). Induction of SOCS-3 is insufficient to confer IRS-1 protein degradation in 3T3-L1 adipocytes. *Biochemical and Biophysical Research Communications*, *344*(1), 95–98. https://doi.org/10.1016/j.bbrc.2006.03.142

He-nan, Z., Yan, W., Miao-na, J., Cai-hua, Z., Shen, L., & Yu-jie, J. (2009). Relation of Cardiotrophin-1 (CT-1) and cardiac transcription factor GATA4 expression in rat's cardiac myocytes hypertrophy and apoptosis. *Pathology - Research and Practice*, *205*(9), 615–625. https://doi.org/10.1016/j.prp.2009.02.010

Herencia, C., Almadén, Y., Ferrín, G., Martínez-Romero, R., De La Mata, M., Ciria, R., Briceño, F. J., & Muñoz-Castañeda, J. R. (2015). Cardiotrophin-1 decreases liver apoptosis through calpastatin induction. *Journal of Surgical Research*, *193*(1), 119–125. https://doi.org/10.1016/j.jss.2014.06.056

Heying, R., Qing, M., Schumacher, K., Sokalska-Duhme, M., Vazquez-Jimenez, J. F., & Seghaye, M.-C. (2014). Myocardial cardiotrophin-1 is Differentially Induced in Congenital Cardiac Defects Depending On Hypoxemia. *Future Cardiology*, *10*(1), 53–62. https://doi.org/10.2217/fca.13.99

Hilger-Eversheim, K., Moser, M., Schorle, H., & Buettner, R. (2000). Regulatory roles of AP-2 transcription factors in vertebrate development, apoptosis and cell-cycle control. *Gene*, *260*(1), 1–12. https://doi.org/10.1016/S0378-1119(00)00454-6

Ho, D. W. (2006). Therapeutic Potential of Cardiotrophin 1 in Fulminant Hepatic Failure: Dual Roles in Antiapoptosis and Cell Repair. *Archives of Surgery*, *141*(11), 1077. https://doi.org/10.1001/archsurg.141.11.1077

Holliger, P., Prospero, T., & Winter, G. (1993). 'Diabodies': Small bivalent and bispecific antibody fragments. *Proceedings of the National Academy of Sciences*, *90*(14), 6444–6448. https://doi.org/10.1073/pnas.90.14.6444

Hu, Z.-Q., Li, H.-P., Zhang, J.-B., Huang, T., Liu, J.-L., Xue, S., Wu, A.-B., & Liao, Y.-C. (2013). A phage-displayed chicken single-chain antibody fused to alkaline phosphatase detects Fusarium pathogens and their presence in cereal grains. *Analytica Chimica Acta*, *764*, 84–92. https://doi.org/10.1016/j.aca.2012.12.022

Hua, X., Shan, Y., Li, D., Xu, D., Zhang, J., Yang, T., Han, L., Shen, C., Xia, Y., Chen, Q., Ma, X., Zhang, J., & Xia, Q. (2015). A Potential Profibrogenic Role of Biliary Epithelium-Derived Cardiotrophin-1 in Pediatric Cholestatic Liver Disease. *Journal of Interferon & Cytokine Research*, *35*(8), 606–612. https://doi.org/10.1089/jir.2014.0128

Hung, H.-C., Lu, F.-H., Ou, H.-Y., Wu, H.-T., Wu, J.-S., Yang, Y.-C., & Chang, C.-J. (2013). Increased cardiotrophin-1 in subjects with impaired glucose tolerance and newly diagnosed diabetes. *International Journal of Cardiology*, *169*(3), e33–e34. https://doi.org/10.1016/j.ijcard.2013.08.112

Hung, H.-C., Lu, F.-H., Wu, H.-T., Ou, H.-Y., Yang, Y.-C., Wu, J.-S., & Chang, C.-J. (2015). Cardiotrophin-1 is inversely associated with obesity in non-diabetic individuals. *Scientific Reports*, *5*(1), 17438. https://doi.org/10.1038/srep17438

Huston, J. S., Mudgett-Hunter, M., Tai, M.-S., McCartney, J., Warren, F., Haber, E., & Oppermann, H. (1991). [3] Protein engineering of single-chain Fv analogs and fusion proteins. In *Methods in Enzymology* (Vol. 203, pp. 46–88). Elsevier. https://doi.org/10.1016/0076-6879(91)03005-2

Iñiguez, M., Berasain, C., Martinez-Ansó, E., Bustos, M., Fortes, P., Pennica, D., Avila, M. A., & Prieto, J. (2006). Cardiotrophin-1 defends the liver against ischemia-reperfusion injury and mediates the protective effect of ischemic preconditioning. *The Journal of Experimental Medicine*, *203*(13), 2809–2815. https://doi.org/10.1084/jem.20061421

Ishikawa, M., Saito, Y., Miyamoto, Y., Kuwahara, K., Ogawa, E., Nakagawa, O., Harada, M., Masuda, I., & Nakao, K. (1996). cDNA Cloning of Rat Cardiotrophin-1 (CT-1): Augmented Expression of CT-1 Gene in Ventricle of Genetically Hypertensive

Rats. *Biochemical and Biophysical Research Communications*, *219*(2), 377–381. https://doi.org/10.1006/bbrc.1996.0241

Ito, Y., Yamamoto, M., Li, M., Mitsuma, N., Tanaka, F., Doyu, M., Suzumura, A., Mitsuma, T., & Sobue, G. (2000). *Temporal Expression of mRNAs for Neuropoietic Cytokines, Interleukin-11 (IL-11), Oncostatin M (OSM), Cardiotrophin-1 (CT-1) and Their Receptors (IL-11R␣ and OSMR␤) in Peripheral Nerve Injury*.

Jia, G., Leng, B., Wang, H., & Dai, H. (2017). Inhibition of cardiotrophin-1 overexpression is involved in the anti-fibrotic effect of Astrogaloside IV. *Molecular Medicine Reports*, *16*(6), 8365–8370. https://doi.org/10.3892/mmr.2017.7676

Jiménez-González, M., Jaques, F., Rodríguez, S., Porciuncula, A., Principe, R. M., Abizanda, G., Iñiguez, M., Escalada, J., Salvador, J., Prósper, F., Halban, P. A., & Barajas, M. (2013). Cardiotrophin 1 protects beta cells from apoptosis and prevents streptozotocin-induced diabetes in a mouse model. *Diabetologia*, *56*(4), 838–846. https://doi.org/10.1007/s00125-012-2822-8

Jin, H., Yang, R., Ko, A., Pennica, D., Wood, W. I., & Paoni, N. F. (1998). EFFECTS OF CARDIOTROPHIN-1 ON HAEMODYNAMICS AND CARDIAC FUNCTION IN CONSCIOUS RATS. *Cytokine*, *10*(1), 19–25. https://doi.org/10.1006/cyto.1997.0241

Jougasaki, M., Tachibana, I., Luchner, A., Leskinen, H., Redfield, M. M., & Burnett, J. C. (2000). Augmented Cardiac Cardiotrophin-1 in Experimental Congestive Heart Failure. *Circulation*, *101*(1), 14–17. https://doi.org/10.1161/01.CIR.101.1.14

Jung, C., Fritzenwanger, M., & Figulla, H. R. (2008). Cardiotrophin-1 in Adolescents: Impact of Obesity and Blood Pressure. *Hypertension*, *52*(2). https://doi.org/10.1161/HYPERTENSIONAHA.108.114421

Junk, D. J., Bryson, B. L., Smigiel, J. M., Parameswaran, N., Bartel, C. A., & Jackson, M. W. (2017). Oncostatin M promotes cancer cell plasticity through cooperative STAT3-SMAD3 signaling. *Oncogene*, *36*(28), 4001–4013. https://doi.org/10.1038/onc.2017.33

Khan, S. Q., Kelly, D., Quinn, P., Davies, J. E., & Ng, L. L. (2006). Cardiotrophin-1 Predicts Death or Heart Failure Following Acute Myocardial Infarction. *Journal of Cardiac Failure*, *12*(8), 635–640. https://doi.org/10.1016/j.cardfail.2006.06.470

Klinger, M., Brandl, C., Zugmaier, G., Hijazi, Y., Bargou, R. C., Topp, M. S., Gökbuget, N., Neumann, S., Goebeler, M., Viardot, A., Stelljes, M., Brüggemann, M., Hoelzer, D., Degenhard, E., Nagorsen, D., Baeuerle, P. A., Wolf, A., & Kufer, P. (2012). Immunopharmacologic response of patients with B-lineage acute lymphoblastic leukemia to continuous infusion of T cell–engaging CD19/CD3-bispecific BiTE antibody blinatumomab. *Blood*, *119*(26), 6226–6233. https://doi.org/10.1182/blood-2012-01-400515

Knappik, A. et al. (n.d.). *Fully Synthetic Human Combinatorial Antibody Libraries (HuCAL) Based on Modular Consensus Frameworks and CDRs Randomized with Trinucleotides*.

Kuwahara, K., Saito, Y., Kishimoto, I., Miyamoto, Y., Harada, M., Ogawa, E., Hamanaka, I., Kajiyama, N., Takahashi, N., Izumi, T., Kawakami, R., & Nakao, K. (2000). Cardiotrophin-1 Phosphorylates Akt and BAD, and Prolongs Cell Survival via a PI3K-dependent Pathway in Cardiac Myocytes. *Journal of Molecular and Cellular Cardiology*, *32*(8), 1385–1394. https://doi.org/10.1006/jmcc.2000.1177

Latchman, D. S. (1999). Cardiotrophin-1 (CT-1): A novel hypertrophic and cardioprotective agent. *International Journal of Experimental Pathology*, *80*(4), 189–196. https://doi.org/10.1046/j.1365-2613.1999.00114.x

Leavy, O. (2016). The birth of monoclonal antibodies. *Nature Immunology*, *17*(1), S13–S13. https://doi.org/10.1038/ni.3608

Lefranc, M.-P., & Lefranc, G. (2022). IMGT® Homo sapiens IG and TR Loci, Gene Order, CNV and Haplotypes: New Concepts as a Paradigm for Jawed Vertebrates Genome Assemblies. *Biomolecules*, *12*(3), 381. https://doi.org/10.3390/biom12030381

Liang, Y., Ma, B., Jiang, P., & Yang, H.-M. (2021). Identification of Methylation-Regulated Differentially Expressed Genes and Related Pathways in Hepatocellular Carcinoma: A Study Based on TCGA Database and Bioinformatics Analysis. *Frontiers in Oncology*, *11*, 636093. https://doi.org/10.3389/fonc.2021.636093

Liao, Z. (2002). Cardiotrophin-1 (CT-1) can protect the adult heart from injury when added both prior to ischaemia and at reperfusion. *Cardiovascular Research*, *53*(4), 902–910. https://doi.org/10.1016/S0008-6363(01)00531-4

Liu, J. K. H. (2014). The history of monoclonal antibody development – Progress, remaining challenges and future innovations. *Annals of Medicine and Surgery*, *3*(4), 113–116. https://doi.org/10.1016/j.amsu.2014.09.001

Liu, J., Shen, Q., & Wu, Y. (2008). Simvastatin prevents cardiac hypertrophy in vitro and in vivo via JAK/STAT pathway. *Life Sciences*, *82*(19–20), 991–996. https://doi.org/10.1016/j.lfs.2008.02.012

Liu, X., Xu, Y., Xiong, W., Yin, B., Huang, Y., Chu, J., Xing, C., Qian, C., Du, Y., Duan, T., Wang, H. Y., Zhang, N., Yu, J. S., An, Z., & Wang, R. (2022). Development of a TCR-like antibody and chimeric antigen receptor against NY-ESO-1/HLA-A2 for cancer immunotherapy. *Journal for ImmunoTherapy of Cancer*, *10*(3), e004035. https://doi.org/10.1136/jitc-2021-004035

López, B., González, A., Lasarte, J. J., Sarobe, P., Borrás, F., Díaz, A., Barba, J., Tomás, L., Lozano, E., Serrano, M., Varo, N., Beloqui, O., Fortuño, M. A., & Díez, J. (2005). Is plasma cardiotrophin-1 a marker of hypertensive heart disease? *Journal of Hypertension*, *23*(3), 625–632. https://doi.org/10.1097/01.hjh.0000160221.09468.d3

López, N., Díez, J., & Fortuño, M. A. (2005). Characterization of the protective effects of cardiotrophin-1 against non-ischemic death stimuli in adult cardiomyocytes. *Cytokine*, *30*(5), 282–292. https://doi.org/10.1016/j.cyto.2005.01.016

López, N., Díez, J., & Fortuño, M. A. (2006). Differential hypertrophic effects of cardiotrophin-1 on adult cardiomyocytes from normotensive and spontaneously

hypertensive rats. *Journal of Molecular and Cellular Cardiology*, *41*(5), 902–913. https://doi.org/10.1016/j.yjmcc.2006.03.433

López-Andrés, N., Calvier, L., Labat, C., Fay, R., Díez, J., Benetos, A., Zannad, F., Lacolley, P., & Rossignol, P. (2013). Absence of Cardiotrophin 1 Is Associated With Decreased Age-Dependent Arterial Stiffness and Increased Longevity in Mice. *Hypertension*, *61*(1), 120–129. https://doi.org/10.1161/HYPERTENSIONAHA.112.201699

López-Andrés, N., Iñigo, C., Gallego, I., Díez, J., & Fortuño, M. A. (2008). Aldosterone Induces Cardiotrophin-1 Expression in HL-1 Adult Cardiomyocytes. *Endocrinology*, *149*(10), 4970–4978. https://doi.org/10.1210/en.2008-0120

López-Yoldi, M., Castilla-Madrigal, R., Lostao, M. P., Barber, A., Prieto, J., Martínez, J. A., Bustos, M., & Moreno-Aliaga, M. J. (2016). Cardiotrophin-1 decreases intestinal sugar uptake in mice and in C aco-2 cells. *Acta Physiologica*, *217*(3), 217–226. https://doi.org/10.1111/apha.12674

López-Yoldi, M., Fernández-Galilea, M., Laiglesia, L. M., Larequi, E., Prieto, J., Martínez, J. A., Bustos, M., & Moreno-Aliaga, M. J. (2014). Cardiotrophin-1 stimulates lipolysis through the regulation of main adipose tissue lipases. *Journal of Lipid Research*, *55*(12), 2634–2643. https://doi.org/10.1194/jlr.M055335

López-Yoldi, M., Marcos-Gomez, B., Romero-Lozano, M. A., Sáinz, N., Prieto, J., Martínez, J. A., Bustos, M., & Moreno-Aliaga, M. J. (2017). Cardiotrophin-1 Regulates Adipokine Production in 3T3-L1 Adipocytes and Adipose Tissue From Obese Mice. *Journal of Cellular Physiology*, *232*(9), 2469–2477. https://doi.org/10.1002/jcp.25590

Lutz, S. Z., Franck, O., Böhm, A., Machann, J., Schick, F., Machicao, F., Fritsche, A., Häring, H.-U., & Staiger, H. (2014). Common Genetic Variation in the Human CTF1 Locus, Encoding Cardiotrophin-1, Determines Insulin Sensitivity. *PLoS ONE*, *9*(7), e100391. https://doi.org/10.1371/journal.pone.0100391

Mallender, W. D., & Voss, E. W. (1994). Construction, expression, and activity of a bivalent bispecific single-chain antibody. *Journal of Biological Chemistry*, *269*(1), 199–206. https://doi.org/10.1016/S0021-9258(17)42334-9

Marquès, J. M., Belza, I., Holtmann, B., Pennica, D., Prieto, J., & Bustos, M. (2007). Cardiotrophin-1 is an essential factor in the natural defense of the liver against apoptosis. *Hepatology*, *45*(3), 639–648. https://doi.org/10.1002/hep.21508

Martínez-Martínez, E., Ibarrola, J., Fernández-Celis, A., Santamaria, E., Fernández-Irigoyen, J., Rossignol, P., Jaisser, F., & López-Andrés, N. (2017). Differential Proteomics Identifies Reticulocalbin-3 as a Novel Negative Mediator of Collagen Production in Human Cardiac Fibroblasts. *Scientific Reports*, *7*(1), 12192. https://doi.org/10.1038/s41598-017-12305-7

Minas, J. N., Thorwald, M. A., Conte, D., Vázquez-Medina, J., Nishiyama, A., & Ortiz, R. M. (2015). Angiotensin and mineralocorticoid receptor antagonism attenuates cardiac oxidative stress in angiotensin II -infused rats. *Clinical and Experimental*

Pharmacology and Physiology, *42*(11), 1178–1188. https://doi.org/10.1111/1440-1681.12473

Monserrat, L., Lopez, B., Gonzalez, A., Hermida, M., Fernandez, X., Ortiz, M., Barriales-Villa, R., Castro-Beiras, A., & Diez, J. (2011). Cardiotrophin-1 plasma levels are associated with the severity of hypertrophy in hypertrophic cardiomyopathy. *European Heart Journal*, *32*(2), 177–183. https://doi.org/10.1093/eurheartj/ehq400

Moreno-Aliaga, M. J., Pérez-Echarri, N., Marcos-Gómez, B., Larequi, E., Gil-Bea, F. J., Viollet, B., Gimenez, I., Martínez, J. A., Prieto, J., & Bustos, M. (2011). Cardiotrophin-1 Is a Key Regulator of Glucose and Lipid Metabolism. *Cell Metabolism*, *14*(2), 242–253. https://doi.org/10.1016/j.cmet.2011.05.013

Natal, C., Fortuño, M. A., Restituto, P., Bazán, A., Colina, I., Díez, J., & Varo, N. (2008). Cardiotrophin-1 is expressed in adipose tissue and upregulated in the metabolic syndrome. *American Journal of Physiology-Endocrinology and Metabolism*, *294*(1), E52–E60. https://doi.org/10.1152/ajpendo.00506.2007

Nomura, N., Asano, M., Saito, T., Sasaki, S., Suzuki, H., Manabe, T., & Mishima, A. (2003). Cardiotrophin-1 is a prophylactic against the development of chronic hypoxic pulmonary hypertension in rats. *The Annals of Thoracic Surgery*, *76*(1), 237–243. https://doi.org/10.1016/S0003-4975(03)00339-4

Novartis Announces FDA Approval of Beovu for the Treatment of Diabetic Macular Edema. (n.d.). Retrieved 25 August 2025, from https://www.drugs.com/newdrugs/novartis-announces-fda-approval-beovu-diabetic-macular-edema-5845.html

Oberle, S., Schober, A., Meyer, V., Holtmann, B., Henderson, C., Sendtner, M., & Unsicker, K. (2006). Loss of Leukemia Inhibitory Factor Receptor β or Cardiotrophin-1 Causes Similar Deficits in Preganglionic Sympathetic Neurons and Adrenal Medulla. *The Journal of Neuroscience*, *26*(6), 1823–1832. https://doi.org/10.1523/JNEUROSCI.4127-05.2006

Okada, T., Akada, M., Fujita, T., Iwata, T., Goto, Y., Kido, K., Okada, T., Matsuzaki, Y., Kobayashi, K., Matsuno, S., Sunamura, M., & Kawakami, Y. (2006). A Novel Cancer Testis Antigen That Is Frequently Expressed in Pancreatic, Lung, and Endometrial Cancers. *Clinical Cancer Research*, *12*(1), 191–197. https://doi.org/10.1158/1078-0432.CCR-05-1206

Okamoto, T., Mukai, Y., Yoshioka, Y., Shibata, H., Kawamura, M., Yamamoto, Y., Nakagawa, S., Kamada, H., Hayakawa, T., Mayumi, T., & Tsutsumi, Y. (2004). Optimal construction of non-immune scFv phage display libraries from mouse bone marrow and spleen established to select specific scFvs efficiently binding to antigen. *Biochemical and Biophysical Research Communications*, *323*(2), 583–591. https://doi.org/10.1016/j.bbrc.2004.08.131

Oppenheim, R. W., Wiese, S., Prevette, D., Armanini, M., Wang, S., Houenou, L. J., Holtmann, B., Götz, R., Pennica, D., & Sendtner, M. (2001). Cardiotrophin-1, a Muscle-Derived Cytokine, Is Required for the Survival of Subpopulations of

Developing Motoneurons. *The Journal of Neuroscience*, *21*(4), 1283–1291. https://doi.org/10.1523/JNEUROSCI.21-04-01283.2001

Pan, J., Dai, Q., Xiang, Z., Liu, B., & Li, C. (2019). Three Biomarkers Predict Gastric Cancer Patients' Susceptibility To Fluorouracil-based Chemotherapy. *Journal of Cancer*, *10*(13), 2953–2960. https://doi.org/10.7150/jca.31120

Pan, J., Fukuda, K., Saito, M., Matsuzaki, J., Kodama, H., Sano, M., Takahashi, T., Kato, T., & Ogawa, S. (1999). Mechanical Stretch Activates the JAK/STAT Pathway in Rat Cardiomyocytes. *Circulation Research*, *84*(10), 1127–1136. https://doi.org/10.1161/01.RES.84.10.1127

Pennica, D., Arce, V., Swanson, T. A., Vejsada, R., Pollock, R. A., Armanini, M., Dudley, K., Phillips, H. S., Rosenthal, A., Kato, A. C., & Henderson, C. E. (1996). Cardiotrophin-1, a Cytokine Present in Embryonic Muscle, Supports Long-Term Survival of Spinal Motoneurons. *Neuron*, *17*(1), 63–74. https://doi.org/10.1016/S0896-6273(00)80281-0

Pennica, D., King, K. L., Shaw, K. J., Luis, E., Rullamas, J., Luoh, S. M., Darbonne, W. C., Knutzon, D. S., Yen, R., & Chien, K. R. (1995). Expression cloning of cardiotrophin 1, a cytokine that induces cardiac myocyte hypertrophy. *Proceedings of the National Academy of Sciences*, *92*(4), 1142–1146. https://doi.org/10.1073/pnas.92.4.1142

Pennica, D., Swanson, T. A., Shaw, K. J., Kuang, W.-J., Gray, C. L., Beatty, B. G., & Wood, W. I. (1996). Human Cardiotrophin-1: Protein and Gene Structure, Biological and Binding Activities, and Chromosomal Localization. *Cytokine*, *8*(3), 183–189. https://doi.org/10.1006/cyto.1996.0026

Perretta-Tejedor, N., Muñoz-Félix, J. M., Düwel, A., Quiros-Luis, Y., Fernández-Martín, J. L., Morales, A. I., López-Hernández, F. J., López-Novoa, J. M., & Martínez-Salgado, C. (2019). Cardiotrophin-1 opposes renal fibrosis in mice: Potential prevention of chronic kidney disease. *Acta Physiologica*, *226*(2), e13247. https://doi.org/10.1111/apha.13247

Popov, A. V., Zou, X., Xian, J., Nicholson, I. C., & Brüggemann, M. (1999). A Human Immunoglobulin λ Locus Is Similarly Well Expressed in Mice and Humans. *Journal of Experimental Medicine*, *189*(10), 1611–1620. https://doi.org/10.1084/jem.189.10.1611

Prieto-Vicente, V., Sánchez-Garrido, A. I., Blanco-Gozalo, V., Arévalo, M., García-Sánchez, E., López-Montañés, D., Quiros, Y., López-Hernández, F. J., Rodríguez-Pérez, A., & López-Novoa, J. M. (2018). Cardiotrophin-1 attenuates experimental colitis in mice. *Clinical Science*, *132*(9), 985–1001. https://doi.org/10.1042/CS20171513

Quiros, Y., Sánchez-González, P. D., López-Hernández, F. J., Morales, A. I., & López-Novoa, J. M. (2013). Cardiotrophin-1 Administration Prevents the Renal Toxicity of Iodinated Contrast Media in Rats. *Toxicological Sciences*, *132*(2), 493–501. https://doi.org/10.1093/toxsci/kft007

R, L., X, L., W, X., & Ks, L. (2017). Tumor-targeting peptides from combinatorial libraries. *Advanced Drug Delivery Reviews*, *110–111*. https://doi.org/10.1016/j.addr.2016.05.009

Rahbarizadeh, F., Rasaee, M. J., Forouzandeh Moghadam, M., Allameh, A. A., & Sadroddiny, E. (2004). Production of Novel Recombinant Single-Domain Antibodies against Tandem Repeat Region of MUC1 Mucin. *Hybridoma and Hybridomics*, *23*(3), 151–159. https://doi.org/10.1089/1536859041224334

Railson, J. E., Lawrence, K., Buddle, J. C., Pennica, D., & Latchman, D. S. (2001). Heat Shock Protein-56 is Induced by Cardiotrophin-1 and Mediates its Hypertrophic Effect. *Journal of Molecular and Cellular Cardiology*, *33*(6), 1209–1221. https://doi.org/10.1006/jmcc.2001.1384

Ravassa, S., Beloqui, O., Varo, N., Barba, J., López, B., Beaumont, J., Zalba, G., Díez, J., & González, A. (2013). Association of cardiotrophin-1 with left ventricular systolic properties in asymptomatic hypertensive patients. *Journal of Hypertension*, *31*(3), 587–594. https://doi.org/10.1097/HJH.0b013e32835ca903

Rees, A. R. (2020). Understanding the human antibody repertoire. *mAbs*, *12*(1), 1729683. https://doi.org/10.1080/19420862.2020.1729683

Rende, D., Baysal, N., & Kirdar, B. (2013). Complex Disease Interventions from a Network Model for Type 2 Diabetes. *PLoS ONE*, *8*(6), e65854. https://doi.org/10.1371/journal.pone.0065854

Rendo-Urteaga, T., García-Calzón, S., Martínez-Ansó, E., Chueca, M., Oyarzabal, M., Azcona-Sanjulián, M. C., Bustos, M., Moreno-Aliaga, M. J., Martínez, J. A., & Marti, A. (2013). Decreased cardiotrophin-1 levels are associated with a lower risk of developing the metabolic syndrome in overweight/obese children after a weight loss program. *Metabolism - Clinical and Experimental*, *62*(10), 1429–1436. https://doi.org/10.1016/j.metabol.2013.05.011

Research, C. for D. E. and. (2024a). FDA approves axicabtagene ciloleucel for second-line treatment of large B-cell lymphoma. *FDA*. https://www.fda.gov/drugs/resources-information-approved-drugs/fda-approves-axicabtagene-ciloleucel-second-line-treatment-large-b-cell-lymphoma

Research, C. for D. E. and. (2024b). FDA approves idecabtagene vicleucel for multiple myeloma. *FDA*. https://www.fda.gov/drugs/resources-information-approved-drugs/fda-approves-idecabtagene-vicleucel-multiple-myeloma

Research, C. for D. E. and. (2024c). FDA approves lisocabtagene maraleucel for second-line treatment of large B-cell lymphoma. *FDA*. https://www.fda.gov/drugs/resources-information-approved-drugs/fda-approves-lisocabtagene-maraleucel-second-line-treatment-large-b-cell-lymphoma

Research, C. for D. E. and. (2024d). FDA approves tebentafusp-tebn for unresectable or metastatic uveal melanoma. *FDA*. https://www.fda.gov/drugs/resources-information-approved-drugs/fda-approves-tebentafusp-tebn-unresectable-or-metastatic-uveal-melanoma

Research, C. for D. E. and. (2024e). FDA approves tisagenlecleucel for relapsed or refractory follicular lymphoma. *FDA*. https://www.fda.gov/drugs/resources-information-approved-drugs/fda-approves-tisagenlecleucel-relapsed-or-refractory-follicular-lymphoma

Research, C. for D. E. and. (2024f). FDA D.I.S.C.O. Burst Edition: FDA approval of CARVYKTI (ciltacabtagene autoleucel) for the treatment of adult patients with relapsed or refractory multiple myeloma after four or more prior lines of therapy, including a proteasome inhibitor, an immunomodulatory agent, and an anti-CD38 monoclonal antibody. *FDA*. https://www.fda.gov/drugs/resources-information-approved-drugs/fda-disco-burst-edition-fda-approval-carvykti-ciltacabtagene-autoleucel-treatment-adult-patients

Research, C. for D. E. and. (2024g). FDA D.I.S.C.O. Burst Edition: FDA approval of Tecartus (brexucabtagene autoleucel) for adult patients with relapsed or refractory B-cell precursor acute lymphoblastic leukemia. *FDA*. https://www.fda.gov/drugs/resources-information-approved-drugs/fda-disco-burst-edition-fda-approval-tecartus-brexucabtagene-autoleucel-adult-patients-relapsed-or

Reusch, U., Burkhardt, C., Fucek, I., Le Gall, F., Le Gall, M., Hoffmann, K., Knackmuss, S. H., Kiprijanov, S., Little, M., & Zhukovsky, E. A. (2014). A novel tetravalent bispecific TandAb (CD30/CD16A) efficiently recruits NK cells for the lysis of $CD30^+$ tumor cells. *mAbs*, *6*(3), 727–738. https://doi.org/10.4161/mabs.28591

Rh, D., S, A., R, P., A, K., & M, K. (2024). A Comprehensive Review of Metabolic Syndrome and Its Role in Cardiovascular Disease and Type 2 Diabetes Mellitus: Mechanisms, Risk Factors, and Management. *Cureus*, *16*(8). https://doi.org/10.7759/cureus.67428

Richards, C. D., Langdon, C., Deschamps, P., Pennica, D., & Shaughnessy, S. G. (2000). STIMULATION OF OSTEOCLAST DIFFERENTIATION IN VITRO BY MOUSE ONCOSTATIN M, LEUKAEMIA INHIBITORY FACTOR, CARDIOTROPHIN-1 AND INTERLEUKIN 6: SYNERGY WITH DEXAMETHASONE. *Cytokine*, *12*(6), 613–621. https://doi.org/10.1006/cyto.1999.0635

Richards, C. D., Langdon, C., Pennica, D., & Gauldie, J. (1996). Murine Cardiotrophin-1 Stimulates the Acute-Phase Response in Rat Hepatocytes and H35 Hepatoma Cells. *Journal of Interferon & Cytokine Research*, *16*(1), 69–75. https://doi.org/10.1089/jir.1996.16.69

Rind, H. B., & Von Bartheld, C. S. (2002). Target-Derived Cardiotrophin-1 and Insulin-like Growth Factor-I Promote Neurite Growth and Survival of Developing Oculomotor Neurons. *Molecular and Cellular Neuroscience*, *19*(1), 58–71. https://doi.org/10.1006/mcne.2001.1069

Robador, P. A., Moreno, M. U., Beloqui, O., Varo, N., Redón, J., Fortuño, A., Zalba, G., & Díez, J. (2010). Protective effect of the 1742(C/G) polymorphism of human cardiotrophin-1 against left ventricular hypertrophy in essential hypertension. *Journal of Hypertension*, *28*(11), 2219–2226. https://doi.org/10.1097/HJH.0b013e32833da326

Robador, P. A., San José, G., Rodríguez, C., Guadall, A., Moreno, M. U., Beaumont, J., Fortuño, A., Díez, J., Martínez-González, J., & Zalba, G. (2011). HIF-1-mediated up-regulation of cardiotrophin-1 is involved in the survival response of cardiomyocytes to hypoxia. *Cardiovascular Research*, *92*(2), 247–255. https://doi.org/10.1093/cvr/cvr202

Rodríguez-Nava, C., Ortuño-Pineda, C., Illades-Aguiar, B., Flores-Alfaro, E., Leyva-Vázquez, M. A., Parra-Rojas, I., Del Moral-Hernández, O., Vences-Velázquez, A., Cortés-Sarabia, K., & Alarcón-Romero, L. D. C. (2023). Mechanisms of Action and Limitations of Monoclonal Antibodies and Single Chain Fragment Variable (scFv) in the Treatment of Cancer. *Biomedicines*, *11*(6), 1610. https://doi.org/10.3390/biomedicines11061610

Rubiś, P., Dziewięcka, E., Szymańska, M., Banyś, R., Urbańczyk-Zawadzka, M., Krupiński, M., Mielnik, M., Wiśniowska-Śmiałek, S., Karabinowska, A., Podolec, P., Winiarczyk, M., Gliniak, M., Kaciczak, M., Robak, J., Karapetyan, A., & Wypasek, E. (2021). Lack of Relationship between Fibrosis-Related Biomarkers and Cardiac Magnetic Resonance-Assessed Replacement and Interstitial Fibrosis in Dilated Cardiomyopathy. *Cells*, *10*(6), 1295. https://doi.org/10.3390/cells10061295

S, R., J, K., F, B., & S, D. (2001). A helper phage to improve single-chain antibody presentation in phage display. *Nature Biotechnology*, *19*(1). https://doi.org/10.1038/83567

Sakamoto, T., Kawazoe, Y., Shen, J., Takeda, Y., Arakawa, Y., Ogawa, J., Oyanagi, K., Ohashi, T., Watanabe, K., Inoue, K., Eto, Y., & Watabe, K. (2003). Adenoviral gene transfer of GDNF, BDNF and TGFβ2, but not CNTF, cardiotrophin-1 or IGF1, protects injured adult motoneurons after facial nerve avulsion. *Journal of Neuroscience Research*, *72*(1), 54–64. https://doi.org/10.1002/jnr.10558

Sari, D., Gozuacik, D., & Akkoc, Y. (2024). Role of autophagy in cancer-associated fibroblast activation, signaling and metabolic reprograming. *Frontiers in Cell and Developmental Biology*, *11*, 1274682. https://doi.org/10.3389/fcell.2023.1274682

Schirone, L., Forte, M., Palmerio, S., Yee, D., Nocella, C., Angelini, F., Pagano, F., Schiavon, S., Bordin, A., Carrizzo, A., Vecchione, C., Valenti, V., Chimenti, I., Falco, E. D., Sciarretta, S., & Frati, G. (2017). A Review of the Molecular Mechanisms Underlying the Development and Progression of Cardiac Remodeling. *Oxidative Medicine and Cellular Longevity*, *2017*, 3920195. https://doi.org/10.1155/2017/3920195

Scoles, D. R., Xu, X., Wang, H., Tran, H., Taylor-Harding, B., Li, A., & Karlan, B. Y. (2010). Liver X receptor agonist inhibits proliferation of ovarian carcinoma cells stimulated by oxidized low density lipoprotein. *Gynecologic Oncology*, *116*(1), 109–116. https://doi.org/10.1016/j.ygyno.2009.09.034

Sheets, M. D., Amersdorfer, P., Finnern, R., Sargent, P., Lindqvist, E., Schier, R., Hemingsen, G., Wong, C., Gerhart, J. C., & Marks, J. D. (1998). Efficient construction of a large nonimmune phage antibody library: The production of high-affinity human single-chain antibodies to protein antigens. *Proceedings of the National Academy of*

Sciences of the United States of America, *95*(11), 6157–6162. https://doi.org/10.1073/pnas.95.11.6157

Sheng, Z., Knowlton, K., Chen, J., Hoshijima, M., Brown, J. H., & Chien, K. R. (1997). Cardiotrophin 1 (CT-1) Inhibition of Cardiac Myocyte Apoptosis via a Mitogen-activated Protein Kinase-dependent Pathway. *Journal of Biological Chemistry*, *272*(9), 5783–5791. https://doi.org/10.1074/jbc.272.9.5783

Singh, G., & Xu, H. (2021). Light Chain Predominant Intact Immunoglobulin Monoclonal Gammopathy Disorders: Shorter Survival in Light Chain Predominant Multiple Myelomas. *Laboratory Medicine*, *52*(4), 390–398. https://doi.org/10.1093/labmed/lmaa057

Stephanou, A., Brar, B., Heads, R., Knight, R. D., Marber, M. S., Pennica, D., & Latchman, D. S. (1998). Cardiotrophin-1 Induces Heat Shock Protein Accumulation in Cultured Cardiac Cells and Protects them from Stressful Stimuli. *Journal of Molecular and Cellular Cardiology*, *30*(4), 849–855. https://doi.org/10.1006/jmcc.1998.0651

Stephens, J., Ravussin, E., & White, U. (2019). The Expression of Adipose Tissue-Derived Cardiotrophin-1 in Humans with Obesity. *Biology*, *8*(2), Article 2. https://doi.org/10.3390/biology8020024

Sun, D., Shi, H., Chen, J., Shi, D., Zhu, Q., Zhang, H., Liu, S., Wang, Y., Qiu, H., & Feng, L. (2012). Generation of a mouse scFv library specific for porcine aminopeptidase N using the T7 phage display system. *Journal of Virological Methods*, *182*(1–2), 99–103. https://doi.org/10.1016/j.jviromet.2012.03.021

T, T., Kn, S., & E, R. (2012). Mapping of vascular ZIP codes by phage display. *Methods in Enzymology*, *503*. https://doi.org/10.1016/B978-0-12-396962-0.00002-1

Terui, K., Enosawa, S., Haga, S., Zhang, H. Q., Kuroda, H., Kouchi, K., Matsunaga, T., Yoshida, H., Engelhardt, J. F., Irani, K., Ohnuma, N., & Ozaki, M. (2004). Stat3 confers resistance against hypoxia/reoxygenation-induced oxidative injury in hepatocytes through upregulation of Mn-SOD. *Journal of Hepatology*, *41*(6), 957–965. https://doi.org/10.1016/j.jhep.2004.08.019

Tian, Y., Shao, Q., Tang, Y., Li, X., Qi, X., Jiang, R., Liang, Y., & Kang, F. (2022). HIF-1α regulates osteoclast activation and mediates osteogenesis during mandibular bone repair via CT-1. *Oral Diseases*, *28*(2), 428–441. https://doi.org/10.1111/odi.13745

Tian, Z., Cui, W., Li, Y., Hao, Y., Du, J., Liu, F., Zhang, H., Zu, X., Liu, S., Chen, L., & An, W. (2004). Different contributions of STAT3, ERK1/2, and PI3-K signaling to cardiomyocyte hypertrophy by cardiotrophin-1. *Acta Pharmacol Sin*.

Vallance, P., Leone, A., Calver, A., Collier, J., & Moncada, S. (1992). Endogenous Dimethylarginine as an Inhibitor of Nitric Oxide Synthesis. *Journal of Cardiovascular Pharmacology*, *20*, S60.

Walker, E. C., McGregor, N. E., Poulton, I. J., Pompolo, S., Allan, E. H., Quinn, J. M., Gillespie, M. T., Martin, T. J., & Sims, N. A. (2008). Cardiotrophin-1 Is an Osteoclast-Derived Stimulus of Bone Formation Required for Normal Bone Remodeling. *Journal*

of Bone and Mineral Research, *23*(12), 2025–2032. https://doi.org/10.1359/jbmr.080706

Wang, L., Zhang, W., Fang, Z., Lu, T., Gu, Z., Sun, T., Han, D., Wang, Y., & Cao, F. (2024). Association between Human Blood Proteome and the Risk of Myocardial Infarction. *Reviews in Cardiovascular Medicine*, *25*(6), 199. https://doi.org/10.31083/j.rcm2506199

Watt, J., Baker, A. H., Meeks, B., Pajevic, P. D., Morgan, E. F., Gerstenfeld, L. C., & Schlezinger, J. J. (2018). Tributyltin induces distinct effects on cortical and trabecular bone in female C57Bl/6J mice. *Journal of Cellular Physiology*, *233*(9), 7007–7021. https://doi.org/10.1002/jcp.26495

Wollert, K. C., Taga, T., Saito, M., Narazaki, M., Kishimoto, T., Glembotski, C. C., Vernallis, A. B., Heath, J. K., Pennica, D., Wood, W. I., & Chien, K. R. (1996). Cardiotrophin-1 Activates a Distinct Form of Cardiac Muscle Cell Hypertrophy. *Journal of Biological Chemistry*, *271*(16), 9535–9545. https://doi.org/10.1074/jbc.271.16.9535

Wu, C., Zhai, Y., Ji, J., Yang, X., Ye, L., Lu, G., Shi, X., & Zhai, G. (2024). Advances in tumor stroma-based targeted delivery. *International Journal of Pharmaceutics*, *664*, 124580. https://doi.org/10.1016/j.ijpharm.2024.124580

Wu, T. T., & Kabat, E. A. (1970). AN ANALYSIS OF THE SEQUENCES OF THE VARIABLE REGIONS OF BENCE JONES PROTEINS AND MYELOMA LIGHT CHAINS AND THEIR IMPLICATIONS FOR ANTIBODY COMPLEMENTARITY. *Journal of Experimental Medicine*, *132*(2), 211–250. https://doi.org/10.1084/jem.132.2.211

Xia, J., Bi, H., Yao, Q., Qu, S., & Zong, Y. (2006). Construction of human ScFv phage display library against ovarian tumor. *Journal of Huazhong University of Science and Technology*, *26*(5), 497–499. https://doi.org/10.1007/s11596-006-0502-y

Xu, C., Miao, W., He, Y., Zu, Y., Liu, X., Li, J., & Liu, X. (2019). Construction of an immunized rabbit phage display antibody library for screening microcystin-LR high sensitive single-chain antibody. *International Journal of Biological Macromolecules*, *123*, 369–378. https://doi.org/10.1016/j.ijbiomac.2018.11.122

Yang, Z. F., Lau, C. K., Ngai, P., Lam, S. P., Ho, D. W., Poon, R. T., & Fan, S. T. (2008). Cardiotrophin-1 enhances regeneration of cirrhotic liver remnant after hepatectomy through promotion of angiogenesis and cell proliferation. *Liver International*, *28*(5), 622–631. https://doi.org/10.1111/j.1478-3231.2008.01687.x

Yin, R., Yang, D., & Li, J. (2004). Effects of cardiotrophin-1 on hemodynamics and cardiomyocyte apoptosis in rats with acute myocardial infarction. *The Journal of Medical Investigation*, *51*(1,2), 29–37. https://doi.org/10.2152/jmi.51.29

Yu, K., & Lieber, M. R. (2019). CURRENT INSIGHTS INTO THE MECHANISM OF MAMMALIAN IMMUNOGLOBULIN CLASS SWITCH RECOMBINATION. *Critical Reviews in Biochemistry and Molecular Biology*, *54*(4), 333. https://doi.org/10.1080/10409238.2019.1659227

Zhang, Z.-F., Liao, W.-H., Yang, Q.-F., Li, H.-Y., Wu, Y.-M., & Zhou, X.-F. (2003). Protective effects of adenoviral cardiotrophin-1 gene transfer on rubrospinal neurons after spinal cord injury in adult rats. *Neurotoxicity Research*, *5*(7), 539–548. https://doi.org/10.1007/BF03033164

Zheng, Z. Z., Tian Fu, X., Liang, J., & Bing Guo, Z. (2015). CT-1 induces angiogenesis by regulating the ADMA/DDAH Pathway. *Biomedical Papers*, *159*(4), 540–546. https://doi.org/10.5507/bp.2015.009

Zolk, O., Ng, L. L., O'Brien, R. J., Weyand, M., & Eschenhagen, T. (2002). Augmented Expression of Cardiotrophin-1 in Failing Human Hearts Is Accompanied by Diminished Glycoprotein 130 Receptor Protein Abundance. *Circulation*, *106*(12), 1442–1446. https://doi.org/10.1161/01.CIR.0000033117.39335.DF

Zvonic, S., Baugh, J. E., Arbour-Reily, P., Mynatt, R. L., & Stephens, J. M. (2005). Cross-talk among gp130 Cytokines in Adipocytes. *Journal of Biological Chemistry*, *280*(40), 33856–33863. https://doi.org/10.1074/jbc.M508020200

Zvonic, S., Hogan, J. C., Arbour-Reily, P., Mynatt, R. L., & Stephens, J. M. (2004). Effects of Cardiotrophin on Adipocytes. *Journal of Biological Chemistry*, *279*(46), 47572–47579. https://doi.org/10.1074/jbc.M403998200